

UNIVERSIDADE DE BRASÍLIA
INSTITUTO DE CIÊNCIAS BIOLÓGICAS
DEPARTAMENTO DE ECOLOGIA

Ray Pinheiro Alves

**Influências geoambientais nas relações organominerais em solos do Planalto
Ocidental Paulista**

Brasília
2019

UNIVERSIDADE DE BRASÍLIA
INSTITUTO DE CIÊNCIAS BIOLÓGICAS
DEPARTAMENTO DE ECOLOGIA

Ray Pinheiro Alves

**Influências geoambientais nas relações organominerais em solos do Planalto
Ocidental Paulista**

Tese apresentada ao Programa de Pós-Graduação
em Ecologia da Universidade de Brasília, para
obtenção do Título de Doutor em Ecologia

Brasília
2019

UNIVERSIDADE DE BRASÍLIA
INSTITUTO DE CIÊNCIAS BIOLÓGICAS
DEPARTAMENTO DE ECOLOGIA

Ray Pinheiro Alves

**Influências geoambientais nas relações organominerais em solos do Planalto
Ocidental Paulista**

Banca Examinadora:

Profa. Dra. Gabriela Bielefeld Nardoto / PPG Ecologia – UnB (Presidente/Orientadora)

Profa. Dra. Heloísa Sinatra Miranda / PPG Ecologia – UnB (Membro Titular)

Prof. Dr. Carlos Eduardo Pellegrino Cerri / PPG Solos e Nutrição de Plantas ESALQ/USP
(Membro Titular)

Prof. Dr. Éder de Souza Martins / PPG Ciências Ambientais – UnB (Membro Titular)

Profa. Dra. Mercedes Maria da Cunha Bustamante / PPG ECL - UnB (Membro Suplente)

DEDICATÓRIA

**Ao meu núcleo familiar Edson, Vera, Georgina, Tatá, Naná, Mari, Manuzim,
Bielzim, Enzo, Théo e à minha amada companheira Isabella**

**Aos meus avós paternos Ana Alves (*in memorian*) e João Alves (*in memorian*)
Aos meus avós maternos Cleonice Pinheiro e Manoel Pinheiro (*in memorian*)**

À minha avó de coração, Olgaíde Cohen (*in memorian*)

À minha madrinha querida, Regina Cohen (*in memorian*)

À minha madrinha de consagração, Fátima Cohen (*in memorian*)

À tia querida Ely Maroccolo (*in memorian*)

**E a todas as pessoas que de alguma forma interagiram comigo e me fizeram ser
quem eu sou**

AGRADECIMENTOS

À minha orientadora Dra. Gabriela Bielefeld Nardoto, pela formação técnico-científica, pela confiança e pela oportunidade de desenvolver este projeto. Agradeço também pelo exemplo de profissionalismo, amizade, conselhos e transparência que estabelecemos ao longo destes anos.

Agradeço aos integrantes da comissão avaliadora, Dra. Heloísa Sinatora Miranda, Dr. Éder de Souza Martins, Dr. Carlos Eduardo Cerri e Dra. Mercedes Maria da Cunha Bustamanete, que aceitaram gentilmente o convite para composição da banca de defesa e pela preciosa análise crítica deste trabalho, trazendo contribuições e agregando experiência para aprimorar a tese.

À toda a galera do laboratório de Solos e Vegetação, pelos conselhos, conversas e compartilhamento de ideias, tornando o ambiente do laboratório de Solos e Vegetação um ambiente propício para a germinação e crescimento deste trabalho. “Kiki”, “little John”, “Fafá”, “Jeh”, “Pomper”, “Giovis”, “Gráubs”, “Carlinha”, “Fabão”, “Pedrão” e “Andrézão” queria dizer que aprendi muito com vocês, tanto no âmbito pessoal como profissional. Não poderia deixar de agradecer o Dr. Vinicius Vasconcelos por me incentivar e apoiar nos estudos geomorfológicos, planejamento e suporte nas coletas.

Ao grupo CSME da UNESP Jaboticabal, que juntamente ao Grupo Origem auxiliaram com o suporte logístico para saídas de campo. Nesse sentido, gostaria de agradecer especialmente ao professor Dr. José Marques Junior, coordenador do grupo CSME, pela confiança e apoio. Além disso gostaria de agradecer ao Dr. Diego Silva Siqueira e Laércio Silva Santos pelo suporte e troca de experiências.

À Universidade da Califórnia – UC Merced, em especial à Dra. Asmeret Asefaw Berhe, por ter me recebido durante o período sanduíche, me auxiliado em relação à abordagens e análises do doutorado. À Fernanda Santos por todo o suporte em relação ao laboratório de biogeoquímica de solos, dicas sobre Merced e os E.U.A, e troca de ideias sobre ciência. Gostaria de agradecer também à Kimber, Morgan, Manisha, Lixia e Jing, por todas as conversas e suporte no laboratório. Enfim, e a todo o pessoal dos Laboratórios de Física e Biogeoquímica de Solos.

À Universidade de Brasília e ao Programa de Pós-graduação em Ecologia, do Instituto de Ciências Biológicas pela oportunidade de ingressar no curso de doutorado, que possibilitou meu aprimoramento profissional.

Ao Conselho Nacional de Desenvolvimento Científico e Tecnológico (CNPq) e à Coordenação de Aperfeiçoamento de Pessoal de Nível Superior (CAPES), pela concessão da bolsa de doutorado. Ao apoio da CAPES no Programa de Doutorado Sanduíche no Exterior (PDSE).

Ao apoio financeiro concedido pelo CNPq para o projeto temático "Geovariabilidade do Planalto Ocidental Paulista e sua relação com as mudanças climáticas e planejamento estratégico de uso e ocupação do solo" (Edital Universal 01/2016 - Faixa C, Proc.nº 402796/2016-0).

Ao apoio financeiro concedido pela CAPES e a PROPE / UNESP (Pró-reitora de Pesquisa da Universidade Estadual Paulista, Edital Nº 15/2014) pelo apoio financeiro ao projeto de pesquisa de fronteira "Diffuse reflectance spectroscopy and soil erodibility in Western Plateau Paulista, the context of soil-landscape".

À Dra. Regina Silveira Sartori pelo apoio, suporte em análises e ter auxiliado na minha formação ao longo destes anos.

Ao professor Dr. Luiz Fellipe Salemi por todos os papos de Gestão Ambiental/Ecologia que tivemos, bem como ao apoio no grupo NEPAL junto aos professores Dr. Antônio Felipe Couto Junior e Dr. Ludgero Cardoso Galli Vieira.

Agradeço ao povo da minha quebrada Nelia, Valtencio, Carlos, Mábia, Munick, Raynan, Patrick e Guilherme.

Ao meu núcleo familiar, Vera, Edson, Georgina, Tatá, Naná, Mari, Manu e Biel por todo o suporte, carinho e compreensão ao longo destes anos. Vocês são inspiração pra mim.

À minha querida companheira Isabella de Carvalho Vallin por todo apoio, paciência, carinho, amor e companheirismo durante essa trajetória. IY.

A todas as pessoas que tive participaram de alguma forma de minha existência.

À vida e a Deus pela oportunidade de aprender.

Agradeço de todo o meu coração!

“Escolher escrever é rejeitar o silêncio.”

Chimamanda Ngozi Adichie

“Seja a mudança que você quer ver no mundo.”

Mahatma Gandhi

“Sonhem de olhos abertos.”

Glauber Rocha

“Se você tem conhecimento, deixe os outros acenderem as suas velas nele.”

Margaret Fuller

Resumo

O solo é o compartimento terrestre com maior reservatório de C na forma de matéria orgânica no solo (MOS). A decomposição da MOS é responsável por emitir pelo menos 3,5 Pg ano⁻¹ de CO₂ para a atmosfera. Como a persistência da MOS é uma propriedade ecossistêmica, é necessário estudá-la em um contexto multidisciplinar. Nesse contexto, existe uma lacuna científica para entender como o material de origem e a geomorfologia influenciam a estabilidade da MOS. Assim, este estudo avaliou como fatores geológicos e processos geomorfológicos afetam a composição e a estabilidade da MOS no Planalto Ocidental Paulista. Utilizando uma abordagem *machine learning* com o algoritmo *random forest*, a suscetibilidade magnética medida em baixa frequência (MS_{lf}) foi identificada como a variável ambiental mais importante para prever carbono (C) e δ¹⁵N no solo, na profundidade de 0-20 cm. Além disso, variáveis topográficas e climáticas ajudaram a predizer C e δ¹⁵N. A relação entre C e δ¹⁵N também foi investigada com diferentes métricas de óxido de ferro, como MS_{lf}, variação de suscetibilidade magnética (MS_{fd%}), ditionito de ferro (Fe_d), oxionato de ferro (Fe_o), hematita (Hm) , goethita (Gt), bem como as razões Fed/Feo, [Hm/(Hm + Gt)] e Silte/Argila. Além disso, um modelo foi aplicado para estimar a estabilidade relativa do MOS (η) em áreas naturais. Posteriormente, investigou-se o efeito da profundidade e da MS_{lf} nas sobre η e grupos funcionais orgânicos obtidos por Espectroscopia de Infravermelho com Transformada de Fourier. As relações entre as métricas de ferro com C e δ¹⁵N reforçam a importância dos óxidos de ferro para estabilizar a MOS e destacam a necessidade de usar variáveis mineralógicas para modelar e predizer C e δ¹⁵N no solo. Considerando diferentes contextos de domínios geoambientais, a MS_{lf} figurou como um pedoindicador integrador na paisagem do Planalto Ocidental Paulista.

Palavras chave: suscetibilidade magnética, matéria orgânica no solo, isótopos estáveis, basaltos, arenitos

Abstract

The soil is the terrestrial compartment with the largest C reservoir in the form of soil organic matter (SOM). Decomposing SOM is responsible for emitting at least 3.5 Pg year⁻¹ of CO₂ to the atmosphere. As the persistence of SOM is an ecosystem property, it is necessary to study it in a multidisciplinary context. Furthermore, there is a scientific gap to understand how source material and geomorphology influence the stability of soil organic matter. In this context, this study evaluated how geological factors and geomorphological processes affect the composition and stability of SOM in the Western Paulista Plateau. Using a machine learning approach with the random forest algorithm the magnetic susceptibility measured at low frequency (MS_{lf}) was identified as the most important environmental variable to predict carbon (C) and δ¹⁵N in the soil, at 0-20 cm depth. Also, topographic and climatic variables aided to predict C and δ¹⁵N. The relationship between C and δ¹⁵N was also investigated, at 0-20 cm depth, with different iron oxide metrics such as MS_{lf}, magnetic susceptibility variation (MS_{fd%}), iron dithionite (Fe_d), iron oxalate (Fe_o), hematite (Hm), goethite (Gt), as well the Fe_d/Fe_o, [Hm/(Hm+Gt)] and Silt/Clay ratios. Further, a model was applied to estimate MOS relative stability (η) in natural areas. Later the effect of the depth and the MS_{lf} on η and organic functional groups ratios obtained by Fourier Transformed Infrared Spectroscopy were investigated. The relationships between iron metrics with C and δ¹⁵N reinforce the importance of iron oxides to stabilize MOS and highlight the need to use mineralogical variables for modeling and predict C and δ¹⁵N in the soil. Considering different contexts of geoenvironmental domains, MS_{lf} figured as an integrating pedoindicator on the landscape of the Western Paulista Plateau.

Keywords: magnetic susceptibility, soil organic matter, stable isotopes, basalts, sandstones

Sumário

1. Introdução Geral	13
2. Objetivos e contexto da tese.....	17
3. Principais resultados e discussão geral	17
4. Conclusões Gerais	23
5. Perspectivas futuras	23
6. Referências Bibliográficas	24
Capítulo 1 – Use of machine learning to predict carbon and nitrogen stable isotope in soils from the Western Paulista Plateau	33
Capítulo 2 – Relationships between soil organic matter stabilization and mineralogy in highly weathered soils from southeastern Brazil.....	63
Capítulo 3 – Application of relative stability of soil carbon in a neo-tropical context ...	86

Lista de Abreviações

C – Carbono

N – Nitrogênio

MOS ou SOM – Matéria Orgânica do Solo

CO₂ – Dióxido de carbono

$\delta^{15}\text{N}$ – composição isotópica de nitrogênio

$\delta^{13}\text{C}$ – composição isotópica de carbono

MS_{lf} – Suscetibilidade magnética em baixa frequência

MS_{hf} – Suscetibilidade magnética em alta frequência

MS_{fd%} – Percentual de dependência da frequência (variação) da suscetibilidade magnética

DSVMP – Domínio das coberturas sedimentares e vulcanossedimentares mesozoicas e paleozoicas, pouco a moderadamente consolidadas, associadas a grandes e profundas bacias sedimentares do tipo sinéclise

DVM – Domínio do vulcanismo fissural mesozoico do tipo *plateau*

%IncMSE – Precisão da diminuição média

Fe_d – Ferro ditionito

Fe_o – Ferro oxalato

Hm – Hematita

Gt – Goethita

Fe_o/Fe_d – Razão ferro oxalato/ferro ditionito

[Hm/(Hm+Gt)] – Razão Hematita/Hematita+Goethita

MOP – Matéria Orgânica Particulada

MOM – Matéria Orgânica associada a Minerais

η – Índice de estabilidade da matéria orgânica do solo

MAP – Precipitação média anual

MAT – Temperatura média anual

PET – Evapotranspiração potencial

AI – Índice de aridez

GPP – Produtividade Primária Bruta

Cross – Curvatura cross-section

Long – Curvatura longitudinal

Min – Curvatura mínima

Max – Curvatura máxima

RuBisCo – ribulose-1,5-bisfosfato carboxilase oxigenase

PEP carboxilase – fosfoenolpiruvato carboxilase

SHMP – Hexametafosfato de sódio

POM – Matéria orgânica particulada

POM-C ou C_p – Carbono orgânico particulado

TOC – Carbono orgânico total da amostra *bulk*

MOM-C ou C_m – Carbono orgânico associado à minerais

δ_p – $\delta^{15}\text{N}$ da matéria orgânica particulada

δ_m – $\delta^{15}\text{N}$ da matéria orgânica associada a minerais

f_C – Proporção de carbono perdido

f_N – Proporção de nitrogênio perdido

r_p – Razão carbono/nitrogênio da matéria orgânica particulada

r_m – Razão carbono/nitrogênio da matéria orgânica associada a minerais

ϵ – Fator de enriquecimento

DEM – Modelo Digital de Elevação

SRTM – *Shuttle Radar Topography Mission*

HYDROSHEDS – *Hydrological data and maps on SHuttle Elevation Derivatives at multiple Scales*

1. Introdução Geral

As propriedades dos solos de um ecossistema são provenientes dos processos de formação e perda de solo (Chapin et al. 2011). Esses processos são fruto da interação dos fatores clima, organismos, topografia, material de origem e tempo (Jenny 1941). Tornando os solos mediadores do fluxo de energia e matéria, portanto dos ciclos biogeoquímicos (Quinton et al. 2010), bem como de diversos serviços ecossistêmicos de suporte, provisão, regulação e serviços culturais à humanidade (Wall et al. 2012). O solo é o compartimento terrestre com o maior reservatório de C, na forma de matéria orgânica do solo (MOS), chegando a ter pelo menos três vezes mais C em relação à atmosfera e a vegetação (Fargione et al. 2008). No entanto, as condições de estado de equilíbrio do planeta tem sido alteradas, agravando mudanças nos ciclos biogeoquímicos do carbono (C) e nitrogênio (N) (Steffen et al. 2015). Estas mudanças no estado de equilíbrio dinâmico entre os reservatórios resultam, por exemplo, no aumento de emissão de C dos solos para a atmosfera (Falloon et al. 2007).

A decomposição da MOS é responsável por pelo menos 3,5 Pg/ano de CO₂ (Houghton 2007). Assim, distúrbios como o desmatamento (Bustamante et al. 2015), drenagem artificial (Hooijer et al. 2010), intervenções agrícolas (Smith et al. 2016) e queimadas (Nave et al. 2011) favorecem a perda líquida de C e N (Steffen et al. 2015) para a atmosfera. Esses distúrbios acontecem diretamente sobre o solo, sejam eles realizados de forma predatória ou em virtude da necessidade da humanidade em desempenhar atividades para suprir a demanda mundial por alimentos (Godfray et al. 2010), fibras e energia (Adhikari e Hartemink 2016).

O tipo de distúrbio sobre o solo, bem como os mecanismos de estabilização e desestabilização são fatores que indicam a vulnerabilidade da MOS em um ecossistema (Schmidt et al. 2011). Nesse contexto, a qualidade e a dinâmica da MOS apresentam-se como parte integrante de funções e serviços ecossistêmicos, pois a MOS é mediadora do fornecimento de macro e micronutrientes, que são determinantes para a provisão de alimentos e segurança alimentar (Lal 2016). Devido à sua importância diversos estudos têm procurado avaliar a MOS em ecossistemas naturais e agroecossistemas na Europa (Conen et al. 2008; De Clercq et al. 2015), Ásia (Hooijer et al. 2010; Xu et al. 2016), América do Norte (Torn et al. 1997; Berhe et al. 2012; Fissore et al. 2017) América Latina (Weintraub et al. 2015; Coward et al. 2018) e Brasil (Corazza et al. 1999; Bayer et al. 2004; Figueiredo et al. 2013; Brandani et al. 2017).

A MOS tem sido considerada uma propriedade ecossistêmica, por ser o produto da interação entre atributos ambientais físicos, químicos e biológicos (Schmidt et al. 2011). Em outras palavras, a MOS reflete a relação entre os fatores de formação do solo apresentados por Jeny (1941). A vegetação e o uso da terra são fatores, bem documentados na literatura, que influenciam a MOS em ecossistemas terrestres. Embora estudos sobre MOS tenham aumentado, a relação entre a decomposição da MOS e os fatores que influenciam a sua estabilidade permanecem como lacuna do conhecimento (Berhe e Kleber 2013). Nesse sentido, compreender como outros fatores de estado (Chapin et al. 2011) como o material de origem e a geomorfologia influenciam a estabilidade da MOS em escala de paisagem, carece de mais informações científicas.

Recentemente Barré et al. (2017) indicaram o material de origem como um vetor de influência sobre a MOS em escala regional. Nesse trabalho, realizado na França, foi observado que a influência do uso do solo sobre a MOS foi modulada pelos diferentes tipos de geologia, sobretudo nas camadas de 0-30 cm.

Outros trabalhos tem integrado abordagens geomorfológicas para avaliar padrões espaciais da MOS. McCorkle et al. (2016) por exemplo, ao avaliar formas do terreno no estado da Califórnia nos E.U.A, perceberam que a concentração de C em áreas de deposição (côncavas) apresentavam maiores concentrações de C nos horizontes 0-10 cm, quando comparadas a outras formas do terreno na paisagem analisada. Neste mesmo trabalho, os autores utilizaram isótopos estáveis de ^{13}C , ^{15}N para avaliar padrões espaciais da MOS e observaram que essa técnica foi eficiente para determinar a origem da MOS na paisagem.

Berhe et al. (2008) também utilizaram a geomorfologia aliada a análise isotópica e avaliaram a contribuição de diferentes formas do terreno para o sequestro de C em uma paisagem dominada por gramíneas. Nesse trabalho os autores observaram que a produtividade primária líquida (PPL) variou em função das diferentes formas do terreno e o inventário de C também variou de acordo com as formas. As menores taxas de decomposição e maiores estoque de C foram encontrados em zonas de deposição. Esses trabalhos exemplificam como a abordagem geomorfológica, através da análise do terreno apresenta-se como ferramenta que pode auxiliar na avaliação da dinâmica da MOS(Berhe e Kleber 2013).

Para realizar análise do terreno, diversos modelos têm sido desenvolvidos para avaliar padrões do relevo, usando Sistemas de Informação Geográfica (SIG) e Modelos Digitais de Elevação (MDE) (Vasconcelos et al. 2012; De Reu et al. 2013). Características

topográficas geradas de MDE, como curvatura, declividade, altitude e formas do terreno tem auxiliado a compreensão do processo de evolução da paisagem (MacMillan e Shary 2009; Bishop et al. 2012), mas também tem auxiliado a entender os processos de distribuição da MOS na paisagem (Grimm et al. 2008; Berhe et al. 2008; McCorkle et al. 2016; Wiesmeier et al. 2019). Variáveis topográficas como declividade, convergência e curvatura são características geomorfológicas que exercem controle sobre as taxas de redistribuição do solo e influenciam a persistência da MOS (Yoo et al. 2005; Hancock et al. 2010; Berhe et al. 2012; Fissore et al. 2017).

Uma outra técnica que tem sido fundamental para entender processos na escala da paisagem é a suscetibilidade magnética (SM). A SM depende da concentração de minerais no solo, como óxidos de ferro e pode indicar minerais litogenéticos, ou minerais pedogenéticos (Allan et al. 1988; Torrent et al. 2010; Marques Jr. et al. 2014). Essa técnica tem apresentado correspondências com MOS e parâmetros magnéticos minerais na fração argila (Hanesch and Scholger 2005; Siqueira et al. 2010; Jordanova et al. 2013; Marques Jr. et al. 2014; Quijano et al. 2014; Pingguo Yang et al. 2016; Jakšík et al. 2016).

Craine et al. (2015) observaram que propriedades do solo como o teor de argila influenciam a decomposição da MOS. Os autores perceberam padrões entre $\delta^{15}\text{N}$ e gradientes climáticos, indicando que as argilas estabilizam o $\delta^{15}\text{N}$ enriquecido da MOS, em ecossistemas quentes e/ou secos. Outros trabalhos também têm indicado que propriedades do solo como o teor de argila, controlam a decomposição da MOS (Balesdent et al. 2000; Xu et al. 2016) devido à interação com superfícies minerais que protegem a MOS da atividade enzimática (Baldock e Skjemstad 2000; Six et al. 2002; Fissore et al. 2017). Complementando essa perspectiva, outros autores indicaram que os valores de $\delta^{15}\text{N}$ aumentam a medida que o tamanho de partículas do solo diminui, ou ao passo que a associação com minerais é mais forte (Baisden et al. 2002; Liao et al. 2006; Marin-Spiotta et al. 2009).

Nesse contexto, o uso de isótopos estáveis ($\delta^{13}\text{C}$ e $\delta^{15}\text{N}$) tem se destacado como ferramenta para avaliar a estabilidade da MOS em suas frações (Liao et al. 2006; Conen et al. 2008; Heckman et al. 2014; De Clercq et al. 2015). Por exemplo, De Clercq et al. (2015) usaram o $\delta^{15}\text{N}$ e a razão C:N para determinar o tempo médio de residência da MOS através da avaliação da estabilidade da MOM (matéria orgânica ligada a minerais) em relação à MOP (matéria orgânica particulada) em áreas de manejo agrícola intenso. Os autores se basearam no fracionamento de $\delta^{15}\text{N}$ ao longo do processo de decomposição da MOS, que ocorre juntamente com o decréscimo da razão C:N. Durante esse processo,

ocorre o fracionamento cinético, que discrimina os isótopos de N mais leves e mais pesados (Högberg 1997), deixando a MOM mais enriquecida em $\delta^{15}\text{N}$. As vantagens do modelo proposto por Conen et al. (2008) é que ele é menos caro que análises de ^{14}C e não é influenciado pelas mudanças possíveis mudanças na vegetação C3 e C4, como o método da diferença relativa na estabilidade derivada a partir de $\delta^{13}\text{C}$ proposto por (Balesdent et al. 1987). Além disso, o modelo proposto por Conen et al. (2008), ainda requer testes em áreas tropicais para auxiliar no entendimento da estabilidade da MOS e os processos biogeoquímicos envolvidos.

As propriedades biogeoquímicas do solo se desenvolvem durante o processo de pedogênese e consequentemente os mecanismos de estabilidade da MOS acompanham este processo (Lawrence et al. 2015). Ou seja, os valores de C e $\delta^{15}\text{N}$ no solo podem variar em função do desenvolvimento dos solos e como o intemperismo reage com processos biológicos que fazem a ciclagem da MOS. Tanto os serviços de provisão de alimentos, fibras e energia, como os serviços de regulação e suporte (Bouma et al. 2017) dependem das propriedades dos solos e suas interações (Adhikari e Hartemink 2016).

Alguns trabalhos tem apresentado que o intemperismo e a cristalinidade de minerais influenciam a estabilidade de C no solo (Khom et al. 2017), bem como a composição de comunidades de microorganismos e atividade enzimática (Doetterl et al. 2018). Nesse sentido, compreender a biogeoquímica dos solos se torna crucial para a gestão dos serviços ecossistêmicos proporcionados pelos solos (Schmidt et al. 2011). Como a MOS é uma propriedade ecossistêmica (Schmidt et al. 2011), o entendimento das relações da MOS com as mudanças ambientais e fatores de estado (Chapin et al. 2011) requer abordagens em diversas escalas (Schmidt et al. 2011; Wiesmeier et al. 2019).

Diante desse panorama, a geologia e a geomorfologia se destacam como fatores de estado importantes para a avaliação da MOS no contexto da paisagem. A partir disso, este estudo avaliou como fatores geológicos e processos geomorfológicos afetam a composição e estabilidade da MOS no Planalto Ocidental Paulista. A contribuição deste estudo se dá por utilizar uma abordagem multidisciplinar que integra técnicas de sistemas de informação geográfica, geofísica aplicada, pedologia, geomorfologia e ecologia aplicada.

2. Objetivos e contexto da tese

O objetivo do presente estudo foi avaliar como a geologia e a covariação da mineralogia do solo, juntamente com processos geomorfológicos influenciam a estabilidade da MOS no Planalto Ocidental Paulista.

O presente estudo está inserido no contexto de um projeto temático cujo objetivo é caracterizar a geovariabilidade do Planalto Ocidental Paulista para facilitar a compreensão da relação de causa e efeito entre atributos do solo. Para a realização deste projeto de doutorado foi firmada uma parceria entre o laboratório de Solos e Vegetação da Universidade de Brasília (UnB)/grupo Environmental Isotope Studies e o grupo de Caracterização do Solo para fins de Manejo Específico (CSME) da Universidade Estadual Paulista Júlio de Mesquita Filho (UNESP). O grupo EIS contribuiu com análises elementares de C e N, bem como análises isotópicas de $\delta^{13}\text{C}$ e $\delta^{15}\text{N}$, enquanto o grupo CSME contribuiu com o banco de dados de atributos mineralógicos do solo utilizados na tese.

3. Principais resultados e discussão geral

No capítulo 1, identificamos através de uma abordagem usando *machine learning* com o algoritmo *random forest*, que a susceptibilidade magnética medida em baixa frequência (MS_{lf}) foi o preditor mais importante para predizer C e $\delta^{15}\text{N}$ no solo, na profundidade de 0-0.20m do Planalto Ocidental Paulista. Em relação ao C no solo, MS_{lf} apresentou um aumento percentual no erro padrão médio (% IncMSE) de 38,79%. Foi possível identificar que os maiores valores de C no solo estão associados a valores de MS_{lf} maiores que $14 \times 10^{-6} \text{ m}^3 \text{ kg}^{-1}$, os quais são característicos do domínio geoambiental *Domain of Mesozoic fissural volcanism of plateau type* (DVM), cujo material de origem é basalto. Como a MS_{lf} é um indicador de óxidos de ferro no solo (Dearing 1994) este resultados indica a adsorção da MOS por superfícies minerais observadas em outros estudos (Lutzow et al. 2006; Khomo et al. 2017; Coward et al. 2017; Hall et al. 2018).

Embora com menores %IncMSE, os resultados obtidos também indicaram que variáveis topográficas auxiliaram na predição de C no solo. Foram observados %IncMSE de 3,56% para declividade, 1,32% para curvatura longitudinal, 0,95% para curvatura transversal e 0,10% para aspecto. Em geral, menores declividades e côncavas apresentaram maiores valores de C no solo. Resultados semelhantes foram observados

por Berhe et al. (2008), que relataram a presença de maiores estoques de C em áreas concávas em um estudo na escala de bacia realizado na região do Vale Central da Califórnia (Estados Unidos da América).

Além disso, variáveis climáticas e de produtividade apresentaram %IncMSE de 8,82% para precipitação média anual, 4,20% para temperatura média anual e 7,16% para produtividade primária bruta. A relação entre C no solo e precipitação média anual foi positiva e apresentou um maior incremento acima de 730mm. Estudos anteriores vem apresentando a importância do clima no potencial de estocagem de C no solo (Jobágyy e Jackson 2000; McBratney et al. 2006). Geralmente, a precipitação média anual influencia positivamente a produtividade primária bruta em ecossistemas terrestres, o que contribui para uma maior entrada de C no solo (Wiesmeier et al. 2019). A temperatura média anual mostrou uma relação negativa com os valores de C no solo. Esse padrão já foi observado em estudos de escala regional e global, que reportaram o padrão de maiores valores de C no solo em ambientes de clima frio/úmido e menores valores em ambientes de clima quente e seco (Jobágyy e Jackson 2000; McBratney et al. 2006; Craine et al. 2015)

Os valores de $\delta^{15}\text{N}$ no solo apresentaram uma relação positiva com MS_{lf}, apresentando %IncMSE de 18,38%. Quando os valores de MS_{lf} ficaram acima de $25 \times 10^{-6} \text{ m}^3 \text{ kg}^{-1}$, os valores de $\delta^{15}\text{N}$ tenderam a estabilizar. Como MS_{lf} é um indicador de óxidos de ferro na fração argila, os resultados indicam que os óxidos de ferro na fração argila estão se ligando à MOS como observado em outros estudos (Quijano et al. 2014; Pingguo Yang et al. 2016). Corroborando portanto a ligação entre C e superfícies minerais, além de indicar a estabilização da MOS por interações com óxidos de Fe (Liao et al. 2006; Marin-Spiotta et al. 2009; Craine et al. 2015). Minerais na fração argila tem sido apontados como fatores que contribuem para estabilizar a MOS com valores enriquecidos de $\delta^{15}\text{N}$ (Craine et al. 2015). Além disso, os valores de $\delta^{15}\text{N}$ tendem a aumentar conforme a associação com minerais se torna mais forte (Baisden et al. 2002; Liao et al. 2006; Marin-Spiotta et al. 2009).

Assim como para o C no solo, as variáveis topográficas também se apresentaram relevância para predizer $\delta^{15}\text{N}$. A declividade, por exemplo, apresentou um %IncMSE de 9,93%, com uma relação negativa entre 2° e 7,2°, ao passo que a curvatura transversal apresentou 1,15%. Os resultados apresentados neste estudo sugerem que ambientes mais declivosos e estáveis do ponto de vista geomorfológico, apresentaram maiores valores de $\delta^{15}\text{N}$. Este padrão indica que ambientes mais dissecados, podem perder nitrogênio através da erosão, que é um processo que não fraciona $\delta^{15}\text{N}$ (Weintraub et al. 2015).

A precipitação média anual apresentou uma relação negativa bem definida com os valores de $\delta^{15}\text{N}$, indicando que os maiores valores de $\delta^{15}\text{N}$ foram encontrados onde a precipitação é menor. Esta relação entre $\delta^{15}\text{N}$ e precipitação média anual apresentou um %IncMSE de 4,51%. Ao passo que a temperatura média anual teve um %IncMSE de 7.98%. Esta relação entre $\delta^{15}\text{N}$ e temperatura média anual apresentou um padrão bimodal. Foi observada uma correlação positiva entre 20 e 20,5 °C, com os valores de $\delta^{15}\text{N}$ e negativa entre 20,6 e 21,4 °C. Entre 21,5 °C e 22,3 °C a relação foi novamente positiva, mas apresentou uma maior amplitude dos valores de $\delta^{15}\text{N}$, esta amplitude também foi observada na relação negativa entre 22,4 °C e 23,0 °C. Em geral, maiores valores de $\delta^{15}\text{N}$ são encontrados em ambientes quentes/secos e menores em ambientes frios/úmidos (Craine et al. 2015). Os resultados encontrados representam bem o padrão descrito por Craine et al. (2015) em relação a precipitação. Em relação à temperatura, o padrão observado indicou uma curva bimodal, sugerindo uma covariação dos valores de $\delta^{15}\text{N}$ em função da temperatura, que por sua vez pode estar sendo influenciada por fatores morfoestruturais da paisagem.

O %IncMSE da razão C:N foi de 7.97%. Os valores de $\delta^{15}\text{N}$ apresentaram uma relação negativa com os valores de razão C:N, sendo que os maiores valores de $\delta^{15}\text{N}$ foram encontrados onde a relação C:N foi menor. Os maiores valores de $\delta^{15}\text{N}$ correspondem às áreas de maior produção primária bruta (%IncMSE: 1.88%), que estão no domínio geoambiental DVM. Os maiores valores de C e MS_{If} no solo também foram encontrados no domínio DVM. Estes resultados ressaltam que a maior presença de óxidos de ferro pode contribuir com maiores valores de C e $\delta^{15}\text{N}$ no solo, sugerindo que existe uma dinâmica distinta entre os domínios geoambientais quanto à estabilização da MOS (Liao et al. 2006; Marin-Spiotta et al. 2009; Craine et al. 2015) na paisagem do Planalto Ocidental Paulista.

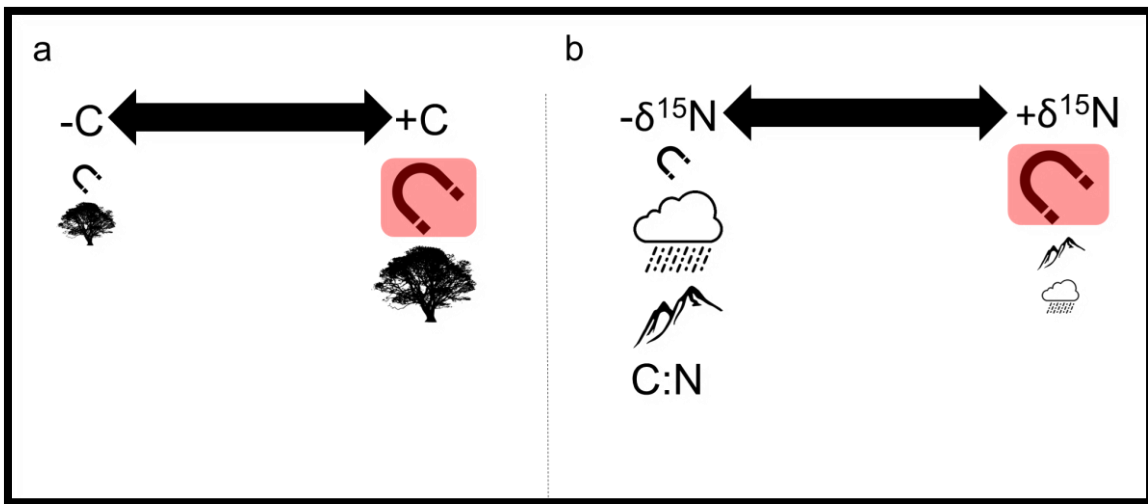


Figura 1 - Quadro ilustrativo dos principais resultados obtidos no capítulo 1. Em “a” indica-se que os maiores valores de C foram obtidos em áreas com maior produtividade primária e com maiores valores de suscetibilidade magnética. Em “b” indica-se que os maiores valores de $\delta^{15}\text{N}$ foram observados em áreas com menores índices de pluviosidade, áreas menos declivosas e com maiores valores de suscetibilidade magnética.

No capítulo 2, foram exploradas as relações entre C e $\delta^{15}\text{N}$ com distintas métricas de óxidos de ferro como MS_{lf}, variação da susceptibilidade magnética (MS_{fd%}), ferro ditionito (Fe_d), ferro oxalato (Fe_o), hematita (Hm), Goethita (Gt), bem como as razões Fe_d/Fe_o, [Hm/Hm+ Gt] e Silte/Argila. Os maiores valores de argila, MS_{lf}, Fe_d, Fe_o, Hm e Gt estiveram associados aos Latossolos do domínio geoambiental DVM, que por sua vez apresentaram os maiores valores de C e $\delta^{15}\text{N}$. O domínio DSVMP apresentou os maiores valores de MS_{fd%}. As diferenças observadas entre os Latossolos Vermelhos originados a partir de contextos geológicos distintos sugere a influência deste comportamento sobre a MS_{lf}, as métricas de Fe e, consequentemente, sobre o fracionamento do $\delta^{15}\text{N}$. Atributos do solo como textura e a mineralogia dos solos são influenciados pelo material de origem (Fontes et al. 2000; Barré et al. 2017; Barbosa et al. 2019), que ficam mais evidentes em contextos de litosequência como o deste estudo.

Posteriormente nós testamos a relações das métricas de Fe e MS_{lf} com C e $\delta^{15}\text{N}$ no solo com a finalidade de caracterizar as ligações organominerais. Os coeficientes de determinação obtidos para Hm, Fed, Feo, SM e argila confirmaram relação com C e $\delta^{15}\text{N}$. Estas relações são atribuídas à formação de complexos organominerais na fração argila (Torn et al. 1997; Lutzow et al. 2006; Adhikari et al. 2016; Khomo et al. 2017; Coward et al. 2017; Hall et al. 2018). Outrossim, ao comparar as relações entre Hm, Fe_d e Fe_o com

C e $\delta^{15}\text{N}$, os maiores coeficientes de determinação foram observados para Hm e Fe_d , indicando um predomínio de relações organominerais com minerais mais cristalizados. Para complementar a verificação da influência da cristalinidade dos minerais sobre C e $\delta^{15}\text{N}$, foi elaborada uma série de modelos lineares múltiplos, seguido de avaliações de modelo médio modelando C e $\delta^{15}\text{N}$ no solo em função de MS_{lf} , $\text{MS}_{\text{fd}\%}$, Fe_d/Fe_o , $[\text{Hm}/(\text{Hm}+\text{Gt})]$ e Silte/Argila. A partir dos modelos gerais, foram selecionados os melhores modelos, os quais apresentaram relações significativas entre C em função de MS_{lf} e razão Silte/Argila ($F_{2,15} = 16.04$, $p < 0.001$, $R^2 = 0.68$, $R^2_{\text{adj}} = 0.63$), enquanto o modelo testando $\delta^{15}\text{N}$ em função de MS_{lf} e $[\text{Hm}/(\text{Hm}+\text{Gt})]$ ($F_{2,15} = 12.11$, $p < 0.001$, $R^2 = 0.62$, $R^2_{\text{adj}} = 0.57$). De acordo com a avaliação dos modelos médios e a importância relativa das variáveis a MS_{lf} foi significativa em todos os modelos que tinham C como variável dependente. Enquanto para $\delta^{15}\text{N}$ a MS_{lf} foi significativa em 86% dos modelos testados.

De acordo com Khomo et al. (2017) relações positivas entre C e Fe_d indicam que óxidos de ferro cristalinos são governadas por quimissorção, também conhecida como adsorção específica, podendo apresentar taxas de *turn-over* de décadas à séculos. No contexto de solos, a quimissorção é considerada uma complexação de esfera interna, que são caracterizadas pela formação de ligações polares covalentes entre a superfície dos átomos e o adsorbato (Kleber et al. 2015). Neste tipo de ligação o adsorbato penetra a célula de coordenação de Fe e através de reações de troca se liga de forma covalente diretamente ao cátion estrutural através de grupos O^- e OH^- (Schwertmann e Taylor 1989).

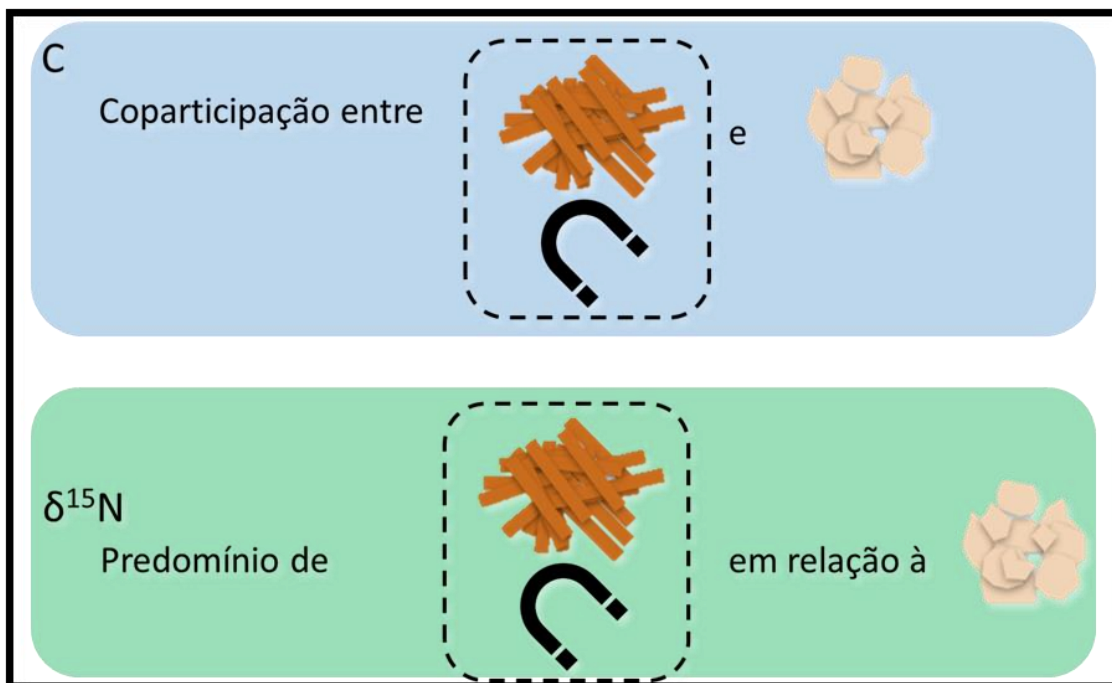


Figura 2 - Quadro ilustrativo dos principais resultados obtidos no capítulo 2. Azul indica que Fe_d e suscetibilidade magnética, bem como Fe_o podem ter uma coparticipação sobre C (com tendências de maiores coeficientes de determinação para SM e Fe_d) magnética e minerais cristalinos). Verde indica que Fe_d e SM apresentaram relações mais fortes com $\delta^{15}\text{N}$ que Fe_o .

No capítulo 3, identificamos que o efeito da profundidade e da MS_{lf} sobre a estabilidade relativa da MOS (η) e razões de grupos funcionais obtidos por Espectroscopia de Infravermelho Próximo com Transformada de Fourier (FTIR). A η é um índice proposto por Conen et al. (2008), que se baseia na razão C:N e $\delta^{15}\text{N}$ como proxy para a degradação e estabilização da MOS. Através de uma análise de componentes principais (PCA), observamos que η está associada com as razões C–H para C=O ($2850+2924/1648 \text{ cm}^{-1}$) e C=C para C=O ($1512/1648 \text{ cm}^{-1}$) que representam a decomposição da MOS.

Os baixos valores de SM_{lf} associados com C = C para C = O ($1512/1648 \text{ cm}^{-1}$) e razão de pico C = C para COO ($1512/1400 \text{ cm}^{-1}$), indicaram a importância de compostos aromáticos para a estabilização da matéria orgânica na profundidade de 5-20 cm em ambos os domínios geológicos DVM e DSVMP. A relação negativa de SM_{lf} com as taxas de pico de FTIR em DVM, indica que a MOS ligada a óxidos de ferro pode ser mais antiga do que a MOS total (global) (Kögel-Knabner et al. 2008; Hall et al. 2018).

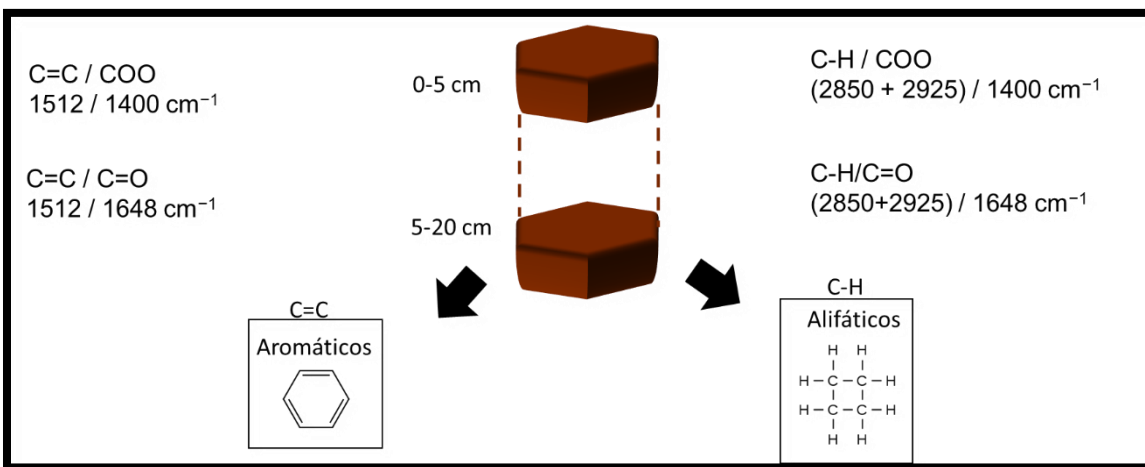


Figura 3 - Quadro ilustrativo dos principais resultados obtidos no capítulo 3, indicando o predomínio de grupos funcionais aromáticos e alifáticos na profundidade de 5-20 cm.

4. Conclusões Gerais

Fatores relacionados a geologia como os óxidos de ferro no solo estudados neste trabalho apresentaram relações com variáveis pertinentes à matéria orgânica do solo como C e $\delta^{15}\text{N}$. Considerando o contexto de diferentes de domínios geoambientais, a suscetibilidade magnética se destacou como um pedoindicador integrador para realizar estudos na escala da paisagem do Planalto Ocidental Paulista. As relações entre métricas de ferro no solo e suscetibilidade magnética com a matéria orgânica reafirmam a importância dos óxidos de ferro na estabilização da matéria orgânica e destacam a necessidade de utilizar variáveis mineralógicas na modelagem e predição de C e $\delta^{15}\text{N}$ no solo. Além disso a interação entre as variáveis mineralógicas com características, topográficas e climáticas auxiliaram na predição de C e $\delta^{15}\text{N}$ reforçando o modelo de formação do solo preconizado por Dokuchaev (1870), posteriormente formulado por Jenny (1940) que vem sendo atualizado por pedólogos e ecólogos.

5. Perspectivas futuras

A partir dos resultados obtidos neste estudo foram adquiridos novos *insights* que certamente irão promover novas pesquisas sobre as relações organominerais em escala de paisagem. Os possíveis desdobramentos desta tese serão: i. Aplicação da metodologia *machine learning* com fins de mapeamento de C e $\delta^{15}\text{N}$ no solo, valendo-se de técnicas *feature-space-based*, *geographic-space-based* ou técnicas híbridas; ii. Realizar métodos

de classificação do terreno com o auxílio de *machine learning* e avaliar a relação com a MOS; iii. Desenvolver novas avaliações sobre as relações organominerais considerando minerais silicatados e óxidos de ferro; iv. Considerando as frações da MOS, pretende-se aplicar razão de estratificação da MOS, considerando áreas nativas e agrícolas; v. Validar a técnica de estimativa de η , utilizando ^{14}C .

6. Referências Bibliográficas

- Adhikari D, Poulson SR, Sumaila S, Dynes JJ, Mcbeth JM, Yang Y (2016) Asynchronous reductive release of iron and organic carbon from hematite – humic acid complexes. *Chemical Geology* 430:13–20. doi: 10.1016/j.chemgeo.2016.03.013
- Adhikari K, Hartemink AE (2016) Linking soils to ecosystem services - A global review. *Geoderma* 262:101–111. doi: 10.1016/j.geoderma.2015.08.009
- Allan JEM, Coey JMD, Resende M, Fabris JD (1988) Magnetic Properties of Iron-Rich Oxisols*. *Physics and Chemistry of Minerals* 15:470–475
- Baisden WT, Amundson R, Cook AC, Brenner DL (2002) Turnover and storage of C and N in five density fractions from California annual grassland surface soils. *Global Biogeochemical Cycles* 16:64-1-64–16. doi: 10.1029/2001GB001822
- Baldock JA, Skjemstad JO (2000) Role of the soil matrix and minerals in protecting natural organic materials against biological attack. *Organic Geochemistry* 31:697–710. doi: 10.1016/S0146-6380(00)00049-8
- Balesdent J, Chenu C, Balabane M (2000) Relationship of soil organic matter dynamics to physical protection and tillage. *Soil and Tillage Research* 53:215–230. doi: 10.1016/S0167-1987(99)00107-5
- Balesdent J, Mariotti A, Guillet B (1987) Natural ^{13}C abundance as a tracer for studies of soil organic matter dynamics. *Soil Biology and Biochemistry* 19:25–30. doi: 10.1016/0038-0717(87)90120-9
- Barbosa RS, Marques Júnior J, Barrón V, Martins Filho MV, Siqueira DS, Peluco RG, Camargo LA, Silva LS (2019) Prediction and mapping of erodibility factors (USLE and WEPP) by magnetic susceptibility in basalt-derived soils in northeastern São Paulo state, Brazil. *Environmental Earth Sciences* 78:1–12. doi: 10.1007/s12665-

018-8015-0

- Barré P, Durand H, Chenu C, Meunier P, Montagne D, Castel G, Billiou D, Soucémarianadin L, Cécillon L (2017) Geological control of soil organic carbon and nitrogen stocks at the landscape scale. *Geoderma* 285:50–56. doi: 10.1016/j.geoderma.2016.09.029
- Bayer C, Martin-Neto L, Mielniczuk J, Pavinato A (2004) Carbon storage in labile fractions of soil organic matter in a tropical no-tillage Oxisol. *Pesquisa Agropecuaria Brasileira* 39:677–683. doi: 10.1590/S0100-204X2004000700009
- Berhe AA, Harden JW, Torn MS, Harte J (2008) Linking soil organic matter dynamics and erosion-induced terrestrial carbon sequestration at different landform positions. *Journal of Geophysical Research: Biogeosciences* 113:1–12. doi: 10.1029/2008JG000751
- Berhe AA, Harden JW, Torn MS, Kleber M, Burton SD, Harte J (2012) Persistence of soil organic matter in eroding versus depositional landform positions. *Journal of Geophysical Research: Biogeosciences* 117:1–16. doi: 10.1029/2011JG001790
- Berhe AA, Kleber M (2013) Erosion, deposition, and the persistence of soil organic matter: mechanistic considerations and problems with terminology. *Earth Surface Processes and Landforms* 38:908–912. doi: 10.1002/esp.3408
- Bishop MP, James LA, Shroder JF, Walsh SJ (2012) Geospatial technologies and digital geomorphological mapping: Concepts, issues and research. *Geomorphology* 137:5–26. doi: 10.1016/j.geomorph.2011.06.027
- Bouma J, Ittersum MK van, Stoorvogel JJ, Batjes NH, Droogers P, Pulleman MM (2017) Soil Capability: Exploring the Functional Potentials of Soils. In: *Global Soil Security*. pp 341–351
- Brandani CB, Abbruzzini TF, Conant RT, Cerri CEP (2017) Soil organic and organomineral fractions as indicators of the effects of land management in conventional and organic sugar cane systems. *Soil Research* 55:145. doi: 10.1071/SR15322
- Bustamante MMC, Roitman I, Aide TM, Alencar A, Anderson LO, Aragão L, Asner GP, Barlow J, Berenguer E, Chambers J, Costa MH, Fanin T, Ferreira LG, Ferreira J,

Keller M, Magnusson WE, Morales-Barquero L, Morton D, Ometto JPHB, Palace M, Peres CA, Silvério D, Trumbore S, Vieira ICG (2015) Toward an integrated monitoring framework to assess the effects of tropical forest degradation and recovery on carbon stocks and biodiversity. *Global Change Biology* 22:92–109. doi: 10.1111/gcb.13087

Chapin FS, Matson PA, Vitousek PM (2011) Principles of Terrestrial Ecosystem Ecology, Second. Springer New York, New York, NY

Conen F, Zimmermann M, Leifeld J, Seth B, Alewell C (2008) Relative stability of soil carbon revealed by shifts in $\delta^{15}\text{N}$ and C:N ratio. *Biogeosciences* 5:123–128. doi: 10.5194/bg-5-123-2008

Corazza EJ, Silva JE, Resck DVS, Gomes AC (1999) Comportamento de diferentes sistemas de manejo como fonte ou depósito de carbono em relação à vegetação do Cerrado. *Revista Brasileira de Ciência do Solo* 23:425–432. doi: 10.1590/S0100-06831999000200025

Coward EK, Ohno T, Plante AF (2018) Adsorption and Molecular Fractionation of Dissolved Organic Matter on Iron-Bearing Mineral Matrices of Varying Crystallinity. *Environmental Science and Technology* 52:1036–1044. doi: 10.1021/acs.est.7b04953

Coward EK, Thompson AT, Plante AF (2017) Iron-mediated mineralogical control of organic matter accumulation in tropical soils. *Geoderma* 306:206–216. doi: 10.1016/j.geoderma.2017.07.026

Craine JM, Elmore AJ, Wang L, Augusto L, Baisden WT, Brookshire ENJ, Cramer MD, Hasselquist NJ, Hobbie EA, Kahmen A, Koba K, Kranabetter JM, Mack MC, Marin-Spiotta E, Mayor JR, McLauchlan KK, Michelsen A, Nardoto GB, Oliveira RS, Perakis SS, Peri PL, Quesada CA, Richter A, Schipper LA, Stevenson BA, Turner BL, Viani RAG, Wanek W, Zeller B (2015) Convergence of soil nitrogen isotopes across global climate gradients. *Scientific Reports* 5:8280. doi: 10.1038/srep08280

De Clercq T, Heiling M, Dercon G, Resch C, Aigner M, Mayer L, Mao Y, Elsen A, Steier P, Leifeld J, Merckx R (2015) Predicting soil organic matter stability in agricultural fields through carbon and nitrogen stable isotopes. *Soil Biology and Biochemistry* 88:29–38. doi: 10.1016/j.soilbio.2015.05.011

De Reu J, Bourgeois J, Bats M, Zwertvaegher A, Gelorini V, De Smedt P, Chu W, Antrop M, De Maeyer P, Finke P, Van Meirvenne M, Verniers J, Crombé P (2013) Application of the topographic position index to heterogeneous landscapes. *Geomorphology* 186:39–49. doi: 10.1016/j.geomorph.2012.12.015

Dearing JA (1994) Environmental magnetic susceptibility. Using the Bartington MS2 system. British Library, England.

Doetterl S, Berhe AA, Arnold C, Bodé S, Fiener P, Finke P, Fuchsleger L, Griepentrog M, Harden JW, Nadeu E, Schnecker J, Six J, Trumbore S, van Oost K, Vogel C, Boeckx P (2018) Links among warming, carbon and microbial dynamics mediated by soil mineral weathering. *Nature Geoscience* 11:589–593. doi: 10.1038/s41561-018-0168-7

Falloon P, Jones CD, Cerri CE, Al-Adamat R, Kamoni P, Bhattacharyya T, Easter M, Paustian K, Killian K, Coleman K, Milne E (2007) Climate change and its impact on soil and vegetation carbon storage in Kenya, Jordan, India and Brazil. *Agriculture, Ecosystems & Environment* 122:114–124. doi: 10.1016/j.agee.2007.01.013

Fargione J, Hill J, Tilman D, Polasky S, Hawthorne P (2008) Land Clearing and the Biofuel Carbon Debt. *Science* 319:1235–1238. doi: 10.1126/science.1152747

Figueiredo CC, Resck DVS, Carneiro MAC, Ramos MLG, Sá JCM (2013) Stratification ratio of organic matter pools influenced by management systems in a weathered Oxisol from a tropical agro-ecoregion in Brazil. *Soil Research* 51:133–141. doi: 10.1071/sr12186

Fissore C, Dalzell BJ, Berhe AA, Voegtle M, Evans M, Wu A (2017) Influence of topography on soil organic carbon dynamics in a Southern California grassland. *Catena* 149:140–149. doi: 10.1016/j.catena.2016.09.016

Fontes MPF, de Oliveira TS, da Costa LM, Campos AAG (2000) Magnetic separation and evaluation of magnetization of Brazilian soils from different parent materials. *Geoderma* 96:81–99. doi: [https://doi.org/10.1016/S0016-7061\(00\)00005-7](https://doi.org/10.1016/S0016-7061(00)00005-7)

Godfray HCJ, Beddington JR, Crute IR, Haddad L, Lawrence D, Muir JF, Pretty J, Robinson S, Thomas SM, Toulmin C (2010) Food Security: The Challenge of Feeding 9 Billion People. *Science* 327:812–818. doi: 10.1126/science.1185383

- Grimm R, Behrens T, Märker M, Elsenbeer H (2008) Soil organic carbon concentrations and stocks on Barro Colorado Island — Digital soil mapping using Random Forests analysis. *Geoderma* 146:102–113. doi: 10.1016/j.geoderma.2008.05.008
- Hall SJ, Berhe AA, Thompson A (2018) Order from disorder: do soil organic matter composition and turnover co-vary with iron phase crystallinity? *Biogeochemistry* 140:93–110. doi: 10.1007/s10533-018-0476-4
- Hancock GR, Murphy D, Evans KG (2010) Hillslope and catchment scale soil organic carbon concentration: An assessment of the role of geomorphology and soil erosion in an undisturbed environment. *Geoderma* 155:36–45. doi: 10.1016/j.geoderma.2009.11.021
- Hanesch M, Scholger R (2005) The influence of soil type on the magnetic susceptibility measured throughout soil profiles. 50–56. doi: 10.1111/j.1365-246X.2005.02577.x
- Heckman K, Throckmorton H, Clingensmith C, González Vila FJ, Horwath WR, Knicker H, Rasmussen C (2014) Factors affecting the molecular structure and mean residence time of occluded organics in a lithosequence of soils under ponderosa pine. *Soil Biology and Biochemistry* 77:1–11. doi: 10.1016/j.soilbio.2014.05.028
- Högberg P (1997) Tansley Review No. 95. ^{15}N natural abundance in soil-plant systems. *New Phytologist* 137:179–203. doi: 10.1046/j.1469-8137.1997.00808.x
- Hooijer A, Page S, Canadell JG, Silvius M, Kwadijk J, Wösten H, Jauhainen J (2010) Current and future CO_2 emissions from drained peatlands in Southeast Asia. *Biogeosciences* 7:1505–1514. doi: 10.5194/bg-7-1505-2010
- Houghton RA (2007) Balancing the global carbon budget. *Annual Review of Earth and Planetary Sciences*, 35, 313-347. doi.org/10.1146/annurev.earth.35.031306.140057
- Jakšík O, Kodešová R, Kapička A, Klement A, Fér M, Nikodem A (2016) Using magnetic susceptibility mapping for assessing soil degradation due to water erosion. *Soil and Water Research* 11:105–113. doi: 10.17221/233/2015-SWR
- Jenny H (1941) Factors of Soil Formation: A System of Quantitative Pedology, McGraw-Hil. Dover Publications, New York
- Jobágyi EG, Jackson RB (2000) The vertical distribution of soil organic carbon and its relation to climate and vegetation. *Ecological Applications* 10:423–436. doi:

10.1890/1051-0761(2000)010[0423:TVDOSO]2.0.CO;2

Jordanova N, Jordanova D, Liu Q, Hu P, Petrov P, Petrovský E (2013) Soil formation and mineralogy of a Rhodic Luvisol - insights from magnetic and geochemical studies. *Global and Planetary Change* 110:397–413. doi: 10.1016/j.gloplacha.2013.08.020

Khom L, Trumbore S, Bern CR, Chadwick OA (2017) Timescales of carbon turnover in soils with mixed crystalline mineralogies. *SOIL* 3:17–30. doi: 10.5194/soil-3-17-2017

Kleber M, Eusterhues K, Keiluweit M, Mikutta C, Mikutta R, Nico PS (2015) Mineral–Organic Associations: Formation, Properties, and Relevance in Soil Environments. In: *Advances in Agronomy*. Elsevier Ltd, pp 1–140

Kögel-Knabner I, Guggenberger G, Kleber M, Kandeler E, Kalbitz K, Scheu S, Eusterhues K, Leinweber P (2008) Organo-mineral associations in temperate soils: Integrating biology, mineralogy, and organic matter chemistry. *Journal of Plant Nutrition and Soil Science* 171:61–82. doi: 10.1002/jpln.200700048

Lal R (2016) Soil health and carbon management. *Food and Energy Security* 5:212–222

Lawrence CR, Harden JW, Xu X, Schulz MS, Trumbore SE (2015) Long-term controls on soil organic carbon with depth and time: A case study from the Cowlitz River Chronosequence, WA USA. *Geoderma* 247–248:73–87. doi: 10.1016/j.geoderma.2015.02.005

Liao JD, Boutton TW, Jastrow JD (2006) Organic matter turnover in soil physical fractions following woody plant invasion of grassland: Evidence from natural ^{13}C and ^{15}N . *Soil Biology and Biochemistry* 38:3197–3210. doi: 10.1016/j.soilbio.2006.04.004

Lutzow M v., Kogel-Knabner I, Ekschmitt K, Matzner E, Guggenberger G, Marschner B, Flessa H (2006) Stabilization of organic matter in temperate soils: mechanisms and their relevance under different soil conditions - a review. *European Journal of Soil Science* 57:426–445. doi: 10.1111/j.1365-2389.2006.00809.x

Marin-Spiotta E, Silver WL, Swanston CW, Ostertag R (2009) Soil organic matter dynamics during 80 years of reforestation of tropical pastures. *Global Change Biology* 15:1584–1597. doi: 10.1111/j.1365-2486.2008.01805.x

Marques Jr. J, Siqueira DS, Camargo LA, Teixeira DDB, Barrón V, Torrent J (2014) Magnetic susceptibility and diffuse reflectance spectroscopy to characterize the spatial variability of soil properties in a Brazilian Haplustalf. *Geoderma* 219–220:63–71. doi: 10.1016/j.geoderma.2013.12.007

McBratney AB, Minasny B, Viscarra Rossel R (2006) Spectral soil analysis and inference systems: A powerful combination for solving the soil data crisis. *Geoderma* 136:272–278. doi: 10.1016/j.geoderma.2006.03.051

McCorkle EP, Berhe AA, Hunsaker CT, Johnson DW, McFarlane KJ, Fogel ML, Hart SC (2016) Tracing the source of soil organic matter eroded from temperate forest catchments using carbon and nitrogen isotopes. *Chemical Geology* 445:172–184. doi: 10.1016/j.chemgeo.2016.04.025

MacMillan, RA, Shary P (2009). Landforms and landform elements in geomorphometry. In Hengl, T., Reuter, H.I. (Eds.), *Geomorphometry: Concepts, Software, Applications*. Elsevier, Amsterdam, pp. 227-254.

Nave LE, Vance ED, Swanston CW, Curtis PS (2011) Fire effects on temperate forest soil C and N storage. *Ecological Applications* 21:1189–1201. doi: 10.1890/10-0660.1

Pingguo Yang, Byrne JM, Yang M (2016) Spatial variability of soil magnetic susceptibility, organic carbon and total nitrogen from farmland in northern China. *Catena* 145:92–98. doi: 10.1016/j.catena.2016.05.025

Quijano L, Chaparro MAE, Marie DC, Gaspar L, Navas A (2014) Relevant magnetic and soil parameters as potential indicators of soil conservation status of Mediterranean agroecosystems. *Geophysical Journal International* 198:1805–1817. doi: 10.1093/gji/ggu239

Quinton JN, Govers G, Van Oost K, Bardgett RD (2010) The impact of agricultural soil erosion on biogeochemical cycling. *Nature Geoscience* 3:311–314. doi: 10.1038/ngeo838

Schmidt MWI, Torn MS, Abiven S, Dittmar T, Guggenberger G, Janssens IA, Kleber M, Kögel-Knabner I, Lehmann J, Manning DAC, Nannipieri P, Rasse DP, Weiner S, Trumbore SE (2011) Persistence of soil organic matter as an ecosystem property. *Nature* 478:49–56. doi: 10.1038/nature10386

Schwertmann U, Taylor RM (1989) Iron Oxides. In: DIXON JB, WEED SB (eds) Minerals in soil environments. Madison, pp 379–438

Siqueira DS, Marques J, Matias SSR, Barrón V, Torrent J, Baffa O, Oliveira LC (2010) Correlation of properties of Brazilian Haplustalfs with magnetic susceptibility measurements. *Soil Use and Management* 26:425–431. doi: 10.1111/j.1475-2743.2010.00294.x

Six J, Conant RT, Paul EA, Paustian K (2002) Stabilization mechanisms of soil organic matter: Implications for C-saturation of soils. *Plant and soil* 241:155–176. doi: 10.1023/A:1016125726789

Smith P, House JI, Bustamante M, Sobocka J, Harper R, Pan G, West PC, Clark JM, Adhya T, Rumpel C, Paustian K, Kuikman P, Cotrufo MF, Elliott JA, McDowell R, Griffiths RI, Asakawa S, Bondeau A, Jain AK, Meersmans J, Pugh TAM (2016) Global change pressures on soils from land use and management. *Global Change Biology* 22:1008–1028. doi: 10.1111/gcb.13068

Steffen W, Richardson K, Rockstrom J, Cornell SE, Fetzer I, Bennett EM, Biggs R, Carpenter SR, de Vries W, de Wit CA, Folke C, Gerten D, Heinke J, Mace GM, Persson LM, Ramanathan V, Reyers B, Sorlin S (2015) Planetary boundaries: Guiding human development on a changing planet. *Science* 347:1259855–1259855. doi: 10.1126/science.1259855

Torn MS, Trumbore SE, Chadwick OA, Vitousek PM, Hendricks DM (1997) Mineral control of soil organic carbon storage and turnover. *Nature* 389:170–173. doi: 10.1038/38260

Torrent J, Liu QS, Barrón V (2010) Magnetic minerals in Calcic Luvisols (Chromic) developed in a warm Mediterranean region of Spain: Origin and paleoenvironmental significance. *Geoderma* 154:465–472. doi: 10.1016/j.geoderma.2008.06.020

Vasconcelos V, Carvalho Junior OA, Martins EDS, Couto Junior AF, Guimarães RF, Gomes RAT (2012) Sistema de classificação geomorfométrica baseado em uma arquitetura sequencial em duas etapas: árvore de decisão e classificador espectral, no Parque Nacional Serra da Canastra. *Revista Brasileira de Geomorfologia* 13:171–186. doi: 10.20502/rbg.v13i2.248

Wall DH, Bardgett RD, Behan-Pelletier V, Herrick JE; Jones TH, Six J, Strong DR (2012)

Soil Ecology and Ecosystem Services. Oxford University Press, UK.

Weintraub SR, Taylor PG, Porder S, Cleveland CC, Asner GP, Townsend AR (2015) Topographic controls on soil nitrogen availability in a lowland tropical forest. *Ecology* 96:1561–1574. doi: 10.1890/14-0834.1

Wiesmeier M, Urbanski L, Hobley E, Lang B, von Lützow M, Marin-Spiotta E, van Wesemael B, Rabot E, Ließ M, Garcia-Franco N, Wollschläger U, Vogel H-J, Kögel-Knabner I (2019) Soil organic carbon storage as a key function of soils - A review of drivers and indicators at various scales. *Geoderma* 333:149–162. doi: 10.1016/j.geoderma.2018.07.026

Xu X, Shi Z, Li D, Rey A, Ruan H, Craine JM, Liang J, Zhou J, Luo Y (2016) Soil properties control decomposition of soil organic carbon: Results from data-assimilation analysis. *Geoderma* 262:235–242. doi: 10.1016/j.geoderma.2015.08.038

Yoo K, Amundson R, Heimsath AM, Dietrich WE (2005) Erosion of upland hillslope soil organic carbon: Coupling field measurements with a sediment transport model. *Global Biogeochemical Cycles* 19:1–17. doi: 10.1029/2004GB002271

Capítulo 1 – Use of machine learning to predict soil organic carbon and nitrogen stable isotopic composition in soils from the Western Paulista Plateau

Abstract

The soil provides several ecosystem goods and services for human well-being. Furthermore, soil is the biggest terrestrial pool of C, as soil organic matter (SOM), reaching more carbon (C) than atmosphere and vegetation together. Due to the importance of SOM for the C biogeochemical cycle, which support and provide goods and services, emerged a growing demand for C soil prediction. Among the variety of statistical techniques used for C prediction, some machine learning algorithms are figuring as tools capable of recognizing and identifying non-linear correlations for data sets with several variables and observations. As biogeochemical process are influenced by interactions between geomorphic, pedogenic, and ecological process across the landscape, this work aims to model an efficient prediction for both soil organic carbon (SOC), and $\delta^{15}\text{N}$ for the Western Paulista Plateau (WPP), based on the evaluation of two machine learning algorithms. The data set was composed by 194 samples collected in field, and 18 auxiliary variables from laboratory analysis and global datasets. The random forest algorithm (RF) performed the higher R-squared, and the lower errors (RMSE and MAE) for SOC and $\delta^{15}\text{N}$ predictions. The variable importance measurement presented magnetic susceptibility measured at low frequency (MS_{lf}) as the most important variable for SOC and $\delta^{15}\text{N}$ models. However, climatic variables as mean annual precipitation (MAP) and mean annual temperature (MAT), as well topographic features as slope and curvature presented relative importance for the tested prediction models.

Keywords: random forest, gradient boosting machine, tropical soils, soil magnetism, modelling

1. Introduction

As an interactive control (Chapin et al. 2011), soil provides several ecosystem goods and services supporting the global demand for food, fiber, water, and energy, also helping to mitigate climate change and maintain biodiversity (McBratney and Field 2015). Soil is the biggest terrestrial pool of carbon (C), as soil organic matter (SOM), reaching more C than atmosphere and vegetation together (Smith et al. 2016). Develop better predictions of soil organic matter (SOM) has received attention from the scientific community, and a wide variety of techniques has been employed to predict SOM. The theoretical background for SOM prediction has a basis on the factorial model that consider soil as a product of the interaction between climate, organisms, relief, parent material and time (CLORPT) (Jenny 1941). Lately, the CLORPT model was reframed to consider soil properties and spatially explicit environmental predictors, also known as SCORPAN (S: Soil, C: Climate, O: Organism, R: Relief, P: Parent material, A: Age, and N: spatial coordinate) (McBratney et al. 2003).

Among the statistical techniques used to apply the factorial model framework, some studies have used feature-space-based model, as machine learning algorithms to predict SOC (Grimm et al. 2008; Rodriguez-Galiano and Chica-Rivas 2014; Hengl et al. 2017; Gomes et al. 2019). Some machine learning algorithms are recognized for identifying non-linear correlations, as RandomForest (Breiman 2001) and Gradient Boosting (Friedman 2002), which are decision trees techniques that can be used to classification and regression analysis.

Lately, studies have been recommended indicator based approach as an alternative to assess soil functions, especially for extensive areas (Wiesmeier et al. 2019). Mean annual precipitation (MAP) and mean annual temperature (MAT) are examples of indicators generally used to predict SOC (Jobágyi and Jackson 2000; Viscarra Rossel et al. 2014; Craine et al. 2015). Topographical features have also been used as indicators to better understand both SOM distribution across the landscape (Grimm et al. 2008; Berhe et al. 2008; McCorkle et al. 2016; Wiesmeier et al. 2019). Another promising proxy to understand some landscape process is the magnetic susceptibility (MS), this technique has been presented correspondence between SOM and mineral magnetic parameters (Jordanova et al. 2013; Quijano et al. 2014; Pingguo Yang et al. 2016; Jakšík et al. 2016). In these studies, the authors found significant correlations between low field MS and C.

The relations between C and MS can be explained by the binding of SOM to mineral surfaces, as iron oxides (Six et al. 2002; Lutzow et al. 2006; Wiesmeier et al. 2019). Due to the dependence of MS and iron oxides, this technique has the potential to identify the soil formation process in a landscape context (Marques Jr. et al. 2014). The MS can indicate lithogenic minerals or pedogenic minerals (Torrent et al. 2010).

Clays have been reported as a factor contributing to stabilizing the enriched $\delta^{15}\text{N}$ in SOM (Craine et al. 2015), controlling SOM decomposition due to the interaction with mineral surfaces (Six et al. 2002; Lutzow et al. 2006; Wiesmeier et al. 2019). Also, $\delta^{15}\text{N}$ values tend to increase as the particle size of soil decreases, or as the association with minerals becomes stronger (Baisden et al. 2002; Liao et al. 2006a; Marin-Spiotta et al. 2009). As biogeochemical process are influenced by interactions between geomorphic, pedogenic, and ecological process across the landscapes (Berhe and Kleber 2013), this work aims to model an efficient prediction for both SOC and $\delta^{15}\text{N}$ for the Western Paulista Plateau (WPP), based on the evaluation of two machine learning algorithms.

2. Material and Methods

2.1 Field study area

The Western Paulista Plateau (WPP) corresponds to 48% of São Paulo area, a Brazilian state that holds an area of 13 million hectares. The Western Paulista Plateau is compartmentalized in two geological domains (Figure 1): i. Domain of sedimentary and volcano-sedimentary of Mesozoic and Paleozoic deposits, little to moderately consolidated, associated with large and deep sedimentary basins of the syncline type (DSVMP); and Domain of Mesozoic fissural volcanism of plateau type (DVM) (Peixoto 2010). The geological outline is characterized by sandy, clay and gravel sediments, volcanic basic rocks, and mainly psammitic sedimentary sequences, which may include pyroclastic. The WPP geological formations are divided into two groups: i Caiuá Group, composed by the Santo Anastácio and Paraná River Formations in the state of São Paulo, corresponding to deposits of dry climate sand, accumulated in long and monotonous desert plains, margins of the large sand dune complexes (Caiuá Desert) extending to the northern region of the state of Paraná; and Bauru Group, which consists of the Uberaba, Rio do Peixe Valley, Araçatuba, São José do Rio Preto, Presidente Prudente and Marília

formations. It also includes the Taiúva Analcimites, volcanic rocks locally interspersed in sequence (Fernandes 2004; Fernandes et al. 2007)

The area has a Tropical Atlantic morphoclimatic regime (sea of hills and forested plateaus) (Ab'Saber 1977). According to the Köppen's climate classification map for Brazil (Alvares et al. 2013), the predominant climates are Aw with dry winter, Cfa with hot summer and Cwa with dry winter and hot summer. The natural vegetation of Western Paulista Plateau was Atlantic Forest in the West and Cerrado in the East and Southwest, and the current most representative land use is sugarcane and pasture.

2.2 Laboratory Analysis

2.2.1 Magnetic susceptibility

The magnetic susceptibility was determined through a Bartington MS2, coupled to a sensor Bartington MS2B dual-frequency sensor (Bartington Instruments Ltd., Oxford, UK), measuring in low frequency (lf: 0.47 kHz) and high frequency (hf: 4.7 kHz) (Dearing 1994; Costa et al. 1999). Measures in double frequency can be used to indicate the presence of magnetic materials of simple or multiple domains. The relative MS_{FD} ($MS_{FD}\%$ defined as $100 \times (MS_{lf} - MS_{hf})/MS_{lf}$) was then calculated to determine the relative variations in the grain size distribution of pedogenic maghemite particles.

2.2.2 Elemental Analysis

The soil was sampled using a Dutch auger. Every soil sample was air-dried, dismantled, and passed through a 2-mm sieve. Roots and the rest of the plant material were removed before the analysis. From the prepared material, sub-samples of 30 to 35 mg of soil were weighed and packed in tin capsules and loaded into an elemental analyzer (Carlo Erba, model 1110, Milan, Italy), which determine C concentration by combustion. The product of the combustion is purified in a chromatography column and placed directly in a mass spectrometer to isotopic ratio (ThermoQuest-Finnigan Delta Plus, Finnigan-MAT, California, USA).

2.2 Sampling Planning

Were collected 300 soil samples distributed in a grid considering the whole Western Paulista Plateau, 0-20 cm depth, using a Dutch auger. The distance among points ranged between 10km and 60km. The grid was applied to provide a good representation of landscape compartments (relief, geology, soils, stratigraphy, climate, landforms, natural vegetation, and mainly crops). The number of samples was enough to attend the requirements in the first variogram lags (n^o pairs > 30), following Yamamoto and Landim (2013), and the experience acquired in previous works applying geostatistics in the Western Paulista Plateau (Teixeira et al. 2013; Marques Jr. et al. 2015).

From the 300 soil samples were selected 194 samples, to evaluate the distribution of points at the Western Paulista Plateau a semi-automatic method delimitation of basic relief units (BRU) (Soares Neto and Martins 2019). The BRU method is an accurate method to typify geomorphological units without subjectivity. The altimetric data used to BRU is from the Shuttle Radar Topography Mission (SRTM) Digital Elevation Model (DEM), available free from the Hydrological Data and Maps on SHuttle Elevation Derivatives at Multiple Scales (HYDROSHEDS) database. The spatial resolution of the DEM is 3arcsec (~ 90 meters). The SRTM was a mission that obtained topographic data of 80% of the Earth's surface between latitudes 60 ° N and 57 ° S 11 days in the year 2000 (Rabus and Eineder 2003).

From the SRTM altimetric data, the spatial data were processed in GIS environment, using ArcGis 10.2 software (ESRI, 2010). The altimetric amplitude (H), lowest possible amplitude value (h) altimetric amplitude interval (a), total area of the basin analyzed (A) were obtained accordingly to (Soares Neto and Martins 2019). Using the R program (R Development Core Team 2019) and the *polynom* package (Venables et al. 2014), the *lm* function was applied to obtain the topographic correlation curve, with determination coefficient of polynomial regression greater than or equal to 0.9 ($R^2 \geq 0.9$) between the h/H and a/A ratio values. The same procedure was performed with the pixel frequency distribution as a function of the declivity intervals. Using the *polynomial* function, maximum and inflection point values were determined to delimit the amplitude and slope classes. After reclassification of the amplitude and slope classes according to their respective maximum and inflection points, the relief units were determined by

overlapping the amplitude ranges associated with the slope ranges. For this, values were proposed in units for the amplitude classes and in tens for the slope classes, so that the sums of these values determined the BRU.

2.3 Input data and predictor variables

From the geographic coordinates of each sampling point, we collected auxiliary variables from previously published datasets (Table 1) and used them as predictors for the model. The MAP and MAT climatic data used in this paper were taken from the climatic means (1970-2000) acquired from WordlClim (Hijmans et al. 2005). The aridity index (AI) and potential evapotranspiration (PET) data were acquired from the Global Aridity Index and Potential Evapotranspiration Climate Database v.2 (Trabucco et al. 2019). The Gross Primary Production (GPP) dataset used is a MODIS/Terra product (MOD17A2, version 55), with means for the temporal extent 2000-2013 (Running and Zhao 2015). The elevation data were acquired from the Digital Elevation Model (DEM) from the Shuttle Radar Topography (Jarvis et al. 2008). From the DEM were generated morphometric attributes as Longitudinal and Cross curvatures (Wood 1996), as well as Minimum and Maximum (Young 1978). The data obtained from laboratory analysis (described further - MS_{lf}, Clay content, Fe_o, and Fe_d) were also used as auxiliary variables.

Table 1. Predictor variables used to model SOC content and δ¹⁵N.

Predictor	Description	Reference
MAP	Mean Annual Temperature WorldClim (°C)	Hijmans et al. (2005)
MAT	Annual Precipitation WorldClim (mm)	Hijmans et al. (2005)
PET	Potencial Evapotranspiration (annual mean)	Trabucco et al. (2019)
AI	Aridity Index	Trabucco et al. (2019)
GPP	Gross Primary Productivity, 2000-2015 (g C.m ² .yr ⁻¹)	Running and Zhao (2016)
Elevation	DEM - Shuttle Radar Topography, meters	Jarvis et al. (2008)
Slope	Morphometric attribute, degrees	This study, following Wentworth (1930)
Cross	Cross curvature - Morphometric attribute	This study, following Wood (1996)
Long	Longitudinal curvature - Morphometric attribute	This study, following Wood (1996)
Min	Minimum curvature - Morphometric attribute	This study, following Young (1978)

Max	Maximum curvature - Morphometric attribute	This study, following Young (1978)
Fed	Iron dithionite (g kg^{-1})	This study
Feo	Iron Oxalate (g kg^{-1})	This study
MS _{lf}	low-frequency magnetic susceptibility ($10^{-6} \text{ m}^3 \text{ kg}^{-1}$)	This study
MS _{fd%}	magnetic susceptibility frequency dependent (%)	This study
Clay	Clay content (g kg^{-1})	This study
pH CaCl ₂	pH in CaCl ₂	This study

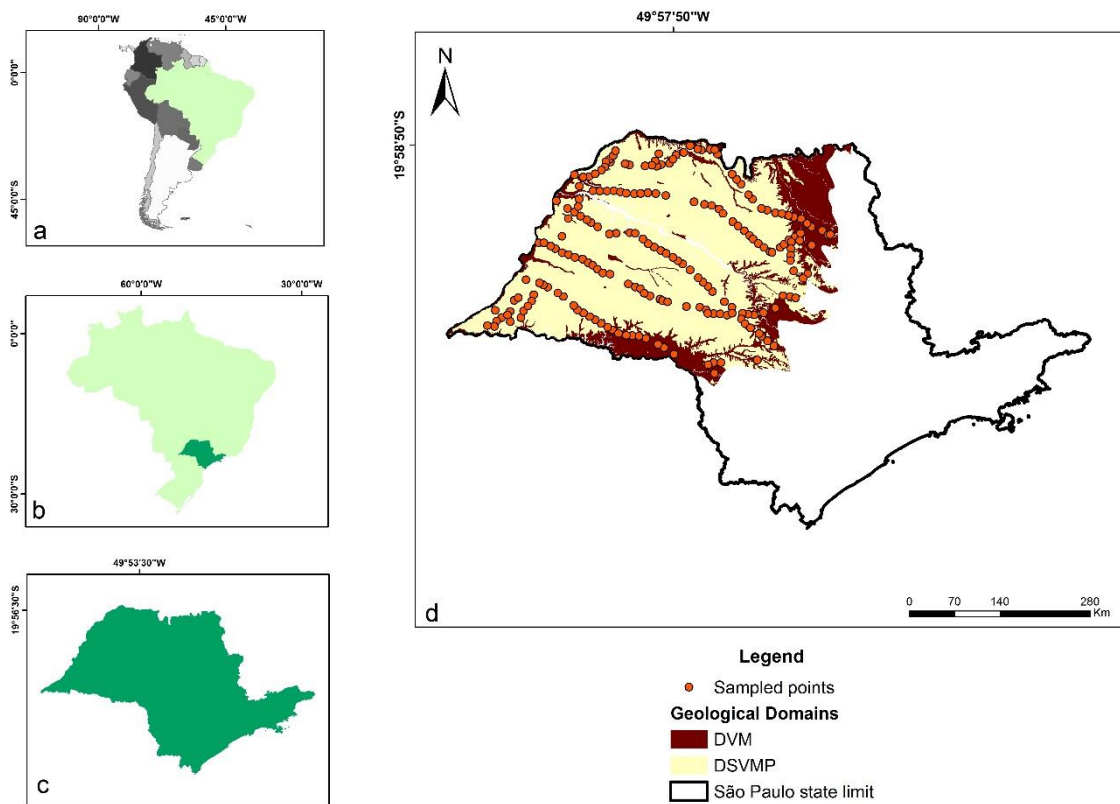


Figure 1. Field study localization context. (a) Highlights Brazil in Latin America context; (b) indicates São Paulo state localization in Brazil; (c) São Paulo state; (d) Western Paulista Plateau area Geological Domains and location of the 197 sampled points (n=197). DSVMP – Domain of sedimentary and volcano-sedimentary of Mesozoic and Paleozoic deposits, little to moderately consolidated, associated with large and deep sedimentary basins of the syncline type; DVM – Domain of Mesozoic fissural volcanism of plateau type.

2.4 Modelling

We built a correlation matrix using the whole data set of predictor variables, to remove a subset of predictors more committed with the most correlations above a given threshold (Kuhn 2008), we considered 0.7 for this study. From the selected predictors, we fitted the models: Random Forest (RF), Gradient Boosting Machine (GBM). The training subset used 70% of the data, and the testing holds out subset used 30% of the data, both drowned randomly. To compare the predictive power of the models, we used 10-fold repeated cross-validation with five repetitions following Bataille et al. (2018). We used three statistical metrics to evaluate the accuracy of the methods used in this study, root mean squared error (RMSE), mean absolute error (MAE), and coefficient of determination (R^2). Finally, to evaluate the best model, we tested the selected model with the testing hold out subset.

Random Forest is an algorithm that was developed to execute classification and regression (Breiman 2001). The RF method is based on ensemble learning (bagging), and couple the predictions of several decision trees to enhance prediction accuracy and minimize variability (Breiman 2001). To do this, RF applies a bootstrapping (Hastie et al. 2009), which is a resampling approach to simulate several random realizations of the original data set. Each decision tree is built from a bootstrap sample of the original data set, and each bootstrap set leaves out ~37% of the original observation, as know as out-of-bag data (OOB) (Hastie et al. 2009). The tuning parameters for RF are the number of trees, the least possible number of data in each terminal node (node size), and the number of features tested in each node (mtry). The mtry is the main hyperparameter for the RF method and is used to optimize the model (Breiman 2001; Hengl et al. 2017).

As RF, GBM can also perform classification and regression, and couple boosting and bagging (Friedman 2001). GBM builts regression trees in sequence, where each new tree learns from the previous one, and emphasizes the observations on week trees, to produce a “committee” to minimize noise (Friedman 2002). The hyperparameters to tune GBM are number of trees, or the number of boosting interactions (n.trees, 500 for this study), the depth of trees (interaction.depth, 30 for this study), and the learning rate (shrinkage, 0.1 for this study) (Greenwell et al. 2019).

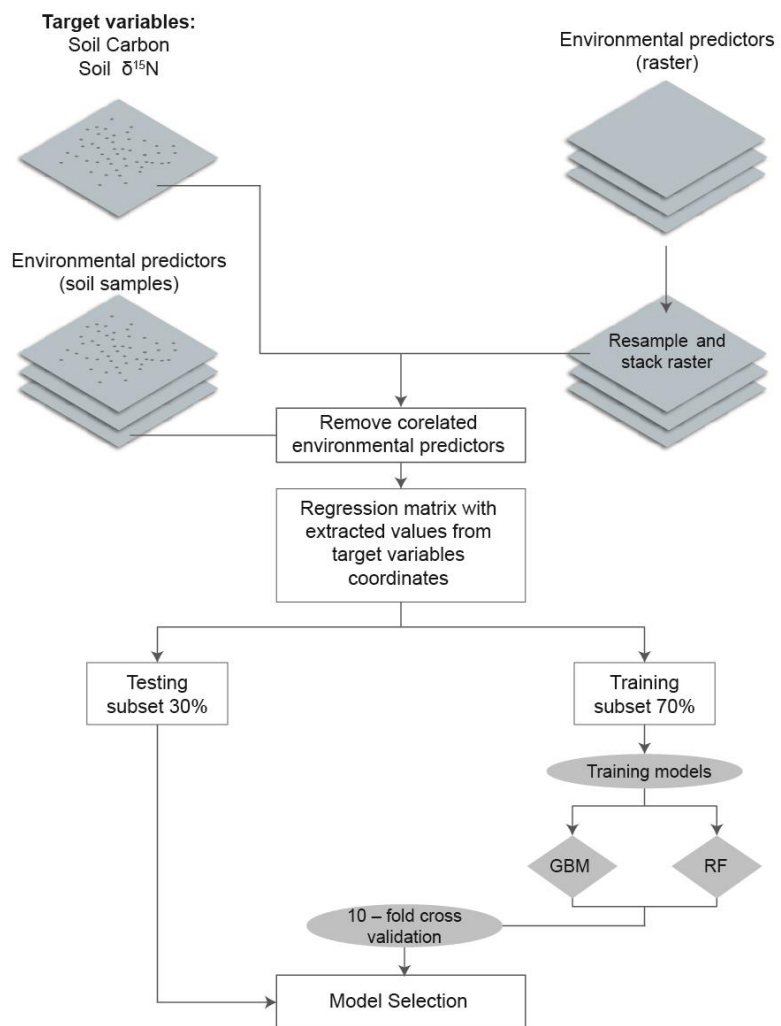


Figure 2. Workflow used for the modeling of soil C and $\delta^{15}\text{N}$. The environmental predictors are listed in Table 1. GBM: Gradient Boosting Machine algorithm; RF: Random Forest algorithm.

We used variable importance quantification to help to indentificate the influence of the environmental predictors used in the models (Nauman and Thompson 2014). Further, we used partial dependence plots to evaluate how environmental predictors influenced the modeled variable (target). In partial dependence plots, the y-axes show the mean marginal effect of a predictor to the final prediction (Friedman 2001).

3. Results

3.1 Basic Relief Units and point distribution

The altimetric amplitude was 806m. After the reclassification to the vertical resolution, were obtained 42 amplitude classes (Table 2), distributed between 0, and 806m, being possible to obtain other altimetric attributes (h , a , h/H and a/A). The topographic correlation curve obtained was $-0.04693006 + 1.148656*x - 3.691659*x^2 + 4.179408*x^3 - 1.588979*x^4$. Where, $R^2 = 0.91$, Adjusted $R^2 = 0.90$, $p\text{-value} < 0.001$. The inflection points were 0.4450234, 0.8701005, and stationary points 0.2445304, 0.7770629, 0.9510927.

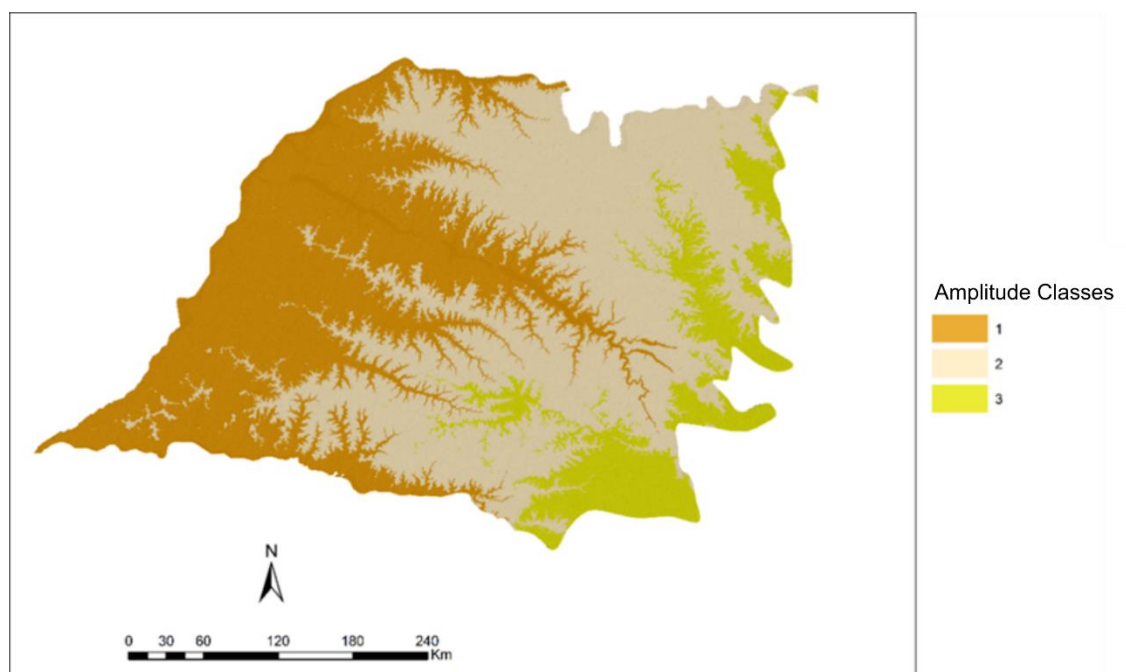


Figure 3. Classification map of altimetric amplitude of the Western Paulista Plateau, obtained from the H_{max} e H_{if} of the topographic correlation curve from the polynom the polynom $-0.04693006 + 1.148656*x - 3.691659*x^2 + 4.179408*x^3 - 1.588979*x^4$.

After the reclassification to the vertical resolution to were obtained 42 slope classes, distributed between 2%, and 86%. With the values of interval and frequency obtained in Table 3, we obtained the curve of the distribution of the pixel frequency as a function of the slope intervals. The polynom obtained was $6636902 - 64881.68x - 139932.3x^2 + 14250.07x^3 - 623.5036x^4 + 14.55345x^5 - 0.1888067x^6 + 0.001285042x^7 - 0.000003580165x^8$. Where, $R^2 = 0.91$, Adjusted $R^2 = 0.90$, $p\text{-value}: < 0.001$. The inflection points were 5.220925, 23.611647, 38.637737, 54.124143, 68.137712,

79.468130, and stationary points: -0.2240626, 18.3074004, 31.6923445, 46.7424955, 61.2737025, 73.5081277, 82.7670030.

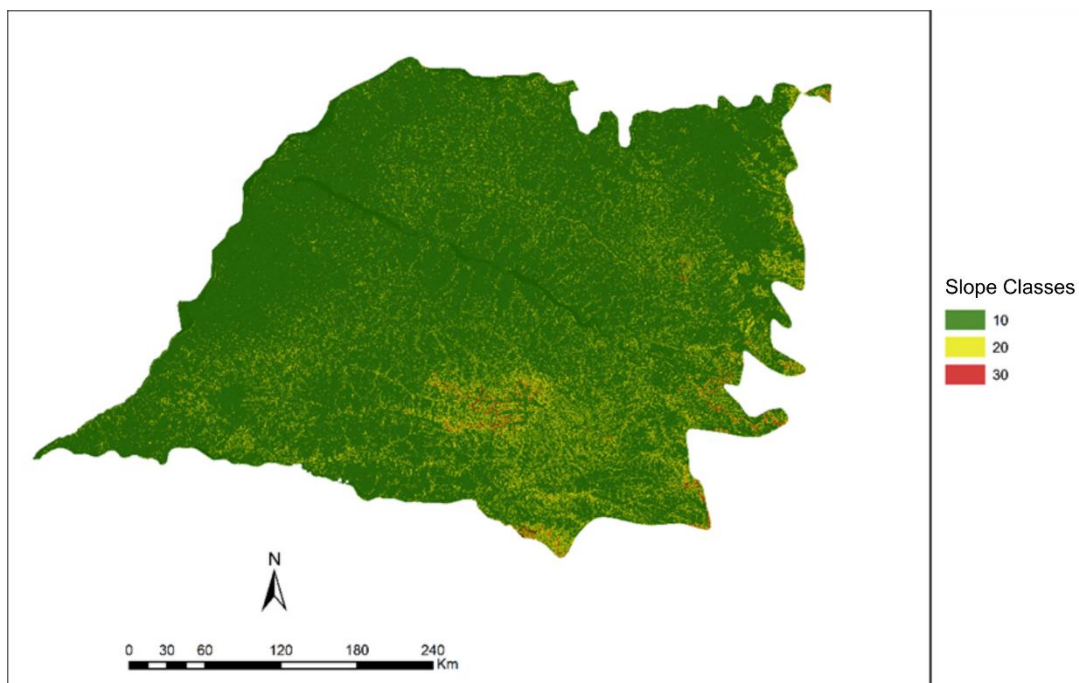
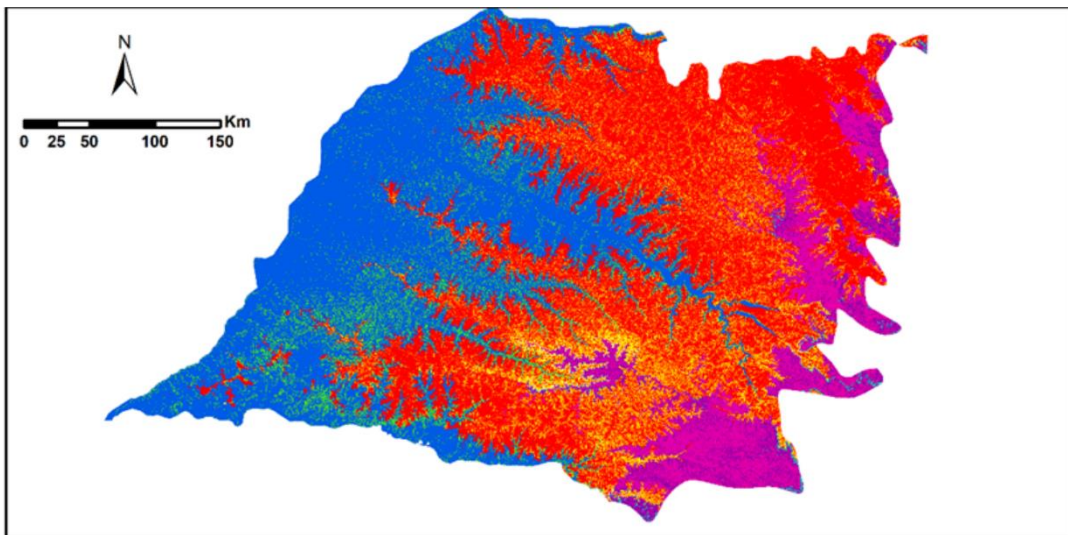


Figure 4. Slope classification map of the Western Paulista Plateau, obtained from the C_{\max} and C_{if} of correlation curve between class intervals and pixel frequency which generated the polynom $6636902 - 64881.68x - 139932.3x^2 + 14250.07x^3 - 623.5036x^4 + 14.55345x^5 - 0.1888067x^6 + 0.001285042x^7 - 0.000003580165x^8$.

Overlapping the amplitude intervals associated with the slope allowed to obtain Basic Relief Units for the morphological limit of the Paulista Western Plateau, according to Soares Neto and Martins (2019).



Basic Relief Units

█ Class 11 - 0 to 200 m, and 0-6% slope	█ Class 12 - 201 to 360 m, and 0-6% slope	█ Class 13 - 361 to 806 m, and 0-6% slope	█ Class 21 - 0 to 200 m, and 6.1-18% slope	█ Class 22 - 201 to 360 m, and 6.1-18% slope	█ Class 23 - 361 to 806 m, and 6.1-18% slope
					█ Class 31 - 0 to 200 m, and >18% slope
					█ Class 32 - 201 to 360 m, and >18% slope
					█ Class 33 - 361 to 806 m, and >18% slope

Figure 5. Final map based on semi-automatic delimitation of Basic Relief Units for the Western Paulista Plateau, following Soares Neto and Martins (2019) methodology.

The delimitation model employed allowed the individualization of twelve BRU to the morphological limit of the Paulista Western Plateau. It was necessary to disregard the existence of inconsistencies in the database and interval values that do not correlate (Soares Neto and Martins 2019). From the delimitation of BRU it was possible to observe that the sampled points were well distributed in relation to the amplitude and slope data.

3.2 Correlation analysis and descriptive statistics

The summary statistics of target variables in the study area are presented in Table 1. SOC ranged from 0.12 to 2.57%, and $\delta^{15}\text{N}$ ranged from 1.64 to 9.46 ‰. From a correlation matrix with 18 environmental predictors (MAP, MAT, PET, AI, GPP, Elevation, Slope, Aspect, Cross, Long, Min, Max, Fe_d, Fe_o, MS_{lf}, MS_{fd%}, Clay, pH CaCl₂) (Figure 2a), were excluded those variables with strongly correlated ($r > 0.7$) represented by dark blue circles in Figure 6. The remaining 9 variables (MAT, MAP, GPP, Slope, Aspect, Cross, MS_{lf}, pH CaCl₂) are presented in Figure 2b.

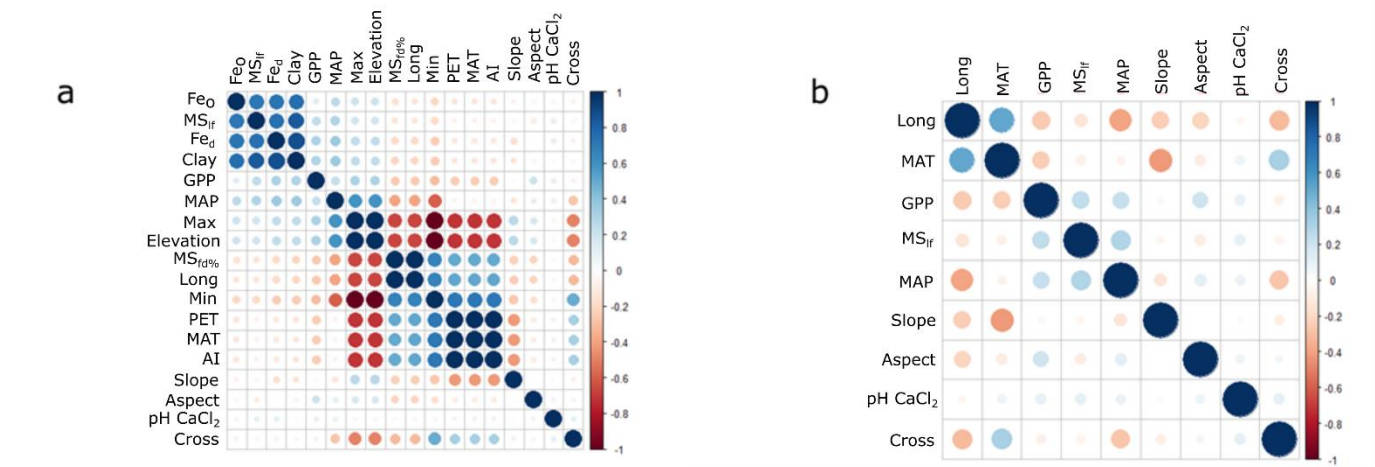


Figure 6. Selection of soil properties used in models to predict C and $\delta^{15}\text{N}$. Figure “a” shows the correlation among the whole set of 18 variables. Figure “b” shows the selected variables. MAP - Mean Annual Temperature WorldClim ($^{\circ}\text{C}$), MAT - Annual Precipitation WorldClim (mm), PET - Potencial Evapotranspiration (annual mean), AI - Aridity Index, GPP – Gross Primary Production ($\text{g C.m}^{-2}.\text{yr}^{-1}$), Elevation (m), Slope (degrees), Cross - Cross curvature, Long - Longitudinal curvature, Min - Minimum curvature, Max - Maximum curvature, Fe_d- Iron dithionite (g kg^{-1}), Fe_o - Iron Oxalate (g kg^{-1}), MS_{lf} - low-frequency magnetic susceptibility ($10^{-6} \text{ m}^3 \text{ kg}^{-1}$), MS_{fd%} - magnetic susceptibility frequency dependent (%), Clay - Clay content (g kg^{-1}), pH CaCl₂ - pH in CaCl₂.

Table 3. Descriptive statistics of soil C contents and $\delta^{15}\text{N}$ in the study area (n=194).

Variable	Min	Median	Mean	Max	SD
C (%)	0.12	0.52	0.66	2.57	0.47
$\delta^{15}\text{N}$ (‰)	1.64	6.42	6.30	9.46	1.56

3.3 Model evaluation

There was no significant difference between RF and GBT (t-test, p-value>0.05). However, comparing the cross-validated RMSE, MAE, and determination coefficient (R^2) among the models, revealed RF as the best algorithm to predict SOC and $\delta^{15}\text{N}$ in the Western Paulista Plateau. The performance of SOC-RF over the 10-fold cross-validation performed $R^2=0.51$ RMSE= 0.31, and MAE=0.22. The same pattern was observed for

$\delta^{15}\text{N}$, where the performance of $\delta^{15}\text{N}$ -RF over the 10-fold cross-validation performed an $R^2=0.29$, RMSE=1.33, and MAE=1.06.

The trained SOC-RF model explained 94% of the variance of the training subset, with an RMSE of 0.12, and 75% of the variance with an RMSE of 0.37 for the testing dataset. While for $\delta^{15}\text{N}$ -RF, the training model explained 93% of the variance, with an RMSE of 0.55, and 14% of the variance with an RMSE of 1.48 for the testing dataset.

The RF model for prediction of SOC content indicated MS_{lf} as the most important predictor for the model SOC-RF, (Figure 7). However, other variables showed to be important for the model as well. In this context, the importance order for SOC-RF is MS_{lf} , with percentual increase in mean standard error (%IncMSE) of 38.79%, followed by GPP (5.67%), MAT (2.93%), MAP (2.31%), Slope (1.90%), longitudinal curvature (1.32%), cross curvature (0.95%), aspect (0.10%), and pH CaCl_2 (0.06%) (Figure 7). The partial dependence plots, showing the relationships between the target variable (SOC) and the environmental predictors are shown in Figure 8.

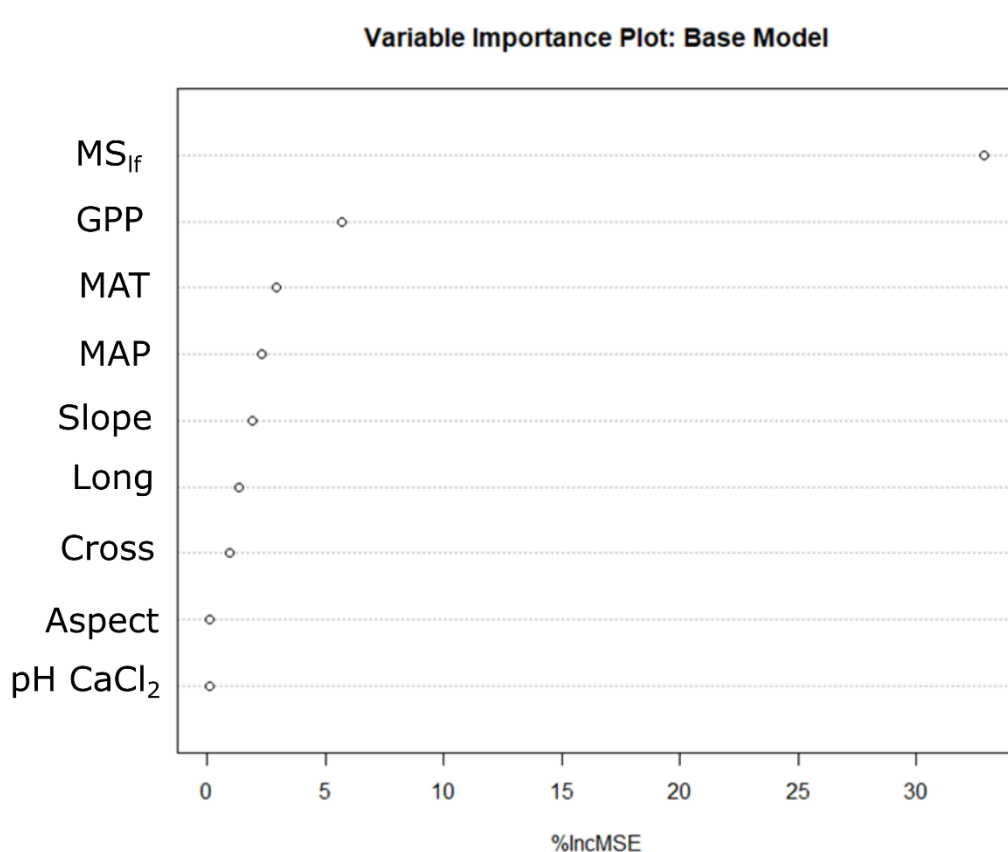


Figure 7. The relative importance of environmental predictors for soil C prediction in the Western Paulista Plateau, using the Random Forest algorithm. %IncMSE refers to a decrease in mean accuracy. MS_{lf} - low-frequency magnetic susceptibility ($10^{-6} \text{ m}^3 \text{ kg}^{-1}$);

GPP – Gross Primary Production ($\text{g C m}^2 \text{ yr}^{-1}$); MAT – Mean Annual Temperature WorldClim ($^{\circ}\text{C}$); MAP - Mean Annual Precipitation WorldClim (mm); Slope (degrees); Long - Longitudinal curvature; Cross - Cross curvature; Aspect; pH CaCl_2 - pH in CaCl_2 .

SOC variations tended to be logarithmically correlated with MS_{lf} (Figure 8a). The increase between 3 and $14 \times 10^{-6} \text{ m}^3 \text{ kg}^{-1}$ corresponds mostly to sandstone areas, while the other values of SM_{lf} correspond to basalt areas where the higher values of SOC content were found. Furthermore, the values of SOC remained constant to 1.6% when MS_{lf} values were higher than $37 \times 10^{-6} \text{ m}^3 \text{ kg}^{-1}$ (Figure 8a). The relationship between SOC and MAP showed an exponential pattern. However, the MAP becomes to be more important for areas with mean annual precipitation higher than 730mm (Figure 8b). Inversely, the relationship between SOC and MAT showed a negative correlation, indicating a decrease of SOC as temperature increases (Figure 8c). Excepting the MAT values above 23.2, that shows an increase that corresponds to a specific area of Serra Geral formation in the west of WPP (Figure 8c). The relationship between SOC and GPP showed a linear trend between 1400 and $2500 \text{ kg C m}^2 \text{ yr}^{-1}$, and a pronounced increase between 2500 and $2600 \text{ kg C m}^2 \text{ yr}^{-1}$.

Further, the relationship between SOC and GPP mean values decreased between 2600 and $2900 \text{ g C m}^2 \text{ yr}^{-1}$ and kept constant (Figure 8d). Slope angle showed an exponential negative correlation with SOC, where the higher values of SOC were found in areas with a slope lower than 2.3° (Figure 8e). To interpret the relationship of the curvatures (cross and longitudinal) with SOC we must consider that negative values correspond to concavity intensity (convergence). In general, there was a negative relationship between SOC and Cross Curvature till -12 value, and then a positive relationship between -11 and -10, tending to be constant as the values were close to 0 (Figure 8f). The longitudinal curvature also showed a negative relationship with SOC, meaning that areas with higher concavity intensity are more propense to store more SOC (Figure 8g). The partial dependence of pH CaCl_2 presented a negative relationship with SOC when pH CaCl_2 values ranged between 3.6 and 4.2 . However, SOC and pH CaCl_2 showed a positive relationship when pH values were higher than 4.2 (Figure 8h).

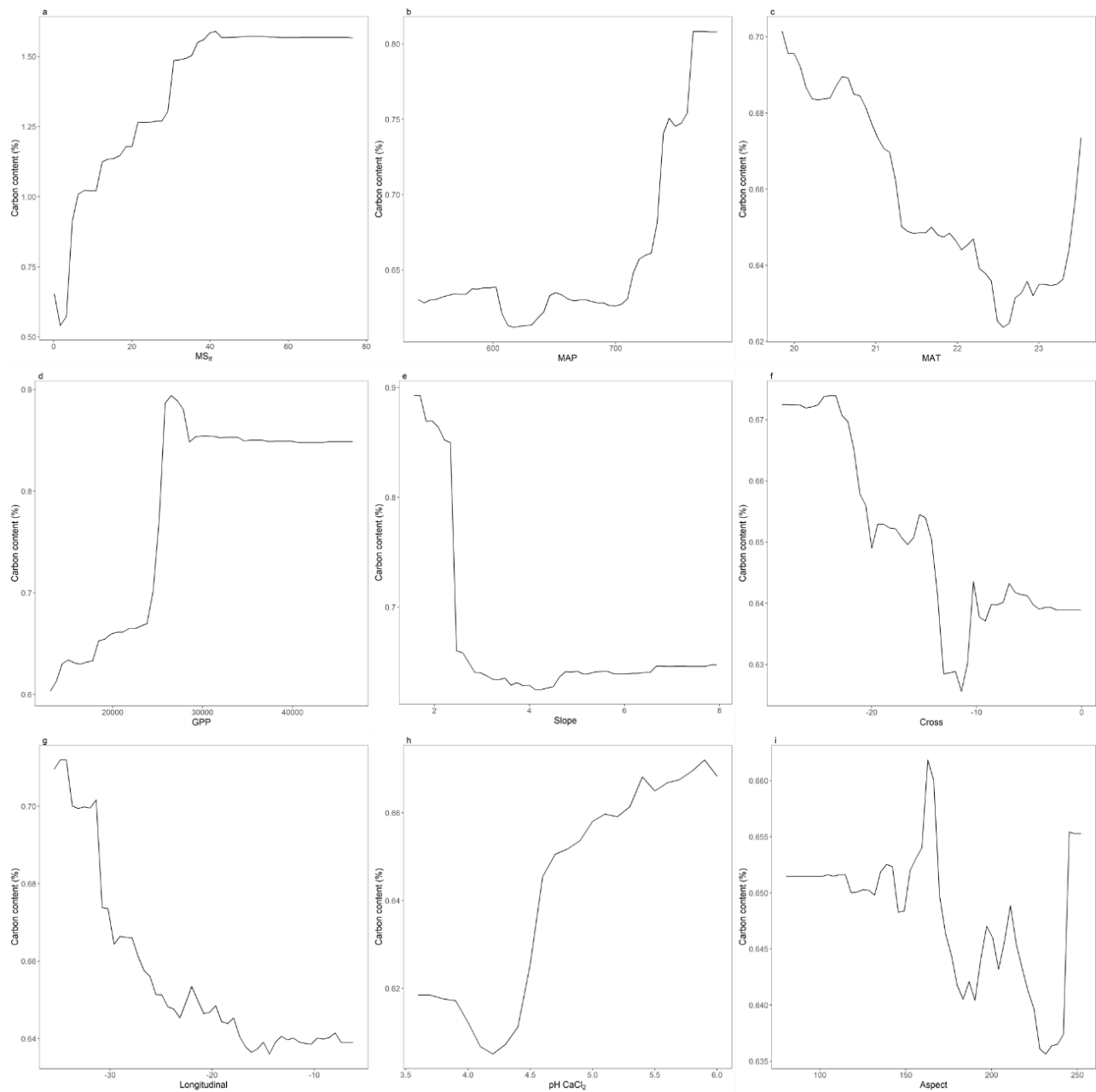


Figure 8. Plots showing the influence of the nine environmental predictors used in the model to predict C in soil using the Random Forest algorithm. a. MS_{lf} - low-frequency magnetic susceptibility ($10^{-6} \text{ m}^3 \text{ kg}^{-1}$); b. MAP - Mean Annual Precipitation WorldClim (mm); c. MAT – Mean Annual Temperature WorldClim (°C); d. GPP – Gross Primary Production ($\text{g C m}^2 \text{ yr}^{-1}$); e. Slope (degrees); f. Cross - Cross curvature; g. Long - Longitudinal curvature; h. pH CaCl₂ - pH in CaCl₂; i. Aspect.

The $\delta^{15}\text{N}$ -RF model also indicated MS_{lf} as the most important predictor for the model (Figure 9). From the variables tested in the model, pH CaCl₂, aspect, and longitudinal curvature showed negative values of %IncMSE, which means that these

variables were not significant enough to the model. Thus, the importance order for $\delta^{15}\text{N}$ -RF is MS_{If}, with an IncMSE of 18.38%, followed by slope (9.93%), MAT (7.98%), C:N ratio (7.97%), MAP (4.51%), GPP (1.88%), and cross curvature (1.15%) (Figure 9). The partial dependence plots, showing the relationships for the $\delta^{15}\text{N}$ -RF model are shown in

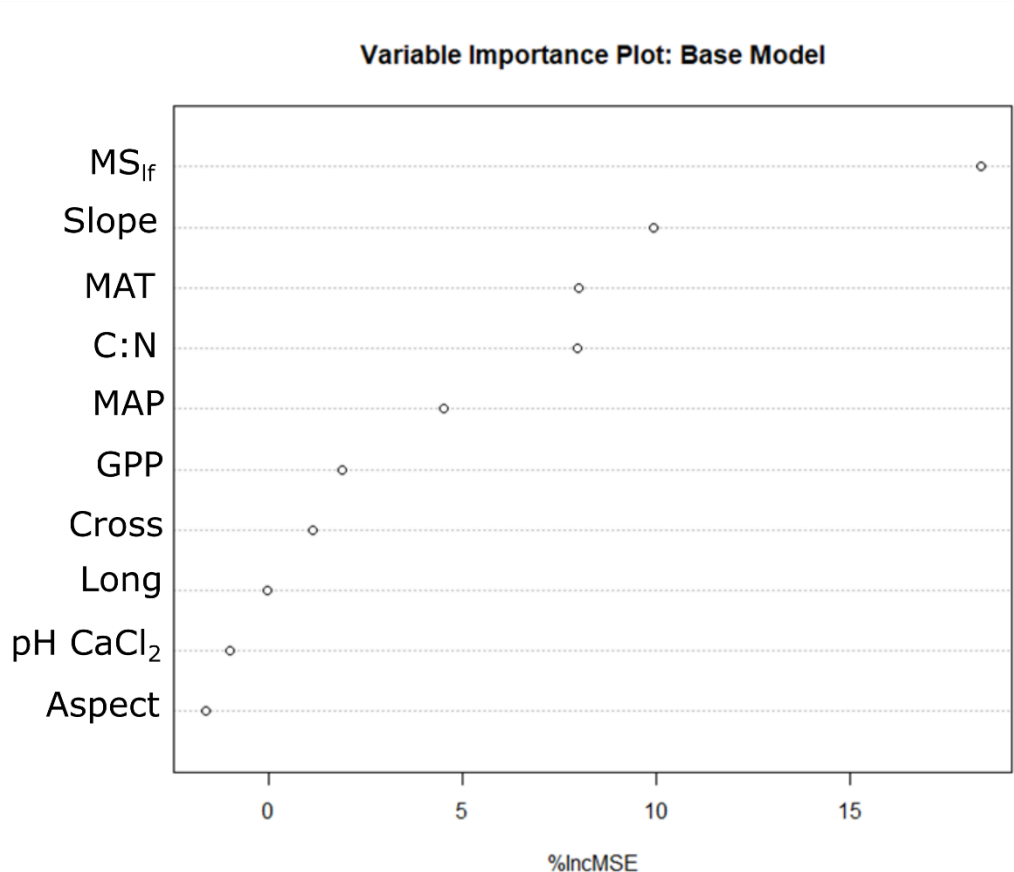


Figure 9. The relative importance of environmental predictors for soil C prediction in the Western Paulista Plateau, using the Random Forest algorithm. %IncMSE refers to a decrease in mean accuracy. MS_{If} - low-frequency magnetic susceptibility ($10^{-6} \text{ m}^3 \text{ kg}^{-1}$); C:N – carbon nitrogen ratio; Slope (degrees); MAT – Mean Annual Temperature WorldClim ($^{\circ}\text{C}$); MAP - Mean Annual Precipitation WorldClim (mm); GPP – Gross Primary Production ($\text{g C m}^{-2} \text{ yr}^{-1}$); Cross – Cross curvature; Long – Longitudinal curvature; pH CaCl₂ - pH in CaCl₂; Aspect.

The partial dependence plot showing the relationship between $\delta^{15}\text{N}$ and MS_{If} showed a positive logarithmic correlation. However, when MS_{If} values were higher than $25 \times 10^{-6} \text{ m}^3 \text{ kg}^{-1}$, $\delta^{15}\text{N}$ values showed near to constant values (Figure 10a). Inversely, slope, and $\delta^{15}\text{N}$ showed a negative correlation between 2° and 7.2° , which indicates that higher values of $\delta^{15}\text{N}$ tended to be found in relatively flat areas (Figure 10e). The

relationship between MAT and $\delta^{15}\text{N}$, showed a bimodal curve, with a positive correlation between 20 and 20.5 °C, a negative correlation between 20.6 and 21.4 °C (Figure 10c). Further, $\delta^{15}\text{N}$ values showed to be highly responsive to MAT between 21.4 and 21.9 °C, where the higher values of $\delta^{15}\text{N}$ were found (Figure 10c). Then, between 22 and 23 °C, the relationship returned to be negative $\delta^{15}\text{N}$ (Figure 10c). The $\delta^{15}\text{N}$ values showed a well-defined pattern with C:N. When C:N was between 10 and 12, $\delta^{15}\text{N}$ values ranged between 6.48 and 6.56 ‰. However, there was an abrupt decrease in $\delta^{15}\text{N}$ values when C:N became higher than 12, showing $\delta^{15}\text{N}$ values between 5.82 and 5.78‰ (Figure 10g). MAP and $\delta^{15}\text{N}$ presented a negative relationship between 550 and 632 mm, with a more pronounced negative relationship between 632 and 642mm. Thus, between 650 and 750mm, the $\delta^{15}\text{N}$ values ranged between 6.16 and 6.2 ‰ (Figure 10b). In general, MAP and $\delta^{15}\text{N}$ correlation indicated that $\delta^{15}\text{N}$ were found in areas with low MAP. The relationship between $\delta^{15}\text{N}$ and GPP showed a positive linear correlation between 1300 and 1910 g C.m².yr⁻¹, but between 1910 and 4350 g C.m².yr⁻¹ the correlation was negative and showed a slight decrease (Figure 10d). The overall relationship between cross curvature and $\delta^{15}\text{N}$ showed a positive correlation indicating that higher values of $\delta^{15}\text{N}$ values were found in flat areas (Figure 10f).

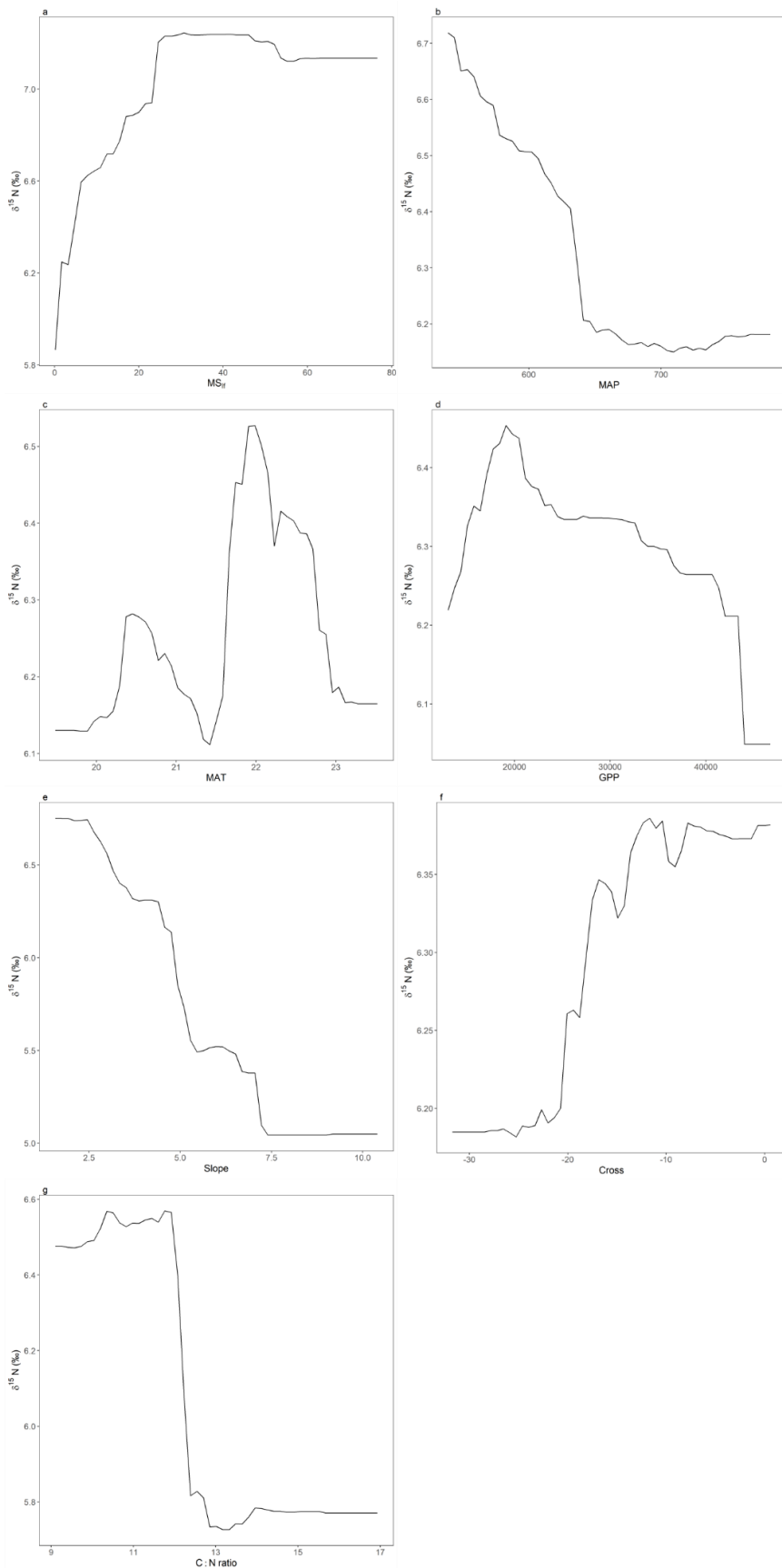


Figure 10. Plots showing the influence of the nine environmental predictors used in the model to predict $\delta^{15}\text{N}$ in soil using the Random Forest algorithm. a. MS_{lf} - low-frequency

magnetic susceptibility ($10^{-6} \text{ m}^3 \text{ kg}^{-1}$); b. MAP - Mean Annual Precipitation WorldClim (mm); c. MAT – Mean Annual Temperature WorldClim ($^{\circ}\text{C}$); d. GPP – Gross Primary Production ($\text{g C m}^2 \text{ yr}^{-1}$); e. Slope (degrees); f. Cross - Cross curvature; g. C:N – carbon nitrogen ratio.

4. Discussion

Through the machine learning approach, our findings indicate that MS_{lf} and topographical features are important to predict SOC and $\delta^{15}\text{N}$ in the soil in 0-0.20 m, on the regional scale of WPP. We assume that parent material is a driver for soil mineralogy, as iron oxides expressed by MS. Our results concur with other studies that suggest topography and iron oxides as important factors for the spatial distribution of SOM in regional studies.

Our results presented RF with the higher R^2 , and lower MAE and RMSE. RF algorithm has been indicated for its accuracy and noise reduction capacity (Rodriguez-Galiano and Chica-Rivas 2014). Machine learning algorithms have been used successfully in ecological prediction and soil mapping (Prasad et al. 2006; Grimm et al. 2008; Hengl et al. 2017; Gomes et al. 2019). Specifically to predict SOC, soil mapping has been used the soil factorial model in machine learning approaches (Gomes et al. 2019; Keskin et al. 2019; Pouladi et al. 2019; Vos et al. 2019; Veronesi and Schillaci 2019).

Climate data, as MAP and MAT, are well-known drivers of SOC storage (Jobbágy and Jackson 2000; McBratney et al. 2006; Craine et al. 2015). In general, MAP influences GPP positively in terrestrial ecosystems and consequently enhances the input of C in soil (Wiesmeier et al. 2019). The decomposition rate of SOM is attributed to enzymatic microbial reactions that are temperature dependent (Conant et al. 2011; Davidson 2015). Thus, MAT increasing stimulates microbial activity, that consumes SOC (Conant et al. 2011; Davidson 2015). The negative relationship between SOC and MAT has been widely reported in other studies (Jobbágy and Jackson 2000; Craine et al. 2015). Coupling the MAP and MAT influences on SOM, SOC values are generally higher in cold/wet climates, and lower values are found in hot/dry climates (Jobbágy and Jackson 2000; McBratney et al. 2006; Craine et al. 2015). The opposite happens for $\delta^{15}\text{N}$, generally higher values of $\delta^{15}\text{N}$ are found in hot/dry climates while, and lower values in cold/wet climates (Craine et al. 2015). Additionally, Craine et al. (2015) ponder that hot/dry ecosystems have soil organic matter with higher $\delta^{15}\text{N}$ values, due to the proportion of nitrogen in organo-mineral bindings.

The IncMSE% of MS_{lf} for SOC-RF and $\delta^{15}\text{N}$ -RF indicates that the Fe oxides represented by MS_{lf} are bound to C and enriched $\delta^{15}\text{N}$. Correlations among clay fractions, as Fe oxides, with C and $\delta^{15}\text{N}$ are reported as organo-mineral bindings (Liao et al. 2006b; Marin-Spiotta et al. 2009; Craine et al. 2015). Furthermore, SOM enrichment of $\delta^{15}\text{N}$ and low C:N ratio are associated with older or more humidified SOM, which correspond to high microbial processed SOM (Liao et al. 2006b; Schmidt et al. 2011; Craine et al. 2015). This older SOM is protected from microbial enzymatic activity due to the organo-mineral binding (Six et al. 2002; Fissore et al. 2017).

Our analyses also indicate that the importance of MS_{lf} for SOC-RF model reflects the role of iron (Fe) oxides for C storage, due to organo-mineral binding (Six et al. 2002; Lutzow et al. 2006; Fissore et al. 2017). Positive correlations of SM_{lf} with SOC were found in different soil types (Jordanova et al. 2013; Quijano et al. 2014; Jakšík et al. 2016) which corroborates the positive relationships of Fe oxides found by other studies (Kaiser and Guggenberger 2000; McNally et al. 2017).

Our results agree with Berhe et al. (2008), who used geomorphology allied to an isotopic approach and evaluated the contribution of different landforms to the sink of C in a landscape dominated by grasses. In this work, the authors observed that the C inventory varied in function of terrain landforms, and the lower rates of decomposition of SOM and the higher C stocks were found in deposition landforms. McCorkle et al. (2016) also used a geomorphologic approach and observed higher concentrations of C in depositional landforms at 0-10 cm depth than in eroding landforms. We found that slope and landscape position are important predictors to $\delta^{15}\text{N}$, these results are consistent with Weintraub et al. (2015), which also found significant effects of slope and landscape on $\delta^{15}\text{N}$ values. The authors reported that steeper slopes presented lower $\delta^{15}\text{N}$ values, and explained their results due to nitrogen loss through non-fractioning pathways as erosion. As places with low inclination and concave landforms contribute to holding water, while abrupt slopes and convex landforms contribute to water flow (Grimm et al. 2008; Wiesmeier et al. 2019), we argue that topographical curvatures showed importance in our models because of their participation in water flow, and erosional process.

5. Conclusion

The use of soil factorial model to guide the machine learning approach showed a satisfactory result to predict both SOC and $\delta^{15}\text{N}$, showing significative determination coefficient with the hold out subset. Our results indicate the high importance of by magnetic susceptibility measured at low frequency, and therefore, the importance of iron oxides represented by this attribute, as a predictor for both SOC and $\delta^{15}\text{N}$. This finding highlighted the relevance of mineralogy predictors for modeling. Additionally, our results corroborate that climate and topographical features can help to predict our target variables on a regional scale.

6. References

- Ab'Saber AN (1977) Domínios morfoclimáticos na América do Sul: primeira aproximação. São Paulo. Instituto de Geografia/USP. Geomorfologia, 52: 1-21.
- Alvares CA, Stape JL, Sentelhas PC, De Moraes Gonçalves JL, Sparovek G (2013) Köppen's climate classification map for Brazil. Meteorologische Zeitschrift 22:711–728. doi: 10.1127/0941-2948/2013/0507
- Baisden WT, Amundson R, Cook AC, Brenner DL (2002) Turnover and storage of C and N in five density fractions from California annual grassland surface soils. Global Biogeochemical Cycles 16:64-1-64–16. doi: 10.1029/2001GB001822
- Bataille CP, von Holstein ICC, Laffoon JE, Willmes M, Liu XM, Davies GR (2018) A bioavailable strontium isoscape for Western Europe: A machine learning approach. PLoS ONE 13:1–27. doi: 10.1371/journal.pone.0197386
- Berhe AA, Harden JW, Torn MS, Harte J (2008) Linking soil organic matter dynamics and erosion-induced terrestrial carbon sequestration at different landform positions. Journal of Geophysical Research: Biogeosciences 113:1–12. doi: 10.1029/2008JG000751
- Berhe AA, Kleber M (2013) Erosion, deposition, and the persistence of soil organic matter: mechanistic considerations and problems with terminology. Earth Surface Processes and Landforms 38:908–912. doi: 10.1002/esp.3408

Breiman L (2001) Random forests. *Machine Learning* 45:5–32. doi: 10.1007/9781441993267_5

Chapin FS, Matson PA, Vitousek PM (2011) Principles of Terrestrial Ecosystem Ecology, Second. Springer New York, New York, NY

Conant RT, Ryan MG, Ågren GI, Birge HE, Davidson EA, Eliasson PE, Evans SE, Frey SD, Giardina CP, Hopkins FM, Hyvönen R, Kirschbaum MUF, Lavallee JM, Leifeld J, Parton WJ, Megan Steinweg J, Wallenstein MD, Martin Wetterstedt JÅ, Bradford MA (2011) Temperature and soil organic matter decomposition rates - synthesis of current knowledge and a way forward. *Global Change Biology* 17:3392–3404. doi: 10.1111/j.1365-2486.2011.02496.x

Costa ACS, Bigham JM, Rhoton FE, Traina SJ (1999) Quantification and Characterization of Maghemite in Soils Derived from Volcanic Rocks in Southern Brazil. *Clays and Clay Minerals* 47:466–473. doi: 10.1346/CCMN.1999.0470408

Craine JM, Elmore AJ, Wang L, Augusto L, Baisden WT, Brookshire ENJ, Cramer MD, Hasselquist NJ, Hobbie EA, Kahmen A, Koba K, Kranabetter JM, Mack MC, Marin-Spiotta E, Mayor JR, McLauchlan KK, Michelsen A, Nardoto GB, Oliveira RS, Perakis SS, Peri PL, Quesada CA, Richter A, Schipper LA, Stevenson BA, Turner BL, Viani RAG, Wanek W, Zeller B (2015) Convergence of soil nitrogen isotopes across global climate gradients. *Scientific Reports* 5:8280. doi: 10.1038/srep08280

Davidson EA (2015) Soil carbon in a beer can. *Nature Geoscience* 8:748–749. doi: 10.1038/ngeo2522

Dearing JA (1994) Environmental magnetic susceptibility. Using the Bartington MS2 system. British Library, England.

Dearing J (1999) Environmental Magnetic Susceptibility Using the Bartington MS2 System, Second. Chi Publ, Kenilworth, UK

Fernandes LA (2004) Mapa litoestratigráfico da parte oriental da Bacia Bauru (PR, SP, MG), escala 1:1.000.000. *Boletim Paranaense de Geociencias* 53–66. doi: 10.5380/geo.v55i0.4283

Fernandes LA, de Castro AB, Basilici G (2007) Seismites in continental sand sea deposits of the Late Cretaceous Caiuá Desert, Bauru Basin, Brazil. *Sedimentary Geology*

199:51–64. doi: 10.1016/j.sedgeo.2005.12.030

Fissore C, Dalzell BJ, Berhe AA, Voegtle M, Evans M, Wu A (2017) Influence of topography on soil organic carbon dynamics in a Southern California grassland. *Catena* 149:140–149. doi: 10.1016/j.catena.2016.09.016

Friedman JH (2002) Stochastic gradient boosting. *Computational Statistics and Data Analysis* 38:367–378. doi: 10.1016/S0167-9473(01)00065-2

Friedman JH (2001) Greedy function machine: A gradient boosting machine. *The Annals of Statistics* 29:1189–1232. doi: doi:10.1214/aos/1013203451

Gomes LC, Faria RM, de Souza E, Veloso GV, Schaefer CEGR, Filho EIF (2019) Modelling and mapping soil organic carbon stocks in Brazil. *Geoderma* 340:337–350. doi: 10.1016/j.geoderma.2019.01.007

Greenwell B, Boehmke B, Cunningham J and GBM Developers (2019). gbm: Generalized Boosted Regression Models. R package version 2.1.5. <https://CRAN.R-project.org/package=gbm>

Grimm R, Behrens T, Märker M, Elsenbeer H (2008) Soil organic carbon concentrations and stocks on Barro Colorado Island — Digital soil mapping using Random Forests analysis. *Geoderma* 146:102–113. doi: 10.1016/j.geoderma.2008.05.008

Hastie T, Tibshirani R, Friedman J (2009) *The Elements of Statistical Learning*. Springer New York, New York, NY

Hengl T, De Jesus JM, Heuvelink GBM, Gonzalez MR, Kilibarda M, Blagotić A, Shangguan W, Wright MN, Geng X, Bauer-Marschallinger B, Guevara MA, Vargas R, MacMillan RA, Batjes NH, Leenaars JGB, Ribeiro E, Wheeler I, Mantel S, Kempen B (2017) SoilGrids250m: Global gridded soil information based on machine learning. *PLoS ONE* 12:1–40. doi: 10.1371/journal.pone.0169748

Hijmans RJ, Cameron SE, Parra JL, Jones PG, Jarvis A (2005) Very high resolution interpolated climate surfaces for global land areas. *International Journal of Climatology* 25:1965–1978. doi: 10.1002/joc.1276

Jarvis A, Reuter HI, Nelson A, Guevara E (2008). Hole-filled SRTM for the globe Version 4. available from the CGIAR-CSI SRTM 90m Database ([http://srtm.cgiar.org](http://srtm.csi.cgiar.org)), 15, 25-54.

- Jakšík O, Kodešová R, Kapička A, Klement A, Fér M, Nikodem A (2016) Using magnetic susceptibility mapping for assessing soil degradation due to water erosion. *Soil and Water Research* 11:105–113. doi: 10.17221/233/2015-SWR
- Jenny H (1941) Factors of Soil Formation: A System of Quantitative Pedology, McGraw-Hil. Dover Publications, New York
- Jobágyi EG, Jackson RB (2000) The vertical distribution of soil organic carbon and its relation to climate and vegetation. *Ecological Applications* 10:423–436. doi: [https://doi.org/10.1890/1051-0761\(2000\)010\[0423:TVDOSO\]2.0.CO;2](https://doi.org/10.1890/1051-0761(2000)010[0423:TVDOSO]2.0.CO;2)
- Jordanova N, Jordanova D, Liu Q, Hu P, Petrov P, Petrovský E (2013) Soil formation and mineralogy of a Rhodic Luvisol - insights from magnetic and geochemical studies. *Global and Planetary Change* 110:397–413. doi: 10.1016/j.gloplacha.2013.08.020
- Kaiser K, Guggenberger G (2000) The role of DOM sorption to mineral surfaces in the preservation of organic matter in soils. *Organic Geochemistry* 31:711–725. doi: 10.1016/S0146-6380(00)00046-2
- Keskin H, Grunwald S, Harris WG (2019) Digital mapping of soil carbon fractions with machine learning. *Geoderma* 339:40–58. doi: 10.1016/j.geoderma.2018.12.037
- Kuhn M (2008) Building Predictive Models in R Using the caret Package. *Journal Of Statistical Software* 28:1–26. doi: 10.1053/j.sodo.2009.03.002
- Liao JD, Boutton TW, Jastrow JD (2006a) Organic matter turnover in soil physical fractions following woody plant invasion of grassland: Evidence from natural ^{13}C and ^{15}N . *Soil Biology and Biochemistry* 38:3197–3210. doi: 10.1016/j.soilbio.2006.04.004
- Liao JD, Boutton TW, Jastrow JD (2006b) Organic matter turnover in soil physical fractions following woody plant invasion of grassland: Evidence from natural ^{13}C and ^{15}N . *Soil Biology & Biochemistry* 38:3197–3210. doi: 10.1016/j.soilbio.2006.04.004
- Lutzow M v., Kogel-Knabner I, Ekschmitt K, Matzner E, Guggenberger G, Marschner B, Flessa H (2006) Stabilization of organic matter in temperate soils: mechanisms and their relevance under different soil conditions - a review. *European Journal of Soil Science* 57:426–445. doi: 10.1111/j.1365-2389.2006.00809.x

- Marin-Spiotta E, Silver WL, Swanston CW, Oster tag R (2009) Soil organic matter dynamics during 80 years of reforestation of tropical pastures. *Global Change Biology* 15:1584–1597. doi: 10.1111/j.1365-2486.2008.01805.x
- Marques Jr. J, Alleoni LRF, Teixeira D de B, Siqueira DS, Pereira GT (2015) Sampling planning of micronutrients and aluminium of the soils of São Paulo, Brazil. *Geoderma Regional* 4:91–99. doi: <http://dx.doi.org/10.1016/j.geodrs.2014.12.004>
- Marques Jr. J, Siqueira DS, Camargo LA, Teixeira DDB, Barrón V, Torrent J (2014) Magnetic susceptibility and diffuse reflectance spectroscopy to characterize the spatial variability of soil properties in a Brazilian Haplustalf. *Geoderma* 219–220:63–71. doi: 10.1016/j.geoderma.2013.12.007
- McBratney A., Mendonça Santos M., Minasny B (2003) On digital soil mapping. *Geoderma* 117:3–52. doi: 10.1016/S0016-7061(03)00223-4
- McBratney A, Field D (2015) Securing our soil. *Soil Science and Plant Nutrition* 61:587–591. doi: 10.1080/00380768.2015.1071060
- McBratney AB, Minasny B, Viscarra Rossel R (2006) Spectral soil analysis and inference systems: A powerful combination for solving the soil data crisis. *Geoderma* 136:272–278. doi: 10.1016/j.geoderma.2006.03.051
- McCorkle EP, Berhe AA, Hunsaker CT, Johnson DW, McFarlane KJ, Fogel ML, Hart SC (2016) Tracing the source of soil organic matter eroded from temperate forest catchments using carbon and nitrogen isotopes. *Chemical Geology* 445:172–184. doi: 10.1016/j.chemgeo.2016.04.025
- McNally SR, Beare MH, Curtin D, Meenken ED, Kelliher FM, Calvelo Pereira R, Shen Q, Baldock J (2017) Soil carbon sequestration potential of permanent pasture and continuous cropping soils in New Zealand. *Global Change Biology* 23:4544–4555. doi: 10.1111/gcb.13720
- Nauman TW, Thompson JA (2014) Semi-automated disaggregation of conventional soil maps using knowledge driven data mining and classification trees. *Geoderma* 213:385–399. doi: 10.1016/j.geoderma.2013.08.024
- Peixoto CAB (2010) Geodiversidade do Estado de São Paulo, CPRM. São Paulo
- Pingguo Yang, Byrne JM, Yang M (2016) Spatial variability of soil magnetic

susceptibility, organic carbon and total nitrogen from farmland in northern China. *Catena* 145:92–98. doi: 10.1016/j.catena.2016.05.025

Pouladi N, Møller AB, Tabatabai S, Greve MH (2019) Mapping soil organic matter contents at field level with Cubist, Random Forest and kriging. *Geoderma* 342:85–92. doi: 10.1016/j.geoderma.2019.02.019

Prasad AM, Iverson LR, Liaw A (2006) Newer classification and regression tree techniques: Bagging and random forests for ecological prediction. *Ecosystems* 9:181–199. doi: 10.1007/s10021-005-0054-1

Quijano L, Chaparro MAE, Marie DC, Gaspar L, Navas A (2014) Relevant magnetic and soil parameters as potential indicators of soil conservation status of Mediterranean agroecosystems. *Geophysical Journal International* 198:1805–1817. doi: 10.1093/gji/ggu239

R Core Team (2019) R: A language and environment for statistical computing. R Foundation for Statistical Computing, Vienna, Austria. URL <https://www.R-project.org/>

Rabus B, Eineder M, Roth A, Bamler R (2003). The shuttle radar topography mission - a new class of digital elevation models acquired by spaceborne radar. *ISPRS journal of photogrammetry and remote sensing*, 57(4), 241-262.

Rodriguez-Galiano VF, Chica-Rivas M (2014) Evaluation of different machine learning methods for land cover mapping of a Mediterranean area using multi-seasonal Landsat images and Digital Terrain Models. *International Journal of Digital Earth* 7:492–509. doi: 10.1080/17538947.2012.748848

Running S, Mu Q, Zhao M. MOD17A2H MODIS/Terra Gross Primary Productivity 8-Day L4 Global 500m SIN Grid V006. (2015), distributed by NASA EOSDIS Land Processes DAAC, <https://doi.org/10.5067/MODIS/MOD17A2H.006>

Schmidt MWI, Torn MS, Abiven S, Dittmar T, Guggenberger G, Janssens IA, Kleber M, Kögel-Knabner I, Lehmann J, Manning DAC, Nannipieri P, Rasse DP, Weiner S, Trumbore SE (2011) Persistence of soil organic matter as an ecosystem property. *Nature* 478:49–56. doi: 10.1038/nature10386

Six J, Conant RT, Paul EA, Paustian K (2002) Stabilization mechanisms of soil organic

matter: Implications for C-saturation of soils. *Plant and soil* 241:155–176. doi: <https://doi.org/10.1023/A:1016125726789>

Smith P, House JI, Bustamante M, Sobocka J, Harper R, Pan G, West PC, Clark JM, Adhya T, Rumpel C, Paustian K, Kuikman P, Cotrufo MF, Elliott JA, McDowell R, Griffiths RI, Asakawa S, Bondeau A, Jain AK, Meersmans J, Pugh TAM (2016) Global change pressures on soils from land use and management. *Global Change Biology* 22:1008–1028. doi: 10.1111/gcb.13068

Soares Neto GB, Martins ÉDS (2019) Método semiautomático de delimitação das Unidades Básicas de Relevo. *Revista Brasileira de Geomorfologia* 20:. doi: 10.20502/rbg.v20i2.1403

Teixeira DDB, Bicalho E da S, Panosso AR, Cerri CEP, Pereira GT, La Scala Júnior N (2013) Spatial variability of soil CO₂ emission in a sugarcane area characterized by secondary information. *Scientia Agricola* 70:195–203. doi: 10.1590/S0103-90162013000300008

Torrent J, Liu QS, Barrón V (2010) Magnetic minerals in Calcic Luvisols (Chromic) developed in a warm Mediterranean region of Spain: Origin and paleoenvironmental significance. *Geoderma* 154:465–472. doi: 10.1016/j.geoderma.2008.06.020

Trabucco A, Zomer R (2019): Global Aridity Index and Potential Evapotranspiration (ET₀) Climate Database v2. figshare. Dataset. doi: 10.6084/m9.figshare.7504448.v3

Veronesi F, Schillaci C (2019) Comparison between geostatistical and machine learning models as predictors of topsoil organic carbon with a focus on local uncertainty estimation. *Ecological Indicators* 101:1032–1044. doi: 10.1016/j.ecolind.2019.02.026

Venables B, Hornik K, Maechler M (2019). polynom: A Collection of Functions to Implement a Class for Univariate Polynomial Manipulations. R package version 1.4-0.

Viscarra Rossel RA, Webster R, Bui EN, Baldock JA (2014) Baseline map of organic carbon in Australian soil to support national carbon accounting and monitoring under climate change. *Global Change Biology* 20:2953–2970. doi: 10.1111/gcb.12569

Vos C, Don A, Hobley EU, Prietz R, Heidkamp A, Freibauer A (2019) Factors controlling the variation in organic carbon stocks in agricultural soils of Germany. European Journal of Soil Science 70:550–564. doi: 10.1111/ejss.12787

Weintraub SR, Taylor PG, Porder S, Cleveland CC, Asner GP, Townsend AR (2015) Topographic controls on soil nitrogen availability in a lowland tropical forest. Ecology 96:1561–1574. doi: 10.1890/14-0834.1

Wiesmeier M, Urbanski L, Hobley E, Lang B, von Lützow M, Marin-Spiotta E, van Wesemael B, Rabot E, Ließ M, Garcia-Franco N, Wollschläger U, Vogel H-J, Kögel-Knabner I (2019) Soil organic carbon storage as a key function of soils - A review of drivers and indicators at various scales. Geoderma 333:149–162. doi: 10.1016/j.geoderma.2018.07.026

Wood J (1996) The Geomorphological Characterization of Digital Elevation Models. Ph.D. Thesis, Department of Geography, University of Leicester, UK.

Yamamoto JK, and Landim PMB (2015) Geoestatística: conceitos e aplicações.

Young M (1978) Terrain analysis: program documentation. Report 5 on Grant DA-ERO-591-73- G0040, Statistical characterization of altitude matrices by computer. Department of Geography, University of Durham, England. 27 p.

Capítulo 2 – Relationships between soil organic matter stabilization and mineralogy in highly weathered soils from southeastern Brazil

Abstract

Few studies have investigated the mineralogical controls over soil organic matter (SOM) in tropical soils. Clay is a factor known for stabilizing enriched nitrogen stable isotope ($\delta^{15}\text{N}$) in SOM. However, clay-sized particles have different potentials to stabilize SOM. This work aimed to investigate the relationship of iron (Fe) oxides with SOM. Were tested the suitability of magnetic susceptibility (MS), iron dithionite (Fed), iron oxalate (Feo), hematite (Hm), and goethite (Gt) to predict carbon (C), and $\delta^{15}\text{N}$ in the Oxisols of the Western Paulista Plateau (WPP). Were sampled 18 representative points through the WPP landscape, 9 points for each geological domain (Domain of Sedimentary and volcano-sedimentary of Mesozoic and Paleozoic deposits – DSVMP, and Domain of Mesozoic fissural volcanism of plateau type – DVM). The mean comparison geological domains showed higher values of Fed, Feo, Hm, Gt, Clay, Ms_{lf}, C, and $\delta^{15}\text{N}$ in Oxisols from DVM. The most markable correlations of $\delta^{15}\text{N}$ with soil attributes were those with Hm, Fe_d, MS_{lf}, Clay, Fe_o, the same pattern was observed for C. Further, were built a series of multiple linear models modeling C and $\delta^{15}\text{N}$ in function of MS_{lf}, MS_{fd%}, Fe_d/Fe_o, [Hm/(Hm+Gt)], and Silt/Clay. From the selected models were found significant relationships between C with MS_{lf} and Silt/Clay ratio, and $\delta^{15}\text{N}$ to MS_{lf} and [Hm/(Hm+Gt)]. The results corroborate that Fe metrics can help to explain SOM stabilization in tropical soils. Additionally, the results also indicate that well-crystallized minerals are providing important mechanisms for storage and stabilizing SOM, in highly weathered soils.

Keywords: carbon, nitrogen, isotope, magnetism, iron oxides, tropical soils

1. Introduction

Due to the critical role of SOM to biogeochemical processes in terrestrial ecosystems, several studies have been carried out in natural systems and agroecosystems. Society demands better understand the mechanisms that control SOM (Minasny et al. 2017). At least 3.5 Pg year⁻¹ of CO₂ emitted to the atmosphere lays on the decomposition of SOM (Houghton et al. 2007). The longevity of SOM, also known as persistence of SOM, is an ecosystem property which is influenced by the interaction of physical, chemical, and biological factors (Schmidt et al. 2011). Although recent studies have been debated the importance of mineral mediated stabilization of SOM (Torn et al. 1997; Schmidt et al. 2011; Doetterl et al. 2015), few studies have investigated the mineralogical controls over SOM in tropical ecosystems (Trumbore 2000; Marin-Spiotta et al. 2008; Coward et al. 2017).

Clays have been reported as a factor contributing to stabilizing enriched δ¹⁵N in SOM (Craine et al. 2015). However, clay size particles have different potentials to stabilize SOM (Rasmussen et al. 2018). Positive relationships among pedogenic Fe-oxides and SOM has been found from local to global scales, pointing out these minerals as relevant drivers of SOM stabilization (Kaiser and Guggenberger 2000; Coward et al. 2017; Hall et al. 2018).

The 2:1 phyllosilicate clay minerals matrices are associated with SOM stabilization, but 1:1 phyllosilicate mineralogy is the more frequent in tropical soils (Kaiser and Guggenberger 2003). Fe oxides can develop an important role for SOM stabilization in tropical soils (Khomoto et al. 2017; Coward et al. 2017; Hall et al. 2018). Magnetite – Mt (Fe₃O₄), maghemite – Mgh (γ-Fe₂O₃), Hematite – Hm (α-Fe₂O₃), and Goethite – Gt (α-FeOOH) are secondary Fe oxides commonly found in tropical and subtropical soils (Schwertmann and Taylor 1989). Mt and Mgh shows strong magnetizations in soils, and are less abundant than Hm and Gt, which are antiferromagnetic (Long et al. 2015).

An efficient technique to identify magnetism and its relationship between soil properties is the magnetic susceptibility (MS) (Grimley and Vepraskas 2000; Siqueira et al. 2010). MS measures how much a mineral is magnetizable (Dearing 1994), and it depends on inherent characteristics of magnetic minerals present in soil (Torrent et al. 2006; Torrent et al. 2007), MS has been presented with potential to identify soil formation

process in tropical landscape contexts (Marques Jr. et al. 2014). MS has presented correspondence between SOM and mineral magnetic parameters with significant correlations between low-frequency MS (MS_{lf}) and C (Jakšík et al. 2016; Jordanova et al. 2013). As MS is a proxy for magnetic Fe oxides (Dearing 1994), the binding of SOM to mineral surfaces (Adhikari et al. 2016; Coward et al. 2017; Hall et al. 2018; Khomo et al. 2017; Lützow et al. 2006) can explain the relations between C and MS.

Most of Oxisols started their development in Tertiary epochs, being considered the oldest soils in the terrestrial crust, and are very prevalent in the Brazilian territory (Schaefer 2001). There is a growing demand to better understand mechanisms between geochemistry and SOM stabilization (Doetterl et al. 2015) specially iron oxides (Adhikari et al. 2016; Coward et al. 2017; Hall et al. 2018; Khomo et al. 2017; Lützow et al. 2006) in highly weathered soils. This study aimed to investigate the relationship of Fe oxides with SOM, testing the inference suitability of MS_{lf} , $MS_{fd\%}$ and some Fe metrics (Fe_d , Fe_o , Hm , and Gt) with C, and $\delta^{15}N$ in Oxisols from the Western Paulista Plateau, a southeastern Brazilian landscape.

2. Material and Methods

2.1 Field study area

The Western Paulista Plateau (WPP) corresponds to 48% of São Paulo area, a Brazilian state that holds an area of 13 million hectares. The Western Paulista Plateau is compartmentalized in two geological domains (Figure 1): i. Domain of sedimentary and volcano-sedimentary of Mesozoic and Paleozoic deposits, little to moderately consolidated, associated with large and deep sedimentary basins of the syncline type (DSVMP); and Domain of Mesozoic fissural volcanism of plateau type (DVM) (Peixoto 2010). The geological outline is characterized by sandy, clay and gravel sediments, volcanic basic rocks, and mainly psammitic sedimentary sequences, which may include pyroclastic. The WPP geological formations are divided into two groups: i Caiuá Group, composed by the Santo Anastácio and Paraná River Formations in the state of São Paulo, corresponding to deposits of dry climate sand, accumulated in long and monotonous desert plains, margins of the large sand dune complexes (Caiuá Desert) extending to the northern region of the state of Paraná; and Bauru Group, which consists of the Uberaba, Rio do Peixe Valley, Araçatuba, São José do Rio Preto, Presidente Prudente and Marília

formations. It also includes the Taiúva Analcimites, volcanic rocks locally interspersed in sequence (Fernandes 2004; Fernandes et al. 2007)

The area has a Tropical Atlantic morphoclimatic regime (sea of hills and forested plateaus) (Ab'Saber 1977). According to the Köppen's climate classification map for Brazil (Alvares et al. 2013), the predominant climates are Aw with dry winter, Cfa with hot summer and Cwa with dry winter and hot summer. The natural vegetation of Western Paulista Plateau was Atlantic Forest in the West and Cerrado in the East and Southwest, and the current most representative land use is sugarcane and pasture.

2.2 Sampling design

Were collected 300 soil samples distributed in a grid considering the whole Western Paulista Plateau, 0-20 cm depth, using a Dutch auger. The distance among points ranged between 10km and 60km. The grid was applied to provide a good representation of landscape compartments (relief, geology, soils, stratigraphy, climate, landforms, natural vegetation, and mainly crops). The number of samples was enough to attend the requirements in the first variogram lags (n° pairs > 30), following Yamamoto and Landim (2013), and the experience acquired in previous works applying geostatistics in the Western Paulista Plateau (Teixeira et al. 2013; Marques Jr. et al. 2015).

From the 300 sampling points, were selected 22 points simulating stratified sampling (Dinkins et al. 2008), to do more sophisticated analysis as diffuse reflectance spectroscopy. These points are representative of the landscape compartments that causes variability. In addition to the landscape compartments, were guided the selection of points by the variability map ($n=300$) of iron dithionite – Fe_d (well-crystallized pedogenic minerals), iron oxalate – Fe_o (less crystallized pedogenic minerals) and magnetic susceptibility (MS). This proceeding granted the same reference interval, being representative of data variation. From the 22 selected areas, were selected 18 points sampling units to perform this study only in Oxisols (Figure 1).

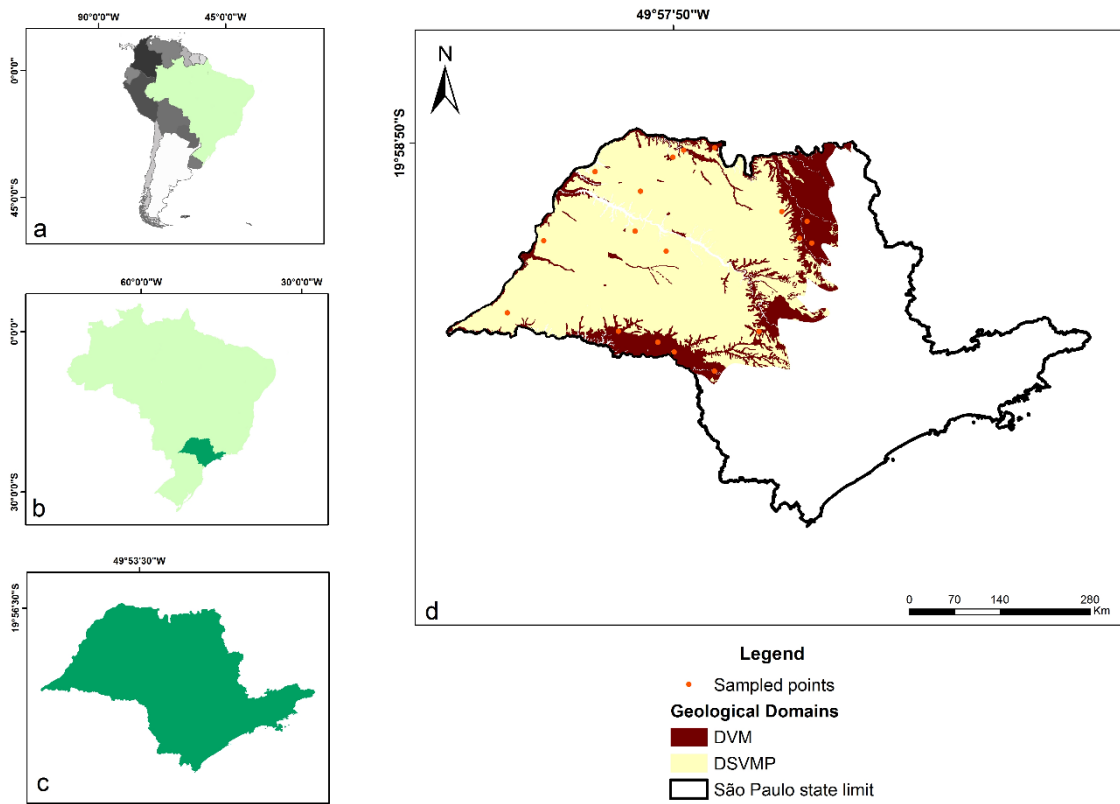


Figure 1. Field study localization context. (a) Highlights Brazil in Latin America context; (b) indicates São Paulo state localization in Brazil; (b) São Paulo state; (b) Western Paulista Plateau area, Geological Domains, and location of 18 sampled points ($n=18$). DSVMP – Domain of sedimentary and volcano-sedimentary of Mesozoic and Paleozoic deposits, little to moderately consolidated, associated with large and deep sedimentary basins of the syncline type; DVM – Domain of Mesozoic fissural volcanism of plateau type.

2.3 Laboratory analysis

Soil granulometry analysis was determined using the pipette method employing 0.1 mol L^{-1} NaOH solution as a dispersant following the procedure described by Donagema (2011). The magnetic susceptibility was determined through a Bartington MS2, coupled to a sensor Bartington MS2B, measuring in low frequency (lf: 0.47 kHz) and high frequency (hf: 4.7 kHz) (Dearing 1994; Costa et al. 1999). Measures in double frequency can be used to indicate the presence of magnetic materials of simple or multiple domains. The value of MS, expressed here in $10^{-6} \text{ m}^3 \text{ kg}^{-1}$, was measured at two frequencies (lf = 0.47 kHz and hf = 4.7 kHz) with a Bartington MS2B dual-frequency sensor (Bartington Instruments Ltd., Oxford, UK). The relative magnetic susceptibility frequency dependent (MS_{fd}%) defined as $100 \times \text{MS}_{\text{lf}} - \text{MS}_{\text{hf}} / \text{MS}_{\text{lf}}$, was then calculated to determine the relative variations in the grain size distribution of pedogenic maghemite

particles. The free iron-oxide contents were extracted using dithionite-citrate-bicarbonate (DCB) solution (Mehra and Jackson 1960), denoted Fe_d . The levels of low-crystallinity oxides, denoted Fe_o , were determined by extraction with ammonium (acid) oxalate solution (c) adapted from Schwertmann (1973).

To characterize hematite (Hm) and goethite (Gt) was conducted a Diffuse Reflectance Spectroscopy analysis on bulk soil using a Lambda 950 (UV/Vis/NIR) spectrophotometer (Perkin Elmer Ltd., Waltham, MA, EUA), coupled to an integrative sphere with 150 mm diameter. Soil samples were grounded to powder, with constant color, on agate mortar and pestle. The spectra were recorded in 0.5 nm intervals, with time integration of 2.43 nm s⁻¹ with an interval between 250 to 2500 nm (VIS and NIR). The powder halon (PTFE) was used as a background reference. To identify goethite (Gt), the minimum intervals were of 415-425 nm, and the maximum of 440-450nm. To identify hematite (Hm), the minimum intervals were 530-545, and maximum of 575-590nm, according to Torrent and Barrón (2008). The spectral data were used to calculate the second derivate of the Kubelka-Munk function over the wavelength range of 380–710 nm (Kubelka and Munk 1931). A spline procedure involving 30 data points was used to estimate the [Hm/(Hm+Gt)] ratio, according to Scheinost et al. (1998).

To do elementary and isotope analysis, every soil sample was air-dried, dismantled, and passed through a 2-mm sieve. Roots and plant material were removed before weight samples of 30 to 35 mg of soil was weighed and packed in tin capsules and loaded into an elemental analyzer (Carlo Erba, model 1110, Milan, Italy), which determine C concentration by combustion. The product of the combustion is purified in a chromatography column and placed directly in a mass spectrometer to the isotopic ratio (ThermoQuest-Finnigan Delta Plus, Finnigan-MAT, California, USA). The natural abundance of and $\delta^{15}\text{N}$ is expressed as deviations per thousand (‰) from an internationally recognized standard, through the equation $\delta = (\text{R sample} / \text{R standard} - 1) \times 1000$, where R is the molar ratio of $^{15}\text{N}/^{14}\text{N}$ in the sample and standard. The standard for N is atmospheric air. The acceptable analytical error to C and $\delta^{15}\text{N}$ is 0.15‰, and 0.30‰, respectively. All samples elemental and isotopic analysis were carried out at the Laboratory of Isotopic Ecology, on the Center to Nuclear Agriculture (CENA), University of São Paulo.

2.4 Data Analysis

The data were analyzed by descriptive statistics, calculating the mean, minimum and maximum values, variance, standard deviation (SD). The relationships between dependent variables (C and $\delta^{15}\text{N}$), and independent variables (MS_{lf}, MS_{fd%}, Fe_d, Fe_o, Hm, Gt) were evaluated using linear regressions (n=18 samples for regressions). Further, a series of multiple linear models were built in R, modeling dependent variables (C and $\delta^{15}\text{N}$), as a function of the independent variables (MS_{lf}, MS_{fd%}, Fe_d/Fe_o, [Hm/(Hm+Gt)], Silt/Clay). Between all the independent variables used, were selected the best fixed-effect structure based on Akaike information criterion corrected for small samples (AIC_C) using the *model.sel* function using package MuMIn (Barton 2019). From the chosen model, were ranked all possible models also according to their AIC_C coefficients using package MuMIn (Barton 2019). Based on this theoretical information approach, the predictor importance was measured by the sum of the AIC_C weights for all models that pursue the predictor (Burnham and Anderson 2002). Independent variables were log+1 transformed when necessary to attempt linear model assumptions. After tests for normality and homoscedasticity, were performed mean comparisons between geological domains (DVM and DSVMP) using the Mann-Whitney U-test for non-parametric populations and T-test for parametric populations.

3. Results

The descriptive statistics results of topsoil (0-20 cm) properties are presented in Table 1.

Table 1. Descriptive statistics for the topsoil (0-20 cm) properties, of Oxisols from Western Paulista Plateau.

Variable	DVM				
	Min	Median	Mean	Max	SD
C (%)	0.7	2.0	1.8	2.6	0.5
$\delta^{15}\text{N} (\text{\textperthousand})$	6.4	7.0	7.3	8.7	0.9
MS _{lf} ($10^{-6} \text{ m}^3 \text{ kg}^{-1}$)	6.15	41.98	39.65	74.72	21.53
MS _{hf} ($10^{-6} \text{ m}^3 \text{ kg}^{-1}$)	5.54	37.97	36.16	67.67	19.77

MS_{fd}(%)	6.09	8.71	9.23	16.61	2.89
Clay (g kg⁻¹)	150.50	476.00	449.50	610.00	138.78
Silt (g kg⁻¹)	77.95	236.50	255.53	490.53	139.19
Sand (g kg⁻¹)	86.47	264.50	294.96	702.52	204.65
Fe_d (g kg⁻¹)	32.60	78.59	75.06	86.27	15.23
Fe_o (g kg⁻¹)	0.49	2.37	2.16	3.53	1.03
Hm (g kg⁻¹)	28.25	70.75	71.35	107.04	21.89
Gt (g kg⁻¹)	5.54	42.16	36.57	57.04	18.57
Fe_d/Fe_o	0.01	0.03	0.02	0.04	0.01
Hm/(Hm+Gt)	0.51	0.60	0.66	0.94	0.14
Silt/Clay	0.139	0.58	0.62	1.15	0.33

DSVMP					
Variables	Min	Median	Mean	Max	SD
C (%)	0.35	0.64	0.81	2.06	0.55
δ¹⁵N (‰)	4.46	6.07	5.89	7.15	1.00
MS_{lf} (10⁻⁶ m³ kg⁻¹)	0.39	1.37	1.85	4.19	1.26
MS_{hf} (10⁻⁶ m³ kg⁻¹)	0.34	1.20	1.62	3.57	1.10
MS_{fd} (%)	8.94	12.66	12.46	14.80	1.65
Clay (g kg⁻¹)	87.00	163.50	157.30	211.50	47.46
Silt (g kg⁻¹)	79.63	118.99	178.63	500.24	140.98
Sand (g kg⁻¹)	298.80	722.00	664.10	817.60	167.44
Fe_d (g kg⁻¹)	13.52	22.63	25.49	42.22	9.68
Fe_o (g kg⁻¹)	0.16	0.64	0.67	1.32	0.32
Hm (g kg⁻¹)	7.31	18.31	21.15	37.74	9.92
Gt (g kg⁻¹)	10.44	13.73	15.94	27.15	6.13
Fe_o/Fe_d	0.01	0.02	0.02	0.05	0.01
Hm/(Hm+Gt)	0.37	0.56	0.55	0.71	0.10
Silt/Clay	0.43	0.93	1.12	2.38	0.65

C: carbon; δ¹⁵N: nitrogen isotope ratio; MS_{lf}: low-frequency magnetic susceptibility; MS_{hf}: high-frequency magnetic susceptibility; MS_{fd}%: magnetic susceptibility frequency per unit mass; Clay: clay content; Silt: silt content; Sand: sand content; Fe_d: iron extracted with dithionite citrate and sodium bicarbonate; Fe_o: iron extracted with ammonium acid oxalate; Hm: hematite; Gt: goethite; Feo/Fed: ratio of oxalate to dithionite-extracted iron; [Hm/(Hm+Gt)]: hematite goethite ratio; Silt/Clay: silt clay ratio.

The mean values of iron oxides extracted by dithionite-citrate-bicarbonate (Fed) showed significant differences among the geological domains DVM and DSVMP ($U=2$, $p<0.001$) (Table 1). The same pattern was observed for Feo ($U=8$; $p<0.001$), hematite (Hm) ($t(16)$: -5.9856, $p<0.001$), goethite (Gt) ($U=14$, $p<0.001$), carbon (C) ($U=9$, $p<0.005$), and $\delta^{15}\text{N}$, $t(16) = -3.2637$, $p<0.005$ (Table 1). Nevertheless, [Hm/(Hm+Gt)] and Fe_d/Fe_o ratio were similar among geological domains. Sand and Clay also showed significant differences between geological domains. Sand presented the higher values in DSVMP ($U=74$, $p<0.005$), while the higher values of Clay were found in DVM, $t(16)=-5.6659$, $p<0.001$. Silt content was similar between geological domains, and the same pattern was also observed for Silt/Clay ratio. The MS_{lf} followed the same trend of Fe metrics and clay content, showing the higher mean values in DVM, $t(16):-8.9808$, $p<0.001$). However, MS_{fd%} showed the higher values in DSVMP, $U= 68$, $p<0.05$ (Table 1). The Fe_o/Fe_d ratios for all samples were bellow of 0.05 (Table 2), and the [Hm/(Hm+Gt)] showed a predominance of Hm over Gt (Table 2)

MS_{lf}, Clay, Fe_d, and Fe_o showed significant relationships with C (R^2 ranging from 40 to 72%) and N (R^2 ranging from 40 to 74%) (Table 2). The simple linear model results for $\delta^{15}\text{N}$ showed values of R^2 (ranging from 26 to 61%). Soil showed a trend to be more enriched in $\delta^{15}\text{N}$, as the concentrations of Fe metrics increased (Table 2). The most markable correlations of $\delta^{15}\text{N}$ with soil attributes were those with Hm, Fe_d, MS_{lf}, Clay, Fe_o, (Table 2), and the same pattern was observed for C (Table 2).

Table 2. Regression results for topsoil C and $\delta^{15}\text{N}$ vs. Fe compositional metrics.

Variable	%C						
	Intercept	Estimate	t value	R²	Adj. R²	F-statistic	p-value
MS_{lf}	0.46 ± 0.23	0.38 ± 0.08	4.430	0.551	0.523	19.650	0.000
MS_{hf}	0.49 ± 0.23	0.38 ± 0.08	4.408	0.548	0.520	19.430	0.000
MS_{fd%}	2.29 ± 0.67	-0.08 ± 0.06	-1.402	0.109	0.054	1.965	0.180
Clay	0.27 ± 0.19	0.003 ± 0.001	6.515	0.726	0.709	42.440	0.000
F_d	0.34 ± 0.26	0.01 ± 0.004	4.450	0.553	0.525	19.810	0.000
Fe_o	0.72 ± 0.24	0.43 ± 0.13	3.331	0.410	0.373	11.100	0.004
Hm	0.53 ± 0.24	0.01 ± 0.004	4.102	0.513	0.482	16.820	0.001
Gt	0.86 ± 0.30	0.01 ± 0.009	1.994	0.199	0.149	3.978	0.063
Fe_o/F_d	1.31 ± 0.43	2.17 ± 13.69	0.159	0.002	0.000	0.025	0.876

Hm/(Hm+Gt)	0.42 ± 0.80	1.55 ± 1.27	1.210	0.085	0.028	1.486	0.241
$\delta^{15}\text{N}$							
Variable	Intercept	Estimate	t value	R²	Adj. R²	F-statistic	p-value
MS_{lf}	5.42 ± 0.42	0.52 ± 0.15	3.464	0.429	0.393	12.000	0.003
MS_{hf}	5.46 ± 0.41	0.53 ± 0.15	3.465	0.429	0.393	12.000	0.003
MS_{fd%}	8.52 ± 0.99	-0.17 ± 0.09	-1.907	0.185	0.134	3.635	0.075
Clay	5.56 ± 0.48	0.003 ± 0.001	2.667	0.308	0.265	7.115	0.017
Fe_d	5.19 ± 0.44	0.02 ± 0.007	3.783	0.472	0.439	14.310	0.002
Fe_o	5.84 ± 0.41	0.56 ± 0.22	2.478	0.277	0.232	6.141	0.025
Hm	5.24 ± 0.33	0.02 ± 0.005	5.044	0.614	0.590	25.440	0.000
Gt	6.35 ± 0.52	0.01 ± 0.01	0.733	0.033	-0.028	0.538	0.474
Fe_o/Fe_d	7.06 ± 0.67	-13.14 ± 21.03	21.038	0.020	0.000	0.390	0.541
[Hm/(Hm+Gt)]	3.21 ± 0.95	5.63 ± 1.52	3.701	0.461	0.428	13.700	0.002

MS_{lf}: low-frequency magnetic susceptibility; MS_{hf}: high-frequency magnetic susceptibility; MS_{fd%}: magnetic susceptibility frequency per unit mass; Clay: clay content; Silt: silt content; Sand: sand content; Fe_d: iron extracted with dithionite citrate and sodium bicarbonate; Fe_o: iron extracted with ammonium acid oxalate; Hm: hematite; Gt: goethite; Fe_o/Fe_d: ratio of oxalate to dithionite-extracted iron; [Hm/(Hm+Gt)]: hematite goethite ratio; Silt/Clay: silt clay ratio.

From the selected model, significant relationships were found between C to MS_{lf} and Silt/Clay ratio (Table 3), and $\delta^{15}\text{N}$ to MS_{lf} and [Hm/(Hm+Gt)] (Table 4). The full linear model relating C to MS_{lf} and Silt/Clay ratio (Figure 2) had significant correlation ($F_{2,15} = 16.04$, $p < 0.001$, $R^2 = 0.68$, $R^2_{adj} = 0.63$). The linear model relating $\delta^{15}\text{N}$ to MS_{lf} and [Hm/Hm+Gt] (Figure 2) was also significant ($F_{2,15} = 12.11$, $p < 0.001$, $R^2 = 0.62$, $R^2_{adj} = 0.57$). Based on the model averaging analysis, and relative importance of each variable, MS_{lf} was significant in all models tested for C (Table 3), while for $\delta^{15}\text{N}$, MS_{lf} was significant in 86% of the tested models (Table 4).

Table 3. Model selection and model-averaged coefficients, and relative importance of multiple linear models relating C to [Hm/Hm+Gt], Fe_o/Fe_d, Silt/Clay, and MS_{lf}, in the Western Paulista Plateau, São Paulo, Brazil.

Model	d.f.	AICc	ΔAICc	wAICc
MS_{lf}+Silt/Clay	4	29.86	0.00	0.57
Fe_o/Fe_d+MS_{lf}+Silt/Clay	5	32.64	2.78	0.14
MS_{lf}	3	32.66	2.80	0.14
[Hm/(Hm+Gt)]+MS_{lf}+Silt/Clay	5	33.78	3.92	0.08
Fe_o/Fe_d+MS_{lf}	4	35.83	5.97	0.03
[Hm/(Hm+Gt)]+MS_{lf}	4	35.96	6.10	0.03
Fe_o/Fe_d+[Hm/(Hm+Gt)]+MS_{lf}+Silt/Clay	6	37.24	7.38	0.01
y Fe_o/Fe_d+[Hm/(Hm+Gt)]+MS_{lf}	5	39.62	9.77	0.00
[Hm/(Hm+Gt)]	3	45.48	15.63	0.00
Silt/Clay	3	46.76	16.91	0.00
Fe_o/Fe_d	3	47.05	17.20	0.00
[Hm/(Hm+Gt)]+Silt/Clay	4	48.82	18.96	0.00
Fe_o/Fe_d+[Hm/(Hm+Gt)]	4	48.84	18.99	0.00
Fe_o/Fe_d+Silt/Clay	4	50.12	20.26	0.00
Fe_o/Fe_d+[Hm/(Hm+Gt)]+Silt/Clay	5	52.74	22.89	0.00
Model Averaged coefficients	Estimate	SE	z	p
Intercept	-0.234706	0.564749	0.395	0.69
[Hm/(Hm+Gt)]	-0.008458	0.337439	0.023	0.95
MS_{lf}	0.492037	0.107972	4.274	>0.001
Silt/Clay	0.481029	0.323739	1.427	0.22
Fe_o/Fe_d	1.344747	4.655999	0.273	0.44
Relative variable importance	[Hm/(Hm+Gt)]	MS_{lf}	Silt/Clay	Fe_o/Fe_d
Importance	0.13	1.00	0.80	0.19

MS_{lf}: low-frequency magnetic susceptibility; Fe_o/Fe_d: ratio of oxalate to dithionite-extracted iron; [Hm/(Hm+Gt)]: hematite goethite ratio; Silt/Clay: silt clay ratio.

Table 4. Model selection and model-averaged coefficients, and relative importance of multiple linear models relating $\delta^{15}\text{N}$ to [Hm/(Hm+Gt)], Fe_o/Fe_d, Silt/Clay, and MS_{lf}, in the Western Paulista Plateau, São Paulo, Brazil.

Model	d.f.	AICc	ΔAICc	wAICc
[Hm/(Hm+Gt)]+ MS_{lf} + Silt/Clay	5	48.99	0.00	0.29
[Hm/(Hm+Gt)]+ MS_{lf}	4	49.00	0.00	0.29
Fe_o/Fe_d + [Hm/(Hm+Gt)]+ MS_{lf}	5	50.53	1.54	0.13
Fe_o/Fe_d + [Hm/(Hm+Gt)]+ MS_{lf} +Silt/Clay	6	51.76	2.77	0.07
[Hm/(Hm+Gt)]	3	51.80	2.81	0.07
Fe_o/Fe_d + [Hm/(Hm+Gt)]	4	52.64	3.65	0.05
MS_{lf}	3	52.86	3.87	0.04
MS_{lf} + Silt/Clay	4	54.62	5.63	0.02
[Hm/(Hm+Gt)]+ Silt/Clay	4	55.12	6.13	0.01
Fe_o/Fe_d + MS_{lf}	4	55.70	6.71	0.01
Fe_o/Fe_d + [Hm/(Hm+Gt)]+ Silt/Clay	5	56.55	7.56	0.01
Fe_o/Fe_d + MS_{lf} + Silt/Clay	5	58.28	9.28	0.00
Silt/Clay	3	62.23	13.24	0.00
Fe_o/Fe_d	3	62.50	13.51	0.00
Fe_o/Fe_d + Fe_o/Fe_d	4	64.97	15.97	0.00
Model Averaged coeffiecents	Estimate	SE	z	P
Intercept	3.1804	1.2297	2.461	0.0139
[Hm/(Hm+Gt)]	4.4830	1.5565	2.669	0.0076
MS_{lf}	0.4257	0.1825	2.333	0.0197
Silt/Clay	0.6492	0.4145	1.445	0.1484
Fe_o/Fe_d	-18.3417	14.210	1.184	0.2363
		0		
Relative variable importance	[Hm/(Hm+Gt)]	MS_{lf}	Silt/Clay	Fe_o/Fe_d
Importance	0.93	0.86	0.40	0.27

MS_{lf}: low-frequency magnetic susceptibility; Fe_o/Fe_d: ratio of oxalate to dithionite-extracted iron; [Hm/Hm+Gt]: hematite goethite ratio; Silt/Clay: silt clay ratio.

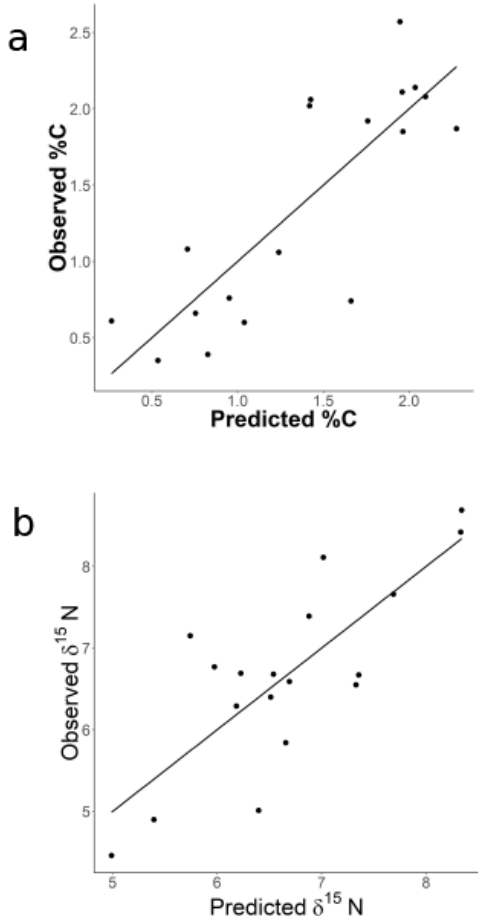


Figure 2. Scatter plots of observed versus predicted values from averaged models. A. model MS_{lf}+Silt/Clay for soil carbon (%C); B. MS_{lf}+Silt/Clay for %N; and C. [Hm/(Hm+Gt)]+MS_{lf} for soil δ¹⁵N.

4. Discussion

The results corroborate that Fe metrics can help to explain SOM stabilization in tropical soils from WPP. The range of MS_{lf} and SM_{hf} values resulted from contrasting Fe amounts, and pedogenic conditions, being important to identify distinct lithologies, presenting MS as a relevant pedological indicator (Torrent et al. 2006). The mean values found are consistent with other studies in the Western Paulista Plateau (Marques Jr. et al. 2014; Siqueira et al. 2016). The higher MS_{lf} values observed in Oxisols from DVM it is due to the higher lithologic influence of basaltic Fe contents on soil magnetism, while low MS_{lf} has been reported for sandstones (Fontes et al. 2000; Torrent al. 2006). Soils

with higher MS_{lf} indicate the presence of magnetite in silt and sand fractions, and maghemite in clay fraction (Torrent et al. 2010). The $SM_{fd\%}$ mean values from DVM Oxisols reveals a mixture of SP grains ($< 0.005 \mu m$) with non-SP grains, while $SM_{FD\%}$ mean values from DSVMP indicates that SP grains with $\sim 0.03 \mu m$ are dominant (Dearing 1994), indicating a higher degree of pedogenesis in DSVMP.

The formation of minerals in clay size and magnetic enhancement during soil formation can explain the relationship between MS_{lf} and the Fe metrics (Torrent et al. 2006). The low Fe_o/Fe_d values, all above 0.05, indicates that Fe oxides are mainly crystallines, typically from high weathered soils (Kämpf et al. 2000). The predominance of Hm over Gt is reported as a pedoclimate contribution to form Hm instead of Gt (Torrent et al. 2006; Torrent et al. 2007), and also reflects the history of water activity in soil (Cornell and Schwertmann 2003).

The differences between Oxisols originated from different parent material, suggests lithological control over Fe metrics, MS_{lf} , and consequently on $\delta^{15}N$ fractioning. Lithological influences on Fe content and other soil attributes have been documented in other studies (Fontes et al. 2000; Barré et al. 2017; Barbosa et al. 2019). The relationships showed by Hm, Fed, Feo, SM, and Clay with C, and $\delta^{15}N$ indicates a binding between SOM and organo-mineral associations in the clay fraction (Adhikari et al. 2016; Coward et al. 2017; Hall et al. 2018; Khomo et al. 2017; Lützow et al. 2006).

Furthermore, these relationships confirm that different bulk Fe compositional metrics can help to explain C and $\delta^{15}N$ patterns in topsoil. Increasing values of $\delta^{15}N$ and decreasing particle size has been reported in the literature (Liao et al. 2006; Marin-Spiotta et al. 2009), and are understood as microbially processed material accumulation in clay-sized mineral fractions (Schmidt et al. 2011; Craine et al. 2015; Hall et al. 2018). The higher significant relationship of C, and $\delta^{15}N$ with Fed than Fe_o , indicates a higher

accumulation of SOM on crystalline minerals. These results are consistent with those found by Khomo et al. (2017), who observed a positive relationship between C and Fed. Besides that, the significant relationship between Hm and $\delta^{15}\text{N}$ also indicates the importance of crystalline minerals to SOM stabilization. In highly weathered soils, binding of SOM to crystalline iron oxides should be driven by chemisorption probably showing decadal–centennial turnover rates (Khomó et al. 2017), and microbially processed material (Hall et al. 2018).

With the model averaged approach, the results showed that MS_{lf} , which is a proxy for magnetic Fe oxides (Dearing 1994), was as a good predictor for C and $\delta^{15}\text{N}$. Similar relationships among C with MS_{lf} were found in different soils types (Quijano et al. 2014; Jakšík et al. 2016), and indicates an organo-mineral binding with magnetic minerals. This findings, reinforce the role of Fe oxides in organo-mineral associations in clay fraction (Lützow et al. 2006; Adhikari et al. 2016; Coward et al. 2017; Hall et al. 2018). The high significant relationship of MS_{lf} and $[\text{Hm}/(\text{Hm}+\text{Gt})]$ with $\delta^{15}\text{N}$ agrees that pedogenic crystalline minerals also contribute to SOM stabilization and storage (Khomó et al. 2017). The importance of $[\text{Hm}/(\text{Hm}+\text{Gt})]$ in the model to predict $\delta^{15}\text{N}$, that not only mineralogy but also the weathering process can influence SOM stabilization (Lawrence et al. 2015; Khomo et al. 2017), as new insights about the relevance of Hm, and its importance to study Fe reduction and SOM stability provided by (Adhikari et al. 2016).

5. Conclusion

Mineralogy explained differences on C content and $\delta^{15}\text{N}$. The data indicated that well-crystallized minerals are providing important mechanisms for storing and stabilizing SOM in highly weathered soils. MS and Fe metrics figured as a helpful indicator to detect relationships between iron oxides with C and $\delta^{15}\text{N}$. Additionally, MS results indicate that

ferrimagnetic iron oxides are also performing SOM stabilization mechanisms. This finding indicates that soil geochemistry and pedogenesis process are important drivers for soil organic matter stabilization in a tropical context.

6. References

- Ab'Saber AN (1977) Domínios morfoclimáticos na América do Sul: primeira aproximação. São Paulo. Instituto de Geografia/USP. Geomorfologia, 52: 1-21.
- Adhikari D, Poulson SR, Sumaila S, Dynes JJ, Mcbeth JM, Yang Y (2016) Asynchronous reductive release of iron and organic carbon from hematite – humic acid complexes. *Chemical Geology* 430:13–20. doi: 10.1016/j.chemgeo.2016.03.013
- Adhikari D, Yang Y (2015) Selective stabilization of aliphatic organic carbon by iron oxide. *Scientific Reports* 5:1–7. doi: 10.1038/srep11214
- Adhikari K, Hartemink AE (2016) Linking soils to ecosystem services - A global review. *Geoderma* 262:101–111. doi: 10.1016/j.geoderma.2015.08.009
- Alvares CA, Stape JL, Sentelhas PC, De Moraes Gonçalves JL, Sparovek G (2013) Köppen's climate classification map for Brazil. *Meteorologische Zeitschrift* 22:711–728. doi: 10.1127/0941-2948/2013/0507
- Barbosa RS, Marques Júnior J, Barrón V, Martins Filho MV, Siqueira DS, Peluco RG, Camargo LA, Silva LS (2019) Prediction and mapping of erodibility factors (USLE and WEPP) by magnetic susceptibility in basalt-derived soils in northeastern São Paulo state, Brazil. *Environmental Earth Sciences* 78:1–12. doi: 10.1007/s12665-018-8015-0
- Barré P, Durand H, Chenu C, Meunier P, Montagne D, Castel G, Billiou D, Soucémarianadin L, Cécillon L (2017) Geological control of soil organic carbon and nitrogen stocks at the landscape scale. *Geoderma* 285:50–56. doi: 10.1016/j.geoderma.2016.09.029
- Barton K (2019) MuMIn: Multi-model inference: R package
- Costa ACS, Bigham JM, Rhoton FE, Traina SJ (1999) Quantification and

Characterization of Maghemite in Soils Derived from Volcanic Rocks in Southern Brazil. *Clays and Clay Minerals* 47:466–473. doi: 10.1346/CCMN.1999.0470408

Coward EK, Thompson A, Plante AF (2018) Contrasting Fe speciation in two humid forest soils: Insight into organomineral associations in redox-active environments. *Geochimica et Cosmochimica Acta* 238:68–84. doi: 10.1016/j.gca.2018.07.007

Coward EK, Thompson AT, Plante AF (2017) Iron-mediated mineralogical control of organic matter accumulation in tropical soils. *Geoderma* 306:206–216. doi: 10.1016/j.geoderma.2017.07.026

Craine JM, Elmore AJ, Wang L, Augusto L, Baisden WT, Brookshire ENJ, Cramer MD, Hasselquist NJ, Hobbie EA, Kahmen A, Koba K, Kranabetter JM, Mack MC, Marin-Spiotta E, Mayor JR, McLauchlan KK, Michelsen A, Nardoto GB, Oliveira RS, Perakis SS, Peri PL, Quesada CA, Richter A, Schipper LA, Stevenson BA, Turner BL, Viani RAG, Wanek W, Zeller B (2015) Convergence of soil nitrogen isotopes across global climate gradients. *Scientific Reports* 5:8280. doi: 10.1038/srep08280

Dearing JA (1994) Environmental magnetic susceptibility. Using the Bartington MS2 system. British Library, England.

Dearing J (1999) Environmental Magnetic Susceptibility Using the Bartington MS2 System, Second. Chi Publ, Kenilworth, UK

Dinkins CP, Jones C, Olson-Rutz K (2008) Soil Sampling Strategies. In: *Soil Sampling Strategies*.

<http://store.msueextension.org/publications/agandnaturalresources/mt200803AG.pdf>

Doetterl S, Berhe AA, Arnold C, Bodé S, Fiener P, Finke P, Fuchsleger L, Griepentrog M, Harden JW, Nadeu E, Schnecker J, Six J, Trumbore S, Van Oost K, Vogel C, Boeckx P (2018) Links among warming, carbon and microbial dynamics mediated by soil mineral weathering. *Nature Geoscience* 11:589–593. doi: 10.1038/s41561-018-0168-7

Doetterl S, Stevens A, Six J, Merckx R, Van Oost K, Casanova Pinto M, Casanova-Katny A, Muñoz C, Boudin M, Zagals Venegas E, Boeckx P (2015) Soil carbon storage controlled by interactions between geochemistry and climate. *Nature Geoscience* 8:780–783. doi: 10.1038/ngeo2516

Fernandes LA (2004) Mapa litoestratigráfico da parte oriental da Bacia Bauru (PR, SP, MG), escala 1:1.000.000. Boletim Paranaense de Geociencias 53–66. doi: 10.5380/geo.v55i0.4283

Fernandes LA, de Castro AB, Basilici G (2007) Seismites in continental sand sea deposits of the Late Cretaceous Caiuá Desert, Bauru Basin, Brazil. *Sedimentary Geology* 199:51–64. doi: 10.1016/j.sedgeo.2005.12.030

Fontes MPF, de Oliveira TS, da Costa LM, Campos AAG (2000) Magnetic separation and evaluation of magnetization of Brazilian soils from different parent materials. *Geoderma* 96:81–99. doi: [https://doi.org/10.1016/S0016-7061\(00\)00005-7](https://doi.org/10.1016/S0016-7061(00)00005-7)

Grimley DA, Vepraskas MJ (2000) Magnetic Susceptibility for Use in Delineating Hydric Soils. *Soil Science Society of America Journal* 64:2174–2180. doi: 10.2136/sssaj2000.6462174x

Hall SJ, Berhe AA, Thompson A (2018) Order from disorder: do soil organic matter composition and turnover co-vary with iron phase crystallinity? *Biogeochemistry* 140:93–110. doi: 10.1007/s10533-018-0476-4

Jakšík O, Kodešová R, Kapička A, Klement A, Fér M, Nikodem A (2016) Using magnetic susceptibility mapping for assessing soil degradation due to water erosion. *Soil and Water Research* 11:105–113. doi: 10.17221/233/2015-SWR

Jordanova N (2017) Applications of soil magnetism

Jordanova N, Jordanova D, Liu Q, Hu P, Petrov P, Petrovský E (2013) Soil formation and mineralogy of a Rhodic Luvisol - insights from magnetic and geochemical studies. *Global and Planetary Change* 110:397–413. doi: 10.1016/j.gloplacha.2013.08.020

Kaiser K, Guggenberger G (2003) Mineral surfaces and soil organic matter. *European Journal of Soil Science* 54:219–236. doi: 10.1046/j.1365-2389.2003.00544.x

Kaiser K, Guggenberger G (2000) The role of DOM sorption to mineral surfaces in the preservation of organic matter in soils. *Organic Geochemistry* 31:711–725. doi: 10.1016/S0146-6380(00)00046-2

Kämpf N, Curi N (2000) Óxidos de ferro: Indicadores de ambientes pedogênicos. In: Novais RF, Alvarez VVH, Schaefer CEGR (eds) Tópicos em ciência do solo, v.1. Sociedade Brasileira de Ciência do Solo, Viçosa-MG, pp 107–138

Khom L, Trumbore S, Bern CR, Chadwick OA (2017) Timescales of carbon turnover in soils with mixed crystalline mineralogies. *SOIL* 3:17–30. doi: 10.5194/soil-3-17-2017

Kubelka P and Munk F (1931). An article on optics of paint layers. *Z. Tech. Phys.*, 12(593-601).

Lawrence CR, Harden JW, Xu X, Schulz MS, Trumbore SE (2015) Long-term controls on soil organic carbon with depth and time: A case study from the Cowlitz River Chronosequence, WA USA. *Geoderma* 247–248:73–87. doi: 10.1016/j.geoderma.2015.02.005

Liao JD, Boutton TW, Jastrow JD (2006) Organic matter turnover in soil physical fractions following woody plant invasion of grassland: Evidence from natural ^{13}C and ^{15}N . *Soil Biology & Biochemistry* 38:3197–3210. doi: 10.1016/j.soilbio.2006.04.004

Long X, Ji J, Balsam W (2011) Rainfall-dependent transformations of iron oxides in a tropical saprolite transect of Hainan Island, South China: Spectral and magnetic measurements. *Journal of Geophysical Research: Earth Surface* 116:. doi: 10.1029/2010JF001712

Long X, Ji J, Balsam W, Barrón V, Torrent J (2015) Grain growth and transformation of pedogenic magnetic particles in red Ferralsols. *Geophysical Research Letters* 42:5762–5770. doi: 10.1002/2015GL064678

Lutzow M v., Kogel-Knabner I, Ekschmitt K, Matzner E, Guggenberger G, Marschner B, Flessa H (2006) Stabilization of organic matter in temperate soils: mechanisms and their relevance under different soil conditions - a review. *European Journal of Soil Science* 57:426–445. doi: 10.1111/j.1365-2389.2006.00809.x

Marin-Spiotta E, Silver WL, Swanston CW, Ostertag R (2009) Soil organic matter dynamics during 80 years of reforestation of tropical pastures. *Global Change Biology* 15:1584–1597. doi: 10.1111/j.1365-2486.2008.01805.x

Marin-Spiotta E, Swanston CW, Torn MS, Silver WL, Burton SD (2008) Chemical and mineral control of soil carbon turnover in abandoned tropical pastures. *Geoderma* 143:49–62. doi: 10.1016/j.geoderma.2007.10.001

Marques Jr. J, Alleoni LRF, Teixeira D de B, Siqueira DS, Pereira GT (2015) Sampling planning of micronutrients and aluminium of the soils of São Paulo, Brazil. *Geoderma* Regional 4:91–99. doi: <http://dx.doi.org/10.1016/j.geodrs.2014.12.004>

Marques Jr. J, Siqueira DS, Camargo LA, Teixeira DDB, Barrón V, Torrent J (2014) Magnetic susceptibility and diffuse reflectance spectroscopy to characterize the spatial variability of soil properties in a Brazilian Haplustalf. *Geoderma* 219–220:63–71. doi: 10.1016/j.geoderma.2013.12.007

Mehra OP, Jackson ML (1960) Iron oxide removal from soils and clay by a dithionite-citrate system buffered with sodium bicarbonate. *Clays Clay Miner* 7:317–327. <https://doi.org/10.1016/B978-0-08-009235-5.50026-7>

Minasny B, Malone BP, McBratney AB, Angers DA, Arrouays D, Chambers A, Chaplot V, Chen ZS, Cheng K, Das BS, Field DJ, Gimona A, Hedley CB, Hong SY, Mandal B, Marchant BP, Martin M, McConkey BG, Mulder VL, O'Rourke S, Richer-de-Forges AC, Odeh I, Padarian J, Paustian K, Pan G, Poggio L, Savin I, Stolbovoy V, Stockmann U, Sulaeman Y, Tsui CC, Vågen TG, van Wesemael B, Winowiecki L (2017) Soil carbon 4 per mille. *Geoderma* 292:59–86

Peixoto CAB (2010) Geodiversidade do Estado de São Paulo, CPRM. São Paulo
Quijano L, Chaparro MAE, Marie DC, Gaspar L, Navas A (2014) Relevant magnetic and soil parameters as potential indicators of soil conservation status of Mediterranean agroecosystems. *Geophysical Journal International* 198:1805–1817. doi: 10.1093/gji/ggu239

Rasmussen C, Heckman K, Wieder WR, Keiluweit M, Lawrence CR, Berhe AA, Blankinship JC, Crow SE, Druhan JL, Hicks Pries CE, Marin-Spiotta E, Plante AF, Schädel C, Schimel JP, Sierra CA, Thompson A, Wagai R (2018) Beyond clay: towards an improved set of variables for predicting soil organic matter content. *Biogeochemistry* 137:297–306. doi: 10.1007/s10533-018-0424-3

Schaefer CER (2001) Brazilian latosols and their B horizon microstructure as long-term biotic constructs. *Australian Journal of Soil Research* 39:909–926. doi: 10.1071/SR00093

Scheinost AC, Chavernas A, Barrón V, Torrent J (1998). Use and limitations of second-derivative diffuse reflectance spectroscopy in the visible to near-infrared range to

identify and quantify Fe oxide minerals in soils. *Clays and Clay Minerals* 46, 528–536, doi.org/10.1346/CCMN.1998.0460506

Schmidt MWI, Torn MS, Abiven S, Dittmar T, Guggenberger G, Janssens IA, Kleber M, Kögel-Knabner I, Lehmann J, Manning DAC, Nannipieri P, Rasse DP, Weiner S, Trumbore SE (2011) Persistence of soil organic matter as an ecosystem property. *Nature* 478:49–56. doi: 10.1038/nature10386

Schwertmann U (1973) Use of oxalate for Fe extraction from soils. *Canadian Journal of Soil Science* 244–246

Schwertmann U, Taylor RM (1989) Iron Oxides. In: DIXON JB, WEED SB (eds) Minerals in soil environments. Madison, pp 379–438

Shenggao L (2000) Lithological factors affecting magnetic susceptibility of subtropical soils , Zhejiang Province , China. 359–373

Siqueira DS, Marques J, Matias SSR, Barrón V, Torrent J, Baffa O, Oliveira LC (2010) Correlation of properties of Brazilian Haplustalfs with magnetic susceptibility measurements. *Soil Use and Management* 26:425–431. doi: 10.1111/j.1475-2743.2010.00294.x

Siqueira DS, Marques Jr J, Teixeira DDB, Matias SSR, Camargo LA, Pereira GT (2016) Magnetic susceptibility for characterizing areas with different potentials for sugarcane production. *Pesquisa Agropecuaria Brasileira* 51:1349–1358. doi: 10.1590/S0100-204X2016000900034

Teixeira DDB, Bicalho E da S, Panosso AR, Cerri CEP, Pereira GT, La Scala Júnior N (2013) Spatial variability of soil CO₂ emission in a sugarcane area characterized by secondary information. *Scientia Agricola* 70:195–203. doi: 10.1590/S0103-90162013000300008

Torn MS, Trumbore SE, Chadwick OA, Vitousek PM, Hendricks DM (1997) Mineral control of soil organic carbon storage and turnover. *Nature* 389:170–173. doi: 10.1038/38260

Torrent J, Barrón V, Liu Q (2006) Magnetic enhancement is linked to and precedes hematite formation in aerobic soil. *Geophysical Research Letters* 33:1–4. doi: 10.1029/2005GL024818

Torrent J, Liu Q, Bloemendal J, Barrón V (2007) Magnetic Enhancement and Iron Oxides in the Upper Luochuan Loess–Paleosol Sequence, Chinese Loess Plateau. *Soil Science Society of America Journal* 71:1570–1578. doi: 10.2136/sssaj2006.0328

Torrent J, Barrón V (2008). Diffuse reflectance spectroscopy. In: Ulery, AL, Drees, LR (Ed.). *Methods of soil analysis: part 5: mineralogical methods*. Madison: Soil Science Society of America, p.367-387. (SSSA Book Series, 5). doi: 10.2136/ ssabookser5.5.c13.

Torrent J, Liu QS, Barrón V (2010) Magnetic minerals in Calcic Luvisols (Chromic) developed in a warm Mediterranean region of Spain: Origin and paleoenvironmental significance. *Geoderma* 154:465–472. doi: 10.1016/j.geoderma.2008.06.020

Trumbore S (2000) Age of soil organic matter and soil respiration: Radiocarbon constraints on belowground C dynamics. *Ecological Applications* 10:399–411. doi: 10.1890/1051-0761(2000)010[0399:AOSOMA]2.0.CO;2

Wiesmeier M, Urbanski L, Hobley E, Lang B, von Lützow M, Marin-Spiotta E, van Wesemael B, Rabot E, Ließ M, Garcia-Franco N, Wollschläger U, Vogel H-J, Kögel-Knabner I (2019) Soil organic carbon storage as a key function of soils - A review of drivers and indicators at various scales. *Geoderma* 333:149–162. doi: 10.1016/j.geoderma.2018.07.026

Yamamoto, JK, and Landim, PMB (2015) *Geoestatística: conceitos e aplicações*. Oficina de textos.

Capítulo 3 – Application of relative stability of soil carbon in a neo-tropical context

Abstract

Human induced changes in the Earth surface have been changing the Carbon (C) and Nitrogen (N) dynamics of soil organic matter (SOM) on terrestrial ecosystems, promoting losses of greenhouse gases (GHGs) to the atmosphere. Changes on soil, influence SOM decomposition, a process that has an essential role in C and N dynamics in terrestrial ecosystems. Several fractionation methods (chemical and physical) were developed, to better understand changes in SOM, determining and identifying SOM pools. Physical fractionation relies on the premise that soil particles organization on soil matrix are essential for SOM dynamics, and the access of microorganisms is a condition to decomposition. SOM stability can also be evaluated using stable isotope ratio composition of C and N ($\delta^{13}\text{C}$ and $\delta^{15}\text{N}$). Thus, some studies have proposed the integration of SOM physical fractionation and isotopic approaches to evaluate natural ecosystems and agroecosystems. In addition, techniques as FTIR (Fourier Transformed Infra Red spectroscopy) can provide information about the composition of organic functional groups. In this study, we hypothesized that relative stability of SOM (η) is affected by depth, as well by magnetic susceptibility measured at low frequency (MS_{lf}), which is a proxy for iron oxides. Furthermore, we used FTIR technique to evaluate the contribution of functional groups to η . We identified the effect of depth and MS_{lf} on the relative stability of MOS (η) and functional group ratios obtained by FTIR. Through a principal component analysis (PCA), we observed that η is associated with the ratios C – H for C = O ($2850 + 2924/1648 \text{ cm}^{-1}$) and C = C for C = O ($1512/1648 \text{ cm}^{-1}$) representing the decomposition of MOS. The low MS_{lf} values associated with C = C to C = O ($1512/1648 \text{ cm}^{-1}$) and peak ratio C = C to COO ($1512/1400 \text{ cm}^{-1}$) indicated the importance of aromatic compounds for the stabilization of organic matter at a depth of 5-20 cm in both studied geological domains. The negative relationship of MS_{lf} with FTIR peak ratios in the Domain of Mesozoic fissural volcanism of plateau type (DVM) indicates that iron oxide-linked SOM may be older than total (global) SOM.

Keywords: soil organic matter, spectral techniques, depth effect, stable isotopes, stability

1. Introduction

Anthropic changes in the Earth surface have been modifying the Carbon (C) and Nitrogen (N) dynamics of soil organic matter (SOM) on terrestrial ecosystems, promoting losses of greenhouse gases (GHGs) to the atmosphere (Trumbore 1997; Smith et al. 2016). Changes on soil, influence SOM decomposition, a process that has an essential role in C and N dynamics in terrestrial ecosystems (Trumbore 1997; Lal 2003).

To better understand changes in SOM, several fractionation methods (chemical and physical) were developed, aiming to determine and identify SOM pools (Lützow et al. 2007). The physical fractionation is supported by the assumption that soil particles organization on soil matrix are essential for SOM dynamics, and the access of microorganisms is a condition to decomposition (Lützow et al. 2007). Some studies have evaluated SOM cycling through wet sieving physical fractionation of SOM, trying to identify labile and stable fractions (Cambardella and Elliot, 1992, Carneiro et al. 2009; Sá et al. 2009; Figueiredo et al. 2013). Labile fractions generally have higher decomposition rates and lower mean residence time in soil (Haynes, 2005). For soil biogeochemistry, mean residence time (MRT) imply that C atoms in SOC are arranged in pools with different turnover rates (Doetterl et al. 2016). MRT is a measure of SOM persistence, and SOM persistence is an ecosystem property because it is the product of the interaction between physical, chemical, and biological factors (Schmidt et al. 2011). MRT can be used as a tool to evaluate the sustainability and the efficiency of C sequester (Zimmermann et al. 2007; De Clercq et al. 2015). A well-known approach to estimate MRT in a temporal scale is ^{14}C because this isotope in SOM can give information about when the C was fixed from the atmosphere, and its stability (Trumbore 2009). However, the ^{14}C method is expensive, which difficult its extensive usage in experiments.

Alternatively, SOM dynamics can also be evaluated using stable isotope ratios of C and N ($\delta^{13}\text{C}$ and $\delta^{15}\text{N}$) (Balesdent and Mariotti 2000; Conen et al. 2008; De Clercq et al. 2015; Figueira et al. 2016; McCorkle et al. 2016). The primary process that contributes to $\delta^{13}\text{C}$ fractioning is the diffusion of CO₂ and the carboxylation. Thus, the fundamental difference of fractioning between C3 and C4 plants are due to the isotopic fractioning among RuBisCO and PEP carboxylase enzymes (Ehleringer et al. 1993). Soil $\delta^{15}\text{N}$ can be used to infer integrated measures of N dynamics along the time (Högberg 1997; Nardoto et al. 2008; Nardoto et al. 2014; Craine et al. 2015).

Some studies have proposed the integration of SOM fractionation and isotopic approaches to evaluate native ecosystems and agroecosystems (Liao et al. 2006; Conen et al. 2008; De Clercq et al. 2015; Heckman et al. 2014). SOM show higher values of $\delta^{15}\text{N}$ as particle size decreases (Baisden et al. 2002; Liao et al. 2006; Marin-Spiotta et al. 2009). Therefore, MOM tends to present a low C:N ratio, higher $\delta^{15}\text{N}$, and it is more stable than POM (Baisden et al. 2002; Liao et al. 2006). During SOM decomposition it occurs the kinetic fractionation, that discriminate N isotopes (Högberg 1997), based on this premise the some approaches have investigated SOM stability in function of changes in C:N, $\delta^{15}\text{N}$ (Conen et al. 2008), and soil depth (Hobbie and Ouiemette 2009; Wang et al. 2009; De Clercq et al. 2015).

For soil biogeochemists, the stability of SOM concerns to a condition in which organic molecules or the concentration of C in the soil remain unchanged for considerable periods (Berhe and Kleber 2013). The stability of SOM can change in function of its distinct compounds, conditions of access to microorganism, and turnover (Schmidt et al. 2011; Lehmann and Kleber 2015; Ellerbrock and Gerke 2013; Ellerbrock et al. 2016).

Spectral techniques as FTIR (Fourier Transformed Infra Red), for example, can provide information about the composition of organic functional groups (Ellerbrock and Gerke 2013). FTIR measures the vibration of molecular bonds, and its absorbances give a mean of organic functional groups (Ellerbrock and Gerke 2013). The attraction of organic functional groups for iron oxides can influence the decomposition dynamics of SOM (Hall et al. 2018).

Some studies reported that iron oxides are generally associated with aromatic and carboxylic than other organic functional groups (Kaiser 2003; Chen et al. 2014). Nonetheless, there are also evidence of stabilization mechanisms between iron oxides with aliphatic and proteinaceous compounds (Liu et al. 2013; Adhikari and Yang 2015). In this context, iron oxides can be accessed by the magnetic susceptibility (MS) technique (Dearing 1994; Marques Jr. et al. 2014; Siqueira et al. 2016) and has been showed correlation with C in other studies (Jordanova et al. 2013; Quijano et al. 2014; Jakšík et al. 2016; Yang et al. 2016).

As the ^{14}C method is expensive, studies of SOM MRT generally are not usual in the Brazilian context, this study aims to apply the model for relative stability of SOM (η) proposed by (Conen et al. 2008) and investigate the relationship between η with magnetic susceptibility in native areas from distinct parent materials. We hypothesize that η is

affected by depth, as well by magnetic susceptibility. Furthermore, we used FTIR technique to evaluate the contribution of functional groups to η .

2. Material and Methods

2.1 Field study area

The Western Paulista Plateau (WPP) corresponds to 48% of São Paulo area, a Brazilian state that holds an area of 13 million hectares. The Western Paulista Plateau is compartmentalized in two geological domains (Figure 1): i. Domain of sedimentary and volcano-sedimentary of Mesozoic and Paleozoic deposits, little to moderately consolidated, associated with large and deep sedimentary basins of the syncline type (DSVMP); and Domain of Mesozoic fissural volcanism of plateau type (DVM) (Peixoto 2010). The geological outline is characterized by sandy, clay and gravel sediments, volcanic basic rocks, and mainly psammitic sedimentary sequences, which may include pyroclastic. The WPP geological formations are divided into two groups: i Caiuá Group, composed by the Santo Anastácio and Paraná River Formations in the state of São Paulo, corresponding to deposits of dry climate sand, accumulated in long and monotonous desert plains, margins of the large sand dune complexes (Caiuá Desert) extending to the northern region of the state of Paraná; and Bauru Group, which consists of the Uberaba, Rio do Peixe Valley, Araçatuba, São José do Rio Preto, Presidente Prudente and Marília formations. It also includes the Taiúva Analcimites, volcanic rocks locally interspersed in sequence (Fernandes 2004; Fernandes et al. 2007)

The area has a Tropical Atlantic morphoclimatic regime (sea of hills and forested plateaus) (Ab'Saber 1977). According to the Köppen's climate classification map for Brazil (Alvares et al. 2013), the predominant climates are Aw with dry winter, Cfa with hot summer and Cwa with dry winter and hot summer. The natural vegetation of Western Paulista Plateau was Atlantic Forest in the West and Cerrado in the East and Southwest, and the current most representative land use is sugarcane and pasture.

2.2 Sampling design

From the 300 sampling points, were selected 22 points simulating stratified sampling (Dinkins et al. 2008), to do more sophisticated analysis as diffuse reflectance spectroscopy. These points are representative of the landscape compartments that causes variability. In addition to the landscape compartments, were guided the selection of points by the variability map ($n=300$) of iron dithionite – Fe_d (well-crystallized pedogenic minerals), iron oxalate – Fe_o (less crystallized pedogenic minerals) and magnetic susceptibility (MS). This proceeding granted the same reference interval, being representative of data variation. To develop a stratified sampling in native areas. From the 22 selected areas, were selected 8 sampling units to perform this study (Figure 1).

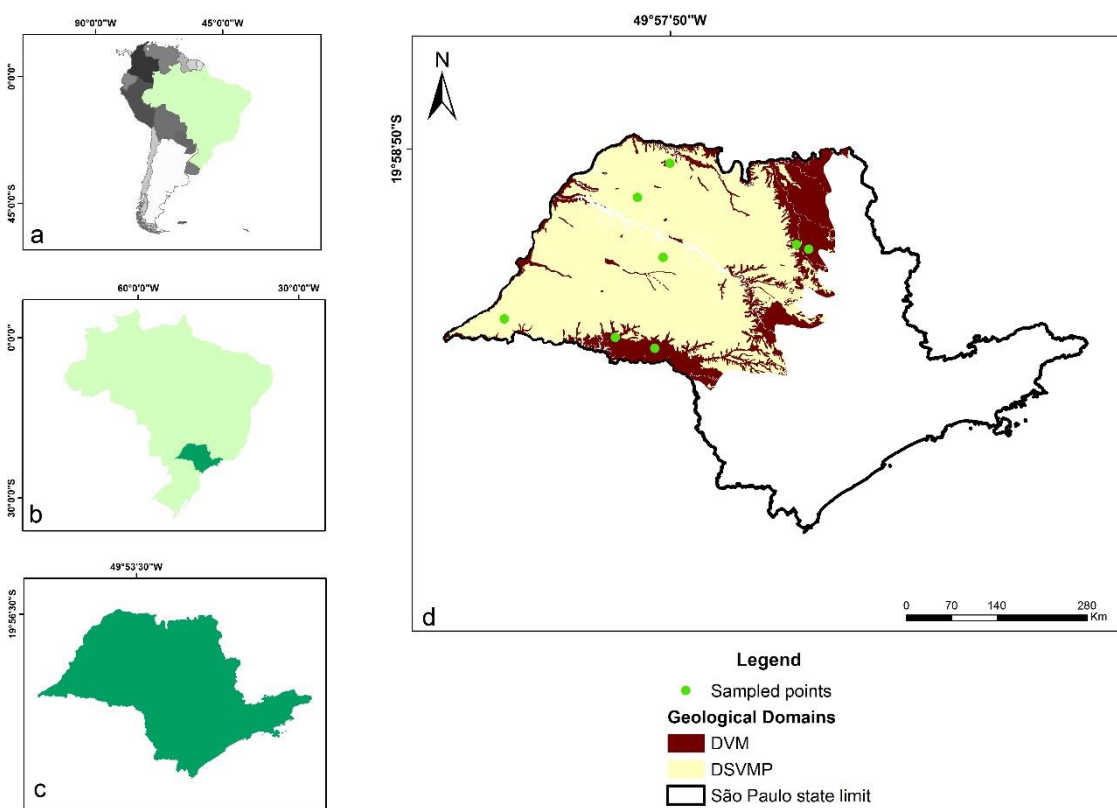


Figure 1. Field study localization context. (a) Highlights Brazil in Latin America context; (b) indicates São Paulo state localization in Brazil; (b) São Paulo state; (b) Western Paulista Plateau area, Geological Domains, and location of 8 sampled points ($n=8$) of native areas. DSVMP – Domain of sedimentary and volcano-sedimentary of Mesozoic and Paleozoic deposits, little to moderately consolidated, associated with large and deep sedimentary basins of the syncline type; DVM – Domain of Mesozoic fissural volcanism of plateau type.

2.3 Magnetic susceptibility and soil texture analysis

The magnetic susceptibility was determined through a Bartington MS2, coupled to a sensor Bartington MS2B, measuring in low frequency (lf: 0.47 kHz) and high frequency (hf: 4.7 kHz) (Costa et al. 1999; Dearing 1999). Measures in double frequency can be used to indicate the presence of magnetic materials of simple or multiple domains. The presence of pedogenetic minerals was determined through the equation (1), according to Dearing (1994):

$$MS_{fd}\% = \frac{(MS_{lf} - MS_{hf})}{MS_{lf}} \times 100$$

Where $MS_{FD}\%$ is the percent of MS in double frequency, MS_{lf} is MS in low frequency; MS_{hf} is MS in high frequency. The values of $MS_{fd}\%$ were classifieds accordingly with Dearing (1994).

2.4 Soil organic matter physical fractioning

The physical fractioning was performed accordingly to Cambardella and Elliot (1992), with adaptations proposed by Bayer et al. (2004) and Bongiovani and Lombartini (2006). The fractioning was realized segregating particulate soil organic matter fractions (labile, >53 µm) and mineral associated soil organic matter (stable, <53 µm). Every soil sample (0-5 and 5-20 cm depth) was air-dried and passed through a 2 mm sieve. Then, 20g of soil were weighted in vial glasses with 70 ml of sodium hexametaphosphate (SHMP), with a concentration of 5 g L⁻¹, and stirred for 15 hours in a stirring table for 190 rpm. The material was passed trough a sieve of 53 µm and washed with a weak jet of distilled water, and dried at 50°C, for 72h, constituting the particulate organic matter (POM>53 µm). After dried, the samples were grounded to powder. Then, the aliquotes were analyzed for their C contents constituting the particulate organic carbon (POM-C). An aliquot of the sub-sample passed in the 2 mm sieve was submitted to the same grinding process. After, this material was analyzed constituting the total organic carbon (TOC) of the bulk sample. Carbon of organic matter associated to minerals (MOM-C) were calculated by the difference between the TOC and POM-C.

2.5 Elemental and Isotope Analysis

All the samples were grounded to powder on a ball mill (8000M Mixer/Mill SPEX SamplePrep, LLC, Metuchen, NJ, USA). The C and N content of bulk soil samples and POM, and their stable nitrogen isotope ratios $\delta^{15}\text{N}$ were determined by combustion on an elemental analyzer (Vario Micro) coupled to an isotope ratio mass spectrometer (Isoprime 100, Elementar, Hanau, Germany), at UC Merced.

2.6 Relative stability os soil organic matter

The equations developed by Conen et al. (2008) were used to calculate the relative stability of SOM. The equations were applied to the context of the soil organic matter physical fractioning presented previously.

$$f_N = 1 - e^{\left(\frac{\delta_m - \delta_p}{\varepsilon}\right)} \quad (2)$$

Where δ_p is the $\delta^{15}\text{N}$ of the POM ($>53 \mu\text{m}$) and δ_m is the $\delta^{15}\text{N}$ of MOM [%]. The proportion of C lost (f_C) can be derived by stoichiometry of the N lost (f_N) and the C:N ratio of POM (r_p) and MOM (r_m).

$$f_C = f_N + (1 - f_N) * \left(1 - \left(\frac{r_m}{r_p}\right)\right) \quad (3)$$

With de mass of C in the particulate organic matter POM-C and MOM-C per soil mass unity (mg g^{-1}), the factor $[\eta]$ can be estimated, by which MOM exceeds the stability of POM in steady-state conditions. Furthermore, the stability of MOM is assumed to be the same mass of MOM-C (C_m) in relation to the mass of POM-C (C_p), which will not be lost during the conversion in mOM-C ($C_p * (1 - f_C)$).

$$\eta = \frac{C_m}{C_p * (1 - f_C)} \quad (4)$$

Thus, the increase of the soil organic matter stability or factor $[\eta]$, is described by ε , changes in $\delta^{15}\text{N}$, C:N ratio and the masses of C as POM and MOM. ε value used for this study was -2%, according to Conen et al. (2008).

2.7 Fourier Transformed Infra Red

To characterize SOM was conducted a Diffuse Infrared Fourier Transform (DRIFT) analyses on bulk soil and POM fractions using a Bruker IFS 66v/S spectrophotometer (Ettlingen, Germany) with a Praying Mantis apparatus (Harrick Scientific, Ossining NY). Samples were grounded to powder on a ball mill (8000M Mixer/Mill SPEX SamplePrep, LLC, Metuchen, NJ, USA). KBr finely powdered was used as a background reference. Absorbance spectra were obtained in the mid-IR range of wavenumbers between 400 and 4000 cm⁻¹ with 32 scannings and resolution of 4cm⁻¹. The spectra were converted to Kulbelka-Munk units. To evaluate the differences in SOM composition in relation to the sampling unities and depth, the diagnostic peaks were recorded after baseline correction, for each sample and sampling unities. The spectra were converted to Kulbelka-Munk units. To evaluate the differences in SOM composition in relation to the sampling unities and depth, the diagnostic peaks were recorded after baseline correction, for each sample and sampling unities using *approxfun* and *integrate* functions from *Stats* package in R (R Development Core Team 2019). The regions used for SOM analysis were followed (Hall et al. 2018). Peaks centered at 2925 and 2850 cm⁻¹ (distances 2898–2976 and 2839–2870 cm⁻¹) were interpreted as aliphatic C–H asymmetric and symmetric stretch. The peak centered close to 1648 cm⁻¹ (distance 1570–1710 cm⁻¹) was interpreted as C=O stretch of amides, quinones, and ketones, with possible contributions from C=C. The peak at 1512 cm⁻¹ (distance 1500–1550 cm⁻¹) was interpreted as aromatic C=C stretch, and the peak at 1400 cm⁻¹ (distance 1360–1450 cm⁻¹) was interpreted as carboxylate C–O (COO) stretch.

2.8 Data analysis

A PCA (Principal Component Analysis) was performed in WPP soil data to investigate the correlation of η and other soil parameters. The PCA was performed using the correlation matrix for soil data. PCA reduces the dimensionality of multivariate data, producing orthogonal variables originated from linear combinations of the original variables (Legendre and Legendre 2012). The first and second principal components for

PCA of soil data were used to evaluate the differences among soils from DVM and DSVMP. General linear models (GLMs) were elaborated to evaluate the effect of depth and MS_{if} on η , and FTIR ratios. Model selection was carried out using *drop1* function (Bates 2015), using F test $p < 0.05$ of significance.

3. Results

The parameters used to calculate η are presented in Table 1. The results show that approximately 75% ($\pm 13\%$) of the SOC (based on the 0-20 cm reserve) was more present in the soil surface (0-5 cm) (Table 1). The $\delta^{15}\text{N}$ values increased with depth, and the same pattern was observed for η . The PCA for soil characteristics indicated that the first two axes explained 71.9% of the variance of the data (Figure 2 and 3).

Table 1. Parameters for η calculation in soil samples from native areas in the Western Paulista Plateau. The η was estimated using Eqs. 2, 3 and 4 in the text.

Geological Domain	Depth	Cp	Cm	δp	δm	rp	rm	η
DSVMP	039NA0-5	4.2	8.1	4.3	1.7	20.42	12.43	0.9
DSVMP	039NA05-20	1.1	6	4.4	4.2	21.39	12.96	8.1
DSVMP	074NA0-5	11.2	4.4	2.6	2.1	20.74	9.01	0.7
DSVMP	074NA05-20	1.2	7.8	3.1	2.8	20.00	14.44	7.7
DSVMP	101NA0-5	17.2	15.6	5.7	3.3	15.44	10.71	0.4
DSVMP	101NA05-20	2.1	11.1	5.7	5	17.50	11.16	5.8
DSVMP	272NA0-5	10.3	2.4	4.1	0.6	25.57	6.51	0.2
DSVMP	272NA05-20	7.2	4.6	6.2	2.7	44.21	8.80	0.6
DVM	102NA0-5	34.7	2.2	6.3	2.7	15.05	2.54	0.1
DVM	102NA05-20	30.4	7	6.8	2.2	15.42	5.83	0.1
DVM	123NA0-5	15.9	14	4.7	2.5	14.96	8.33	0.5
DVM	123NA05-20	4.5	10.6	4.6	4.8	18.10	8.77	5.4
DVM	242NA0-5	7.2	13.3	5.4	3.2	17.14	12.82	0.8
DVM	242NA05-20	2.6	14	6	3.9	16.85	12.37	2.6
DVM	248NA0-5	20.9	15.2	5.5	1.7	16.36	9.28	0.2
DVM	248NA05-20	3.9	12.8	4.3	4.6	21.67	10.74	7.7

Fourier transform infrared spectroscopy (FTIR) permitted to evaluate the SOM on distinct landscape contexts, and depths. Spectra showed a similar pattern between samples. However, a clear enhancement with depth was observed when FTIR peak ratios were used. Following the importance order, the soil properties that showed higher correlation to PC1 were the FTIR peak ratios C=C to COO ($1512/1400\text{ cm}^{-1}$), C=C to C=O ($1512/1648\text{ cm}^{-1}$), C–H to C=O ($2850+2924/1648\text{ cm}^{-1}$), C–H to COO ($2850+2924/1400\text{ cm}^{-1}$), and η . Additionally, the best-related soil properties in PC2 were MS_{lf}, δm , and Depth. PC1 indicated that 5–20 cm soil samples from DSVMP are positively related to FTIR peak ratios and η . Further, in PC1 FTIR peak ratios and η showed positive loadings (Figure 2), while MS_{lf} and Depth showed positive loadings for PC2. MS_{lf} was related positively with samples from DVM geological domain, and negatively related to high values of FTIR peak ratios C=C to COO ($1512/1400\text{ cm}^{-1}$), and C=C to C=O ($1512/1648\text{ cm}^{-1}$), peak ratios C=C to COO ($1512/1400\text{ cm}^{-1}$), C=C to C=O ($1512/1648\text{ cm}^{-1}$), C–H to C=O ($2850+2924/1648\text{ cm}^{-1}$), C–H to COO ($2850+2924/1400\text{ cm}^{-1}$). Depth and δm were positively related to being also associated with 5–20cm soil samples. Finally, SM_{fd%} was more associated with the layer of 0–5 cm.

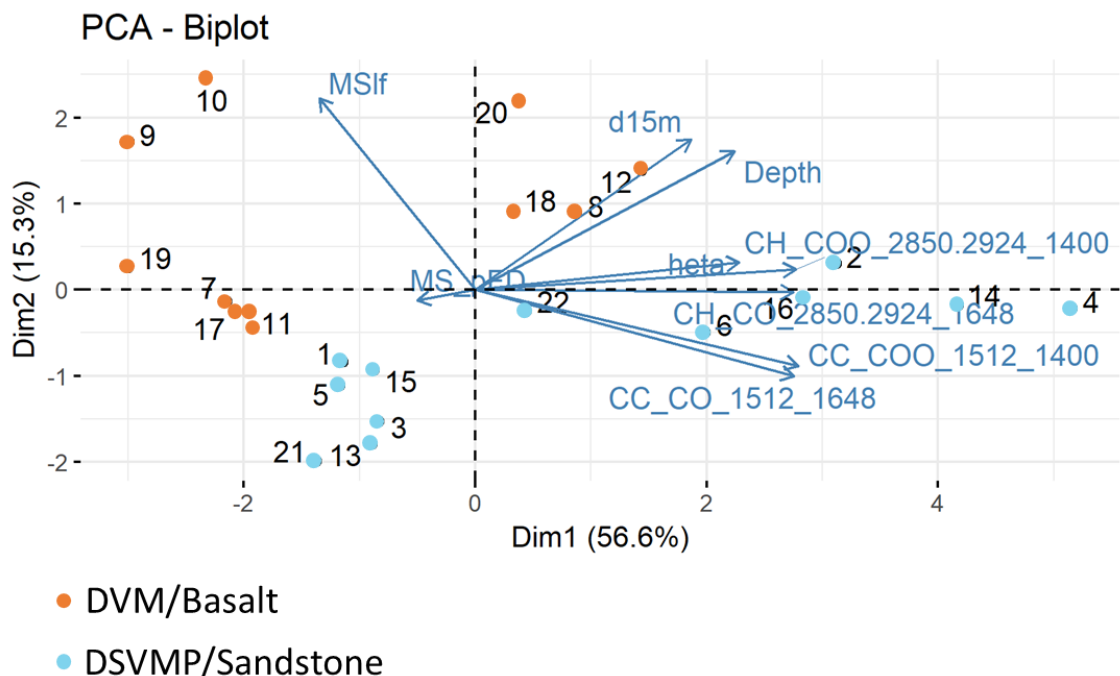


Figure 2. Principal Component Analysis (PCA) of soil variables in native areas of the Western Paulista Plateau. Groups: 1 means DVM, 2 means DSVMP; MS_{lf}: low-frequency

magnetic susceptibility measured in bulskoil; MS_pFD: magnetic susceptibility frequency per unit mass measured in bulskoil ($MS_{fd\%}$); d15m: $\delta^{15}\text{N}$ in mineral fraction (δm); η : relative SOM stability; norm_b_CH_COO_2850.2924_1400: peak ratio C–H to COO ($2850+2924/1400 \text{ cm}^{-1}$); norm_b_CH_CO_2850.2924_1648: peak ratio C–H to C=O ($2850+2924/1648 \text{ cm}^{-1}$); norm_b_CC_COO_1512_1400: peak ratio C=C to COO ($1512/1400 \text{ cm}^{-1}$); norm_b_CC_CO_1512_1648: peak ratio C=C to C=O ($1512/1648 \text{ cm}^{-1}$).

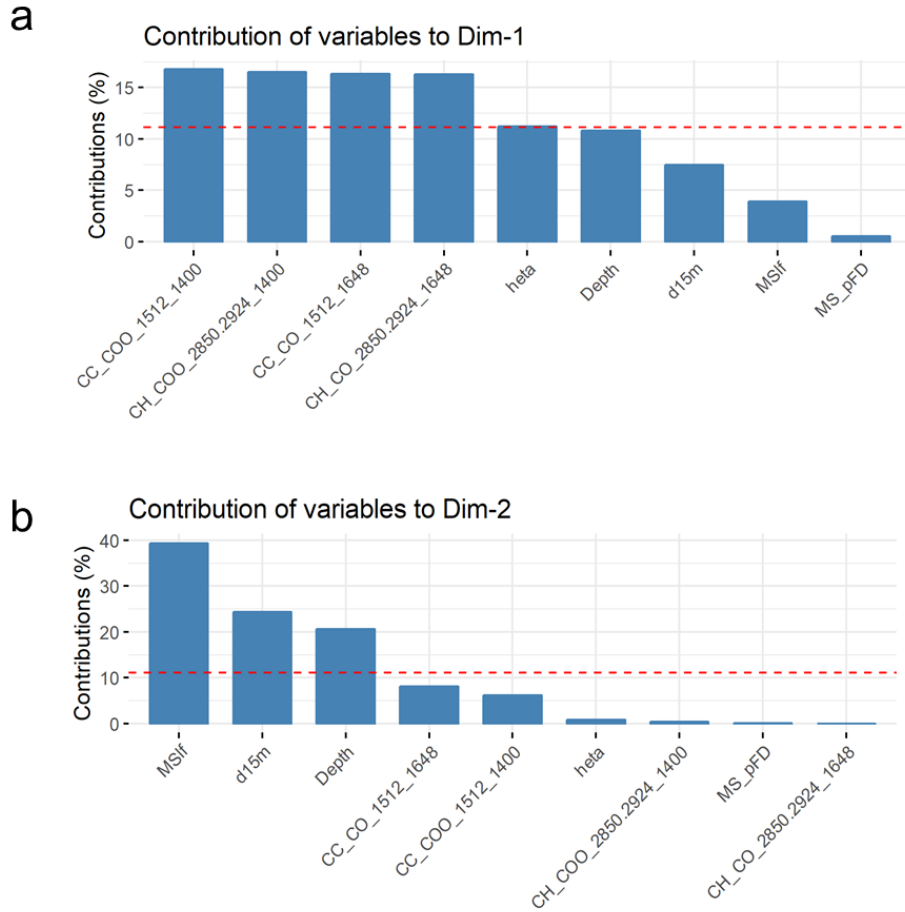


Figure 3. Variance proportion from the data set explained by the different principal components and contribution of each variable to Dimension 1 (Dim 1), and Dimension 2 (Dim 2). BulksoilLF: low-frequency magnetic susceptibility measured in bulskoil (MS_{lf}); Bulskoil_pFD: magnetic susceptibility frequency per unit mass measured in bulskoil ($MS_{fd\%}$); d15m: $\delta^{15}\text{N}$ in mineral fraction (δm); η : relative SOM stability; norm_b_CH_COO_2850.2924_1400: peak ratio C–H to COO ($2850+2924/1400 \text{ cm}^{-1}$); norm_b_CH_CO_2850.2924_1648: peak ratio C–H to C=O ($2850+2924/1648 \text{ cm}^{-1}$); norm_b_CC_COO_1512_1400: peak ratio C=C to COO ($1512/1400 \text{ cm}^{-1}$); norm_b_CC_CO_1512_1648: peak ratio C=C to C=O ($1512/1648 \text{ cm}^{-1}$).

The GLM showed that SM_{lf} and depth affected η ($p < 0.001$), suggesting that this indicator explained 60.98% of the total variation (Table 2). Further, the GLM models applied to analyze the relationships among FTIR peak ratios and SM_{lf} and depth (Table 2). The

GLM model for C=C to C=O ($1512/1648\text{ cm}^{-1}$) peak ratio showed a pseudo R^2 of 75.62% ($p < 0.001$), for peak ratio C=C to COO ($1512/1400\text{ cm}^{-1}$) showed a pseudo- R^2 79.44% ($p < 0.001$), while for peak ratio C–H to C=O ($2850+2924/1648\text{ cm}^{-1}$) showed a pseudo- R^2 of 60.01% ($p < 0.001$), and for peak ratio C–H to COO ($2850+2924/1400\text{ cm}^{-1}$) a pseudo- R^2 of 65.60 %, ($p < 0.001$). Relationships between SM_{fd} with η and FTIR peak ratios showed no significant relationships.

Table 1. Effects of depth and low-frequency magnetic susceptibility measured in bulskoil (MS_{lf}) on organic functional groups on soils from Western Paulista Plateau.

	C=C to C=O	C=C to COO	C–H to C=O	C–H to COO	η
(intercept)	0.16 ± 0.04	0.24 ± 0.05	0.10 ± 0.05	0.14 ± 0.06	-0.56 ± 0.53
Depth	0.10 ± 0.02	0.15 ± 0.03	0.13 ± 0.03	0.20 ± 0.04	1.53 ± 0.31
MS_{lf}	-0.06 ± 0.01	-0.08 ± 0.01	-0.04 ± 0.01	-0.04 ± 0.02	-0.32 ± 0.14
Rd	0.1	0.4	0.2	0.4	9.9
pseudo R^2	75.62	79.43	60.01	65.60	60.97

4. Discussion

The η approach showed convergent information with FTIR analysis, indicating that MS_{lf} and depth are important features to be considered for SOM stabilization in the WPP soils. Our results also agree with other studies which consider C:N ratio and $\delta^{15}\text{N}$ as proxies for SOM decomposition and stabilization.

Following our first and second hypothesis, η was affected by depth, and SM_{lf} , which was corroborated by FTIR peak ratios, as observed in the GLM model. Higher values of Cp were associated with low values of η , which indicate the influence of input of biomass in the studied soils. According to Conen et al. (2008), when η is small, the incorporation of SOM in the soil is more related to plant residues, and higher values of η are associated with mineral interactions and microbially processed materials. Our results also indicate that C:N ratio and $\delta^{15}\text{N}$ can be a suitable proxy for SOM decomposition and stabilization, as observed in other studies (Conen et al. 2008; De Clercq et al. 2015). During the decomposition process, soil organic matter is mineralized (Högberg 1997), which promotes increasing values of $\delta^{15}\text{N}$ with depth. SOM tends to be older as soil depth increases because the input of organic matter in superficial layer depth decomposes with time and move to the bottom layers (Nadelhoffer and Fry 1988). However, SOM age can

decrease as depth increases if the sampled area is in a context of soil redistribution receiving soil from erosion (Torn et al. 2009; Berhe et al. 2012). Similarly, as η increased with depth, we can infer that the studied native areas are not receiving soil from erosion process. We consider that sensitivity of the η approach should be tested further with ^{14}C to validate the technique in a tropical context.

Although it is not possible to determine molecular structures of SOM with FTIR-DRIFTS, this technique can help to obtain the relative contents of SOM functional groups (Ellerbrock and Gerke 2013). Some studies have presented that absolute or relative peak ratio registered to increase in decomposition and microbial transformation (Ryals et al. 2014; Fissore et al. 2017; Hall et al. 2018). The covariation of η with peak ratios C–H to C=O ($2850+2924/1648\text{ cm}^{-1}$) and C–H to COO ($2850+2924/1400\text{ cm}^{-1}$) indicate that η is more related to decomposed organic matter. The low values of SM_{lf} associated with C=C to C=O ($1512/1648\text{ cm}^{-1}$) and peak ratio C=C to COO ($1512/1400\text{ cm}^{-1}$), can indicate the importance of recalcitrant compounds to organic matter stabilization in the context of 20–40 cm soil depth in DSVMP geological domain. The negative relationship of SM_{lf} with FTIR peak ratios in DVM, indicate that the SOM bound to iron oxides can be older than bulskoil SOM (Kögel-Knabner et al. 2008; Hall et al. 2018). The MS_{lf} values associated with DVM soil samples in the PCA are due to the influence of iron oxides as magnetite and maghemite, while lower values of SM_{lf} were reported for sandstones (Fontes et al. 2000; Torrent et al. 2006; Marques Jr. et al. 2014; Siqueira et al. 2016). $\text{SM}_{\text{fd}\%}$ values associated with 0–5 cm soil depth from DSVMP indicates that SP grains with $\sim 0.03\text{ }\mu\text{m}$ dominate in the upper layers (Dearing 1994).

5. Conclusion

The η approach showed to be a suitable technique to be used in WPP, corroborating that C:N ratio and $\delta^{15}\text{N}$ in soil can be used as indicators for SOM decomposition and stabilization. FTIR peak ratios corroborated the results found by η . Furthermore, our results showed that depth and MS_{lf} influenced η and FTIR peak ratios in native areas from WPP. Our findings suggest that SOM quality and ferrimagnetic iron oxides may help to understand stabilization mechanisms on a landscape scale better.

6. References

- Ab'Saber AN (1977). Domínios morfoclimáticos na América do Sul: primeira aproximação. São Paulo. Instituto de Geografia/USP. Geomorfologia, 52: 1-21.
- Adhikari D, Yang Y (2015) Selective stabilization of aliphatic organic carbon by iron oxide. *Scientific Reports* 5:1–7. doi: 10.1038/srep11214
- Alvares CA, Stape JL, Sentelhas PC, De Moraes Gonçalves JL, Sparovek G (2013) Köppen's climate classification map for Brazil. *Meteorologische Zeitschrift* 22:711–728. doi: 10.1127/0941-2948/2013/0507
- Baisden WT, Amundson R, Cook AC, Brenner DL (2002) Turnover and storage of C and N in five density fractions from California annual grassland surface soils. *Global Biogeochemical Cycles* 16:64-1-64–16. doi: 10.1029/2001GB001822
- Bates D, Maechler M, Bolker B, Walker S (2015) Fitting Linear Mixed-Effects Models Using lme4. *Journal of Statistical Software*, 67(1), 1-48. doi: 10.18637/jss. v067.i01.
- Bayer C, Martin-Neto L, Mielniczuk J, Pavinato A. (2004). Armazenamento de carbono em frações lábeis da matéria orgânica de um Latossolo Vermelho sob plantio direto. *Pesquisa Agropecuária Brasileira*, 39(7), 677-683. doi: 10.1590/S0100-204X2004000700009
- Berhe AA, Harden JW, Torn MS, Kleber M, Burton SD, Harte J (2012) Persistence of soil organic matter in eroding versus depositional landform positions. *Journal of Geophysical Research: Biogeosciences* 117:1–16. doi: 10.1029/2011JG001790
- Berhe AA, Kleber M (2013) Erosion, deposition, and the persistence of soil organic matter: mechanistic considerations and problems with terminology. *Earth Surface Processes and Landforms* 38:908–912. doi: 10.1002/esp.3408
- Bongiovanni MD, Lobartini JC (2006) Particulate organic matter, carbohydrate, humic acid contents in soil macro-and microaggregates as affected by cultivation. *Geoderma*, 136(3), 660-665. doi: 10.1016/j.geoderma.2006.05.002
- Cambardella CA, Elliott ET (1992) Particulate soil organic-matter changes across a grassland cultivation sequence. *Soil Science Society of America Journal*, 56(3), 777-783. 10.2136/sssaj1992.03615995005600030017x
- Carneiro MAC, de Souza ED, dos Reis EF, Pereira HS, de Azevedo WR (2009) Atributos

físicos, químicos e biológicos de solo de cerrado sob diferentes sistemas de uso e manejo. Revista Brasileira de Ciencia do Solo 33:147–157. doi: 10.1590/S0100-06832009000100016

Chen C, Dynes JJ, Wang J, Sparks DL (2014) Properties of Fe- organic matter associations via coprecipitation versus adsorption. Environmental Science & Technology 48:13751–13759. doi: 10.1021/es503669u

Conen F, Zimmermann M, Leifeld J, Seth B, Alewell C (2008) Relative stability of soil carbon revealed by shifts in $\delta^{15}\text{N}$ and C:N ratio. Biogeosciences 5:123–128. doi: 10.5194/bg-5-123-2008

Costa ACS, Bigham JM, Rhoton FE, Traina SJ (1999) Quantification and Characterization of Maghemite in Soils Derived from Volcanic Rocks in Southern Brazil. Clays and Clay Minerals 47:466–473. doi: 10.1346/CCMN.1999.0470408

Craine JM, Elmore AJ, Wang L, Augusto L, Baisden WT, Brookshire ENJ, Cramer MD, Hasselquist NJ, Hobbie EA, Kahmen A, Koba K, Kranabetter JM, Mack MC, Marin-Spiotta E, Mayor JR, McLauchlan KK, Michelsen A, Nardoto GB, Oliveira RS, Perakis SS, Peri PL, Quesada CA, Richter A, Schipper LA, Stevenson BA, Turner BL, Viani RAG, Wanek W, Zeller B (2015) Convergence of soil nitrogen isotopes across global climate gradients. Scientific Reports 5:8280. doi: 10.1038/srep08280

De Clercq T, Heiling M, Dercon G, Resch C, Aigner M, Mayer L, Mao Y, Elsen A, Steier P, Leifeld J, Merckx R (2015) Predicting soil organic matter stability in agricultural fields through carbon and nitrogen stable isotopes. Soil Biology and Biochemistry 88:29–38. doi: 10.1016/j.soilbio.2015.05.011

Dearing JA (1994) Environmental magnetic susceptibility. Using the Bartington MS2 system. British Library, England.

Dearing J (1999) Environmental Magnetic Susceptibility Using the Bartington MS2 System, Second. Chi Publ, Kenilworth, UK

Dinkins CP, Jones C, Olson-Rutz K (2008) Soil Sampling Strategies. In: Soil Sampling Strategies.

<http://store.msuextension.org/publications/agandnaturalresources/mt200803AG.pdf>

Doetterl S, Berhe AA, Nadeu E, Wang Z, Sommer M, Fiener P (2016) Erosion, deposition

and soil carbon: A review of process-level controls, experimental tools and models to address C cycling in dynamic landscapes. *Earth-Science Reviews* 154:102–122. doi: 10.1016/j.earscirev.2015.12.005

Ellerbrock RH, Gerke HH (2013) Characterization of organic matter composition of soil and flow path surfaces based on physicochemical principles-a review. *Advances in Agronomy* 121:117–177. doi: 10.1016/B978-0-12-407685-3.00003-7

Ellerbrock RH, Leue M, Gerke HH (2016) Interpretation of infrared spectra for OM characterization of soil structural surfaces of Bt-horizons. *Journal of Plant Nutrition and Soil Science* 179:29–38. doi: 10.1002/jpln.201400619

Fernandes LA (2004) Mapa litoestratigráfico da parte oriental da Bacia Bauru (PR, SP, MG), escala 1:1.000.000. *Boletim Paranaense de Geociencias* 53–66. doi: 10.5380/geo.v55i0.4283

Fernandes LA, de Castro AB, Basilici G (2007) Seismites in continental sand sea deposits of the Late Cretaceous Caiuá Desert, Bauru Basin, Brazil. *Sedimentary Geology* 199:51–64. doi: 10.1016/j.sedgeo.2005.12.030

Figueiredo CC, Resck DVS, Carneiro MAC, Ramos MLG, Sá JCM (2013) Stratification ratio of organic matter pools influenced by management systems in a weathered Oxisol from a tropical agro-ecoregion in Brazil. *Soil Research* 51:133–141. doi: 10.1071/sr12186

Fissore C, Dalzell BJ, Berhe AA, Voegtle M, Evans M, Wu A (2017) Influence of topography on soil organic carbon dynamics in a Southern California grassland. *Catena* 149:140–149. doi: 10.1016/j.catena.2016.09.016

Fontes MPF, de Oliveira TS, da Costa LM, Campos AAG (2000) Magnetic separation and evaluation of magnetization of Brazilian soils from different parent materials. *Geoderma* 96:81–99. doi: [https://doi.org/10.1016/S0016-7061\(00\)00005-7](https://doi.org/10.1016/S0016-7061(00)00005-7)

Hall SJ, Berhe AA, Thompson A (2018) Order from disorder: do soil organic matter composition and turnover co-vary with iron phase crystallinity? *Biogeochemistry* 140:93–110. doi: 10.1007/s10533-018-0476-4

Hobbie EA, Ouimette AP (2009) Controls of nitrogen isotope patterns in soil profiles. *Biogeochemistry* 95:355–371. doi: 10.1007/s10533-009-9328-6

Högberg P (1997) Tansley Review No. 95. ¹⁵N natural abundance in soil-plant systems. *New Phytologist* 137:179–203. doi: 10.1046/j.1469-8137.1997.00808.x

Jakšík O, Kodešová R, Kapička A, Klement A, Fér M, Nikodem A (2016) Using magnetic susceptibility mapping for assessing soil degradation due to water erosion. *Soil and Water Research* 11:105–113. doi: 10.17221/233/2015-SWR

Jordanova N, Jordanova D, Liu Q, Hu P, Petrov P, Petrovský E (2013) Soil formation and mineralogy of a Rhodic Luvisol - insights from magnetic and geochemical studies. *Global and Planetary Change* 110:397–413. doi: 10.1016/j.gloplacha.2013.08.020

Kaiser K (2003) Sorption of natural organic matter fractions to goethite (α -FeOOH): effect of chemical composition as revealed by liquid-state ^{13}C NMR and wet-chemical analysis. *Organic Geochemistry* 34:1569–1579. doi: 10.1016/S0146-6380(03)00120-7

Kögel-Knabner I, Guggenberger G, Kleber M, Kandeler E, Kalbitz K, Scheu S, Eusterhues K, Leinweber P (2008) Organo-mineral associations in temperate soils: Integrating biology, mineralogy, and organic matter chemistry. *Journal of Plant Nutrition and Soil Science* 171:61–82. doi: 10.1002/jpln.200700048

Lal R (2003) Global potential of soil carbon sequestration to mitigate the greenhouse effect. *Critical Reviews in Plant Sciences* 22:151–184. doi: 10.1080/713610854

Legendre P, Legendre LFJ (2012) Numerical ecology. 3rd ed. Amsterdam: Elsevier. vol. 24.

Lehmann J, Kleber M (2015) The contentious nature of soil organic matter. *Nature* 528:1–9. doi: 10.1038/nature16069

Liao JD, Boutton TW, Jastrow JD (2006) Organic matter turnover in soil physical fractions following woody plant invasion of grassland: Evidence from natural ^{13}C and ^{15}N . *Soil Biology & Biochemistry* 38:3197–3210. doi: 10.1016/j.soilbio.2006.04.004

Liu X, Eusterhues K, Thieme J et al (2013) STXM and Nano- SIMS Investigations on EPS fractions before and after adsorption to goethite. *Environmental Science & Technology* 47:3158–3166. doi: 10.1021/es3039505

Lützow M, Kögel-Knabner I, Ekschmitt K, Flessa H, Guggenberger G, Matzner E,

Marschner B (2007) SOM fractionation methods: Relevance to functional pools and to stabilization mechanisms. *Soil Biology and Biochemistry* 39:2183–2207. doi: 10.1016/j.soilbio.2007.03.007

Marin-Spiotta E, Silver WL, Swanston CW, Ostertag R (2009) Soil organic matter dynamics during 80 years of reforestation of tropical pastures. *Global Change Biology* 15:1584–1597. doi: 10.1111/j.1365-2486.2008.01805.x

Marques Jr. J, Siqueira DS, Camargo LA, Teixeira DDB, Barrón V, Torrent J (2014) Magnetic susceptibility and diffuse reflectance spectroscopy to characterize the spatial variability of soil properties in a Brazilian Haplustalf. *Geoderma* 219–220:63–71. doi: 10.1016/j.geoderma.2013.12.007

McCorkle EP, Berhe AA, Hunsaker CT, Johnson DW, McFarlane KJ, Fogel ML, Hart SC (2016) Tracing the source of soil organic matter eroded from temperate forest catchments using carbon and nitrogen isotopes. *Chemical Geology* 445:172–184. doi: 10.1016/j.chemgeo.2016.04.025

Natelhoffer KJ, Fry B (1988) Controls on natural nitrogen-15 and carbon-13 abundances in forest soil organic matter. *Soil Science Society of America Journal*, 52(6), 1633–1640. doi:10.2136/sssaj1988.03615995005200060024x

Nardoto GB, Ometto JPHB, Ehleringer JR, Higuchi N, Bustamante MM da C, Martinelli LA (2008) Understanding the Influences of Spatial Patterns on N Availability Within the Brazilian Amazon Forest. *Ecosystems* 11:1234–1246. doi: 10.1007/s10021-008-9189-1

Nardoto GB, Quesada CA, Patiño S, Saiz G, Baker TR, Schwarz M, Schrodt F, Feldpausch TR, Domingues TF, Marimon BS, Marimon Junior BH, Vieira ICG, Silveira M, Bird MI, Phillips OL, Lloyd J, Martinelli LA (2014) Basin-wide variations in Amazon forest nitrogen-cycling characteristics as inferred from plant and soil ^{15}N : ^{14}N measurements. *Plant Ecology and Diversity* 7:173–187. doi: 10.1080/17550874.2013.807524

Peixoto CAB (2010) Geodiversidade do Estado de São Paulo, CPRM. São Paulo
Quijano L, Chaparro MAE, Marie DC, Gaspar L, Navas A (2014) Relevant magnetic and soil parameters as potential indicators of soil conservation status of Mediterranean agroecosystems. *Geophysical Journal International* 198:1805–1817. doi:

10.1093/gji/ggu239

R Core Team (2019) R: A language and environment for statistical computing. R Foundation for Statistical Computing, Vienna, Austria. URL <https://www.R-project.org/>

Ryals R, Kaiser M, Torn MS, Berhe AA, Silver WL (2014) Impacts of organic matter amendments on carbon and nitrogen dynamics in grassland soils. *Soil Biology and Biochemistry* 68:52–61. doi: 10.1016/j.soilbio.2013.09.011

Sá JCDM, Cerri CC, Lal R, Dick WA, Cassia Piccolo M, Feigl BE (2009) Soil organic carbon and fertility interactions affected by a tillage chronosequence in a Brazilian Oxisol. *Soil and Tillage Research* 104:56–64. doi: 10.1016/j.still.2008.11.007

Schmidt MWI, Torn MS, Abiven S, Dittmar T, Guggenberger G, Janssens IA, Kleber M, Kögel-Knabner I, Lehmann J, Manning DAC, Nannipieri P, Rasse DP, Weiner S, Trumbore SE (2011) Persistence of soil organic matter as an ecosystem property. *Nature* 478:49–56. doi: 10.1038/nature10386

Siqueira DS, Marques Jr J, Teixeira DDB, Matias SSR, Camargo LA, Pereira GT (2016) Magnetic susceptibility for characterizing areas with different potentials for sugarcane production. *Pesquisa Agropecuaria Brasileira* 51:1349–1358. doi: 10.1590/S0100-204X2016000900034

Smith P, House JI, Bustamante M, Sobocka J, Harper R, Pan G, West PC, Clark JM, Adhya T, Rumpel C, Paustian K, Kuikman P, Cotrufo MF, Elliott JA, McDowell R, Griffiths RI, Asakawa S, Bondeau A, Jain AK, Meersmans J, Pugh TAM (2016) Global change pressures on soils from land use and management. *Global Change Biology* 22:1008–1028. doi: 10.1111/gcb.13068

Torn MS, Swanston CW, Castanha C, Trumbore SE (2009) Storage and Turnover of Organic Matter in Soil

Torrent J, Barrón V, Liu Q (2006) Magnetic enhancement is linked to and precedes hematite formation in aerobic soil. *Geophysical Research Letters* 33:1–4. doi: 10.1029/2005GL024818

Trumbore S (2009) Radiocarbon and Soil Carbon Dynamics. *Annual Review of Earth and Planetary Sciences* 37:47–66. doi: 10.1146/annurev.earth.36.031207.124300

Trumbore SE (1997) Potential responses of soil organic carbon to global environmental change. *Proceedings of the National Academy of Sciences* 94:8284–8291. doi: 10.1073/pnas.94.16.8284

Wang L, D'Odorico P, Okin GS, Macko SA (2009) Isotope composition and anion chemistry of soil profiles along the Kalahari Transect. *Journal of Arid Environments* 73:480–486. doi: 10.1016/j.jaridenv.2008.11.010

ANEXO

Sequential steps to perform Basic Relief Units.

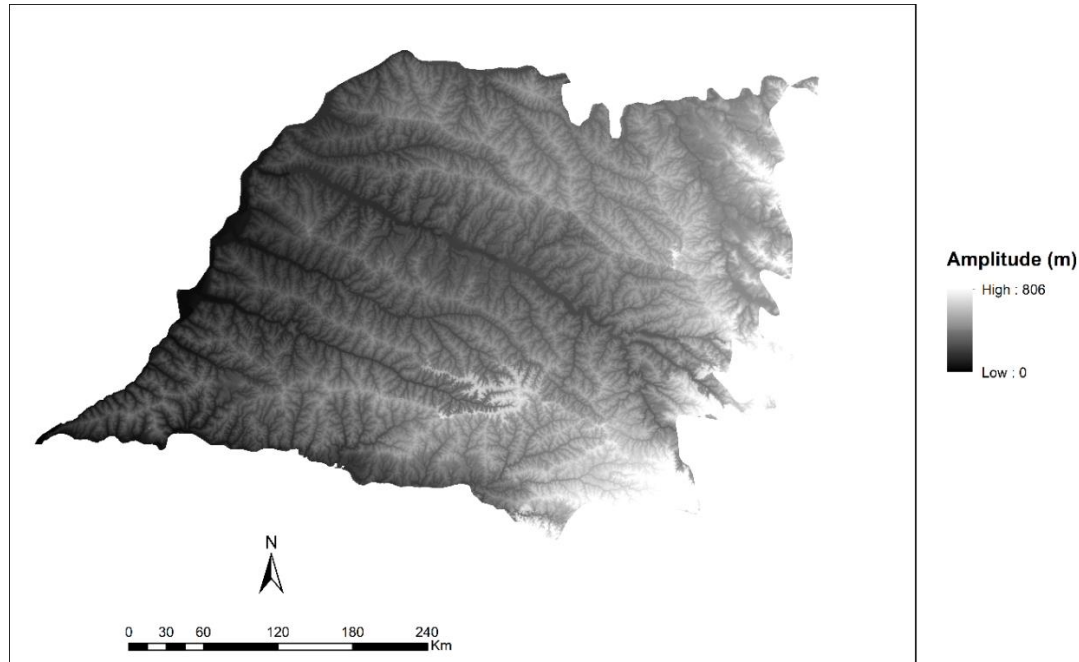


Figure 1. Altimetric amplitude of the Western Paulista Plateau.

The altimetric amplitude was 806m (Figure 1). After the reclassification to the vertical resolution (20m), were obtained 42 amplitude classes, distributed between 0, and 806m, being possible to obtain other altimetric attributes (h , a , h/H and a/A).

Table 1. Altimetric attributes of the Western Paulista Plateau. H : altimetric amplitude; h : the lowest amplitude range value possible; A : means total area of the field study; a : area of each intervalo of altimetric amplitude.

Amplitude	h	H	h/H	a	A	a/A
20	20	806	0.024814	78.2007	134379	0.000582
40	40	806	0.04902	1096.94	134379	0.008163
60	60	806	0.073529	1593.82	134379	0.011861
80	80	806	0.098039	1608.5	134379	0.01197
100	100	806	0.122549	3887.18	134379	0.028927
120	120	806	0.147059	5171.81	134379	0.038487
140	140	806	0.171569	7367.27	134379	0.054825
160	160	806	0.196078	9366.91	134379	0.069705
180	180	806	0.220588	9915.13	134379	0.073785
200	200	806	0.245098	10525	134379	0.078323

220	220	806	0.269608	10015.1	134379	0.074529
240	240	806	0.294118	10169.7	134379	0.075679
260	260	806	0.318627	10203.1	134379	0.075928
280	280	806	0.343137	9671.01	134379	0.071968
300	300	806	0.367647	8853.61	134379	0.065885
320	320	806	0.392157	7532.2	134379	0.056052
340	340	806	0.416667	5998.88	134379	0.044641
360	360	806	0.441176	4608.27	134379	0.034293
380	380	806	0.465686	3439.47	134379	0.025595
400	400	806	0.490196	2648.91	134379	0.019712
420	420	806	0.514706	2156.61	134379	0.016049
440	440	806	0.539216	1750.84	134379	0.013029
460	460	806	0.563725	1365.11	134379	0.010159
480	480	806	0.588235	1090.18	134379	0.008113
500	500	806	0.612745	882.147	134379	0.006565
520	520	806	0.637255	715.665	134379	0.005326
540	540	806	0.661765	572.346	134379	0.004259
560	560	806	0.686275	453.378	134379	0.003374
580	580	806	0.710784	358.213	134379	0.002666
600	600	806	0.735294	300.659	134379	0.002237
620	620	806	0.759804	261.023	134379	0.001942
640	640	806	0.784314	222.088	134379	0.001653
660	660	806	0.808824	185.234	134379	0.001378
680	680	806	0.833333	140.894	134379	0.001048
700	700	806	0.857843	100.164	134379	0.000745
720	720	806	0.882353	47.4627	134379	0.000353
740	740	806	0.906863	17.0235	134379	0.000127
760	760	806	0.931373	5.89779	134379	4.39E-05
780	780	806	0.955882	2.48895	134379	1.85E-05
800	800	806	0.980392	0.768079	134379	5.72E-06
806	806	806	1.004902	0.332585	134379	2.48E-06

The topographic correlation curve obtained was

$$-0.04693006 + 1.148656*x - 3.691659*x^2 + 4.179408*x^3 - 1.588979*x^4$$

Were. R²: 0.912, Adjusted R²: 0.902, p-value: < 2.2e-16,

Inflexion points: 0.4450234, 0.8701005

Stationary points: 0.2445304, 0.7770629, 0.9510927

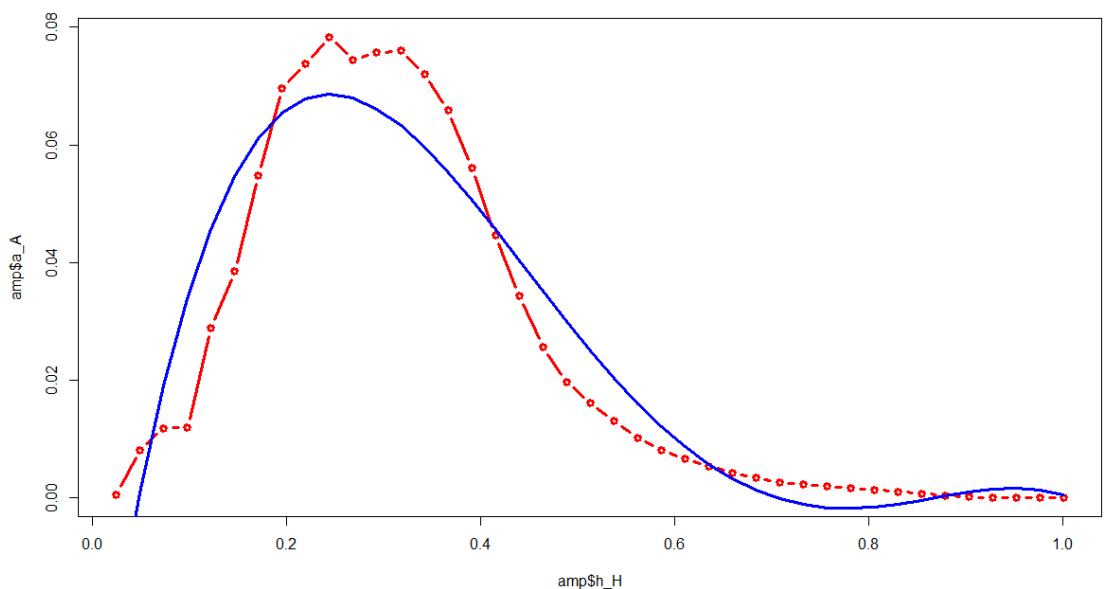


Figure 2. Graphic representation of the topographic correlation curve (red) and the trend curve (blue) of the polynom $-0.04693006 + 1.148656x - 3.691659x^2 + 4.179408x^3 - 1.588979x^4$.

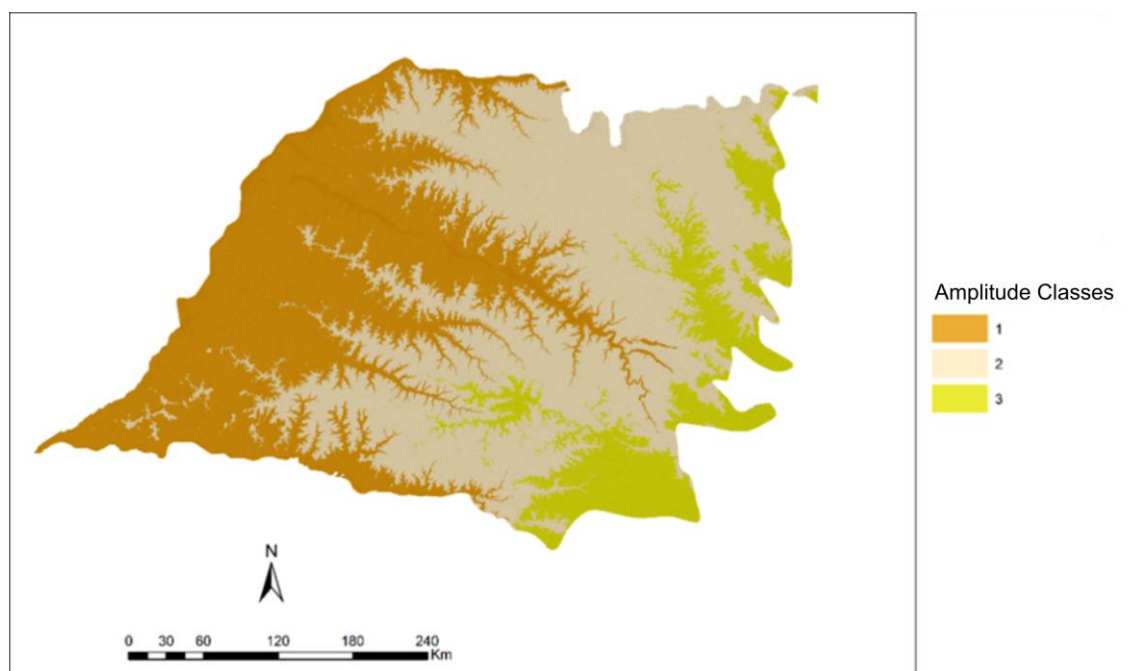


Figure 3. Classification map of the altimetric amplitude of the Western Paulista Plateau, obtained from the H_{\max} e H_{if} of the topographic correlation curve.

After the reclassification to the vertical resolution were obtained 42 slope classes, distributed between 2%, and 86%. With the values of interval and frequency obtained in Table 2, we obtained the curve of the distribution of the pixel frequency as a function of the slope intervals, it was necessary to obtain an eighth order polynomial:

$$6636902 - 64881.68x - 139932.3x^2 + 14250.07x^3 - 623.5036x^4 + 14.55345x^5 - 0.1888067x^6 + 0.001285042x^7 - 0.000003580165x^8$$

Where,

Multiple R-squared: 0.9121, Adjusted R-squared: 0.9005, p-value: < 2.2e-16

Stationary points: -0.2240626, 18.3074004, 31.6923445, 46.7424955, 61.2737025, 73.5081277, 82.7670030.

Inflexion points: 5.220925, 23.611647, 38.637737, 54.124143, 68.137712, 79.468130.

Tabela 2- Slope classification in 2% intervals and pixel frequency of each interval class.

Slope interval (%)	Pixel frequency
2	5009616
4	6820275
6	4017902
8	1366374
10	407730
12	141312
14	61330
16	34224
18	21956
20	15801
22	11937
24	9340
26	7444
28	5922
30	4561
32	3725
34	2888
36	2237
38	1662
40	1361
42	1066
44	725
46	495
48	372
50	261
52	215
54	136

56	111
58	69
60	39
62	34
64	31
66	14
68	11
70	6
72	8
74	7
76	11
78	4
80	1
84	2
86	1

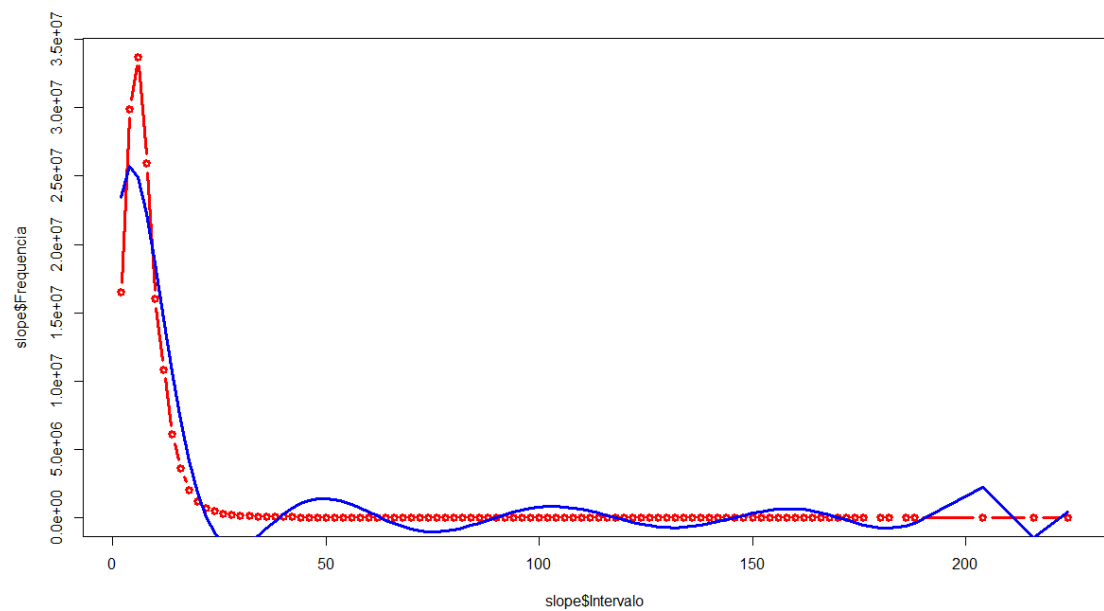


Figure 4 – Graphic representation of correlation curve between frequency interval (red) and tendency curve (blue) of the polynom $6636902 - 64881.68x - 139932.3x^2 + 14250.07x^3 - 623.5036x^4 + 14.55345x^5 - 0.1888067x^6 + 0.001285042x^7 - 0.000003580165x^8$.

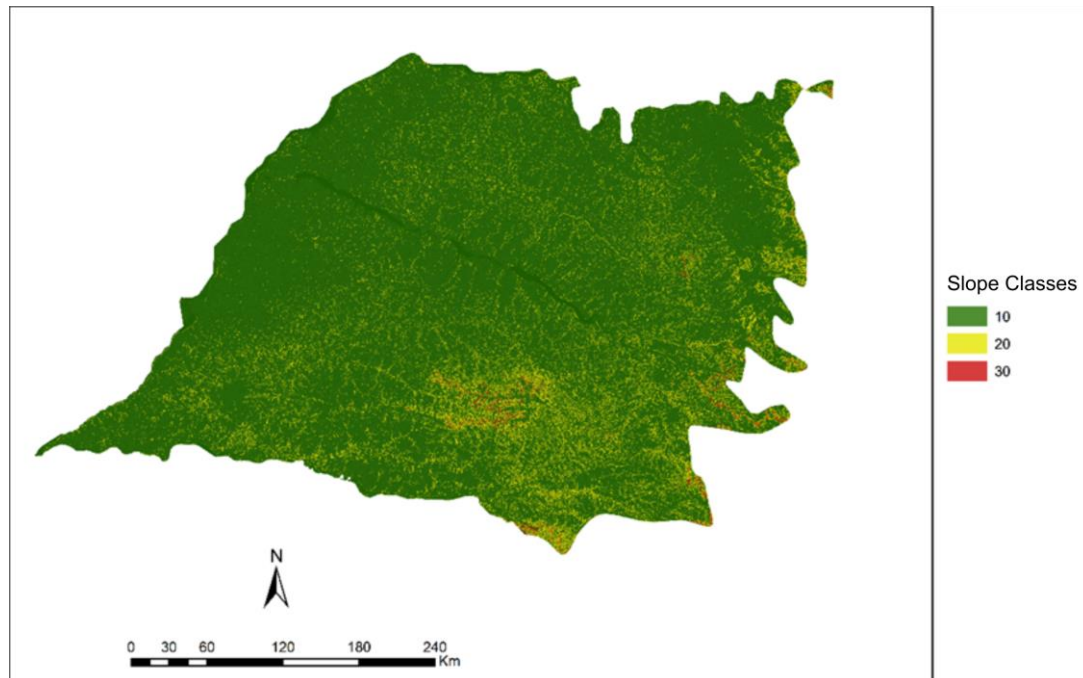
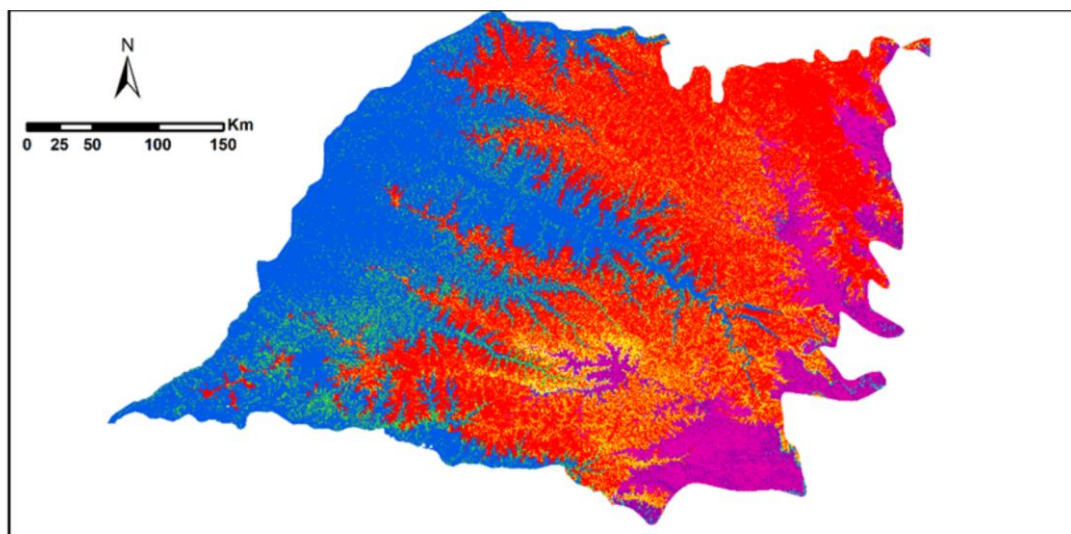


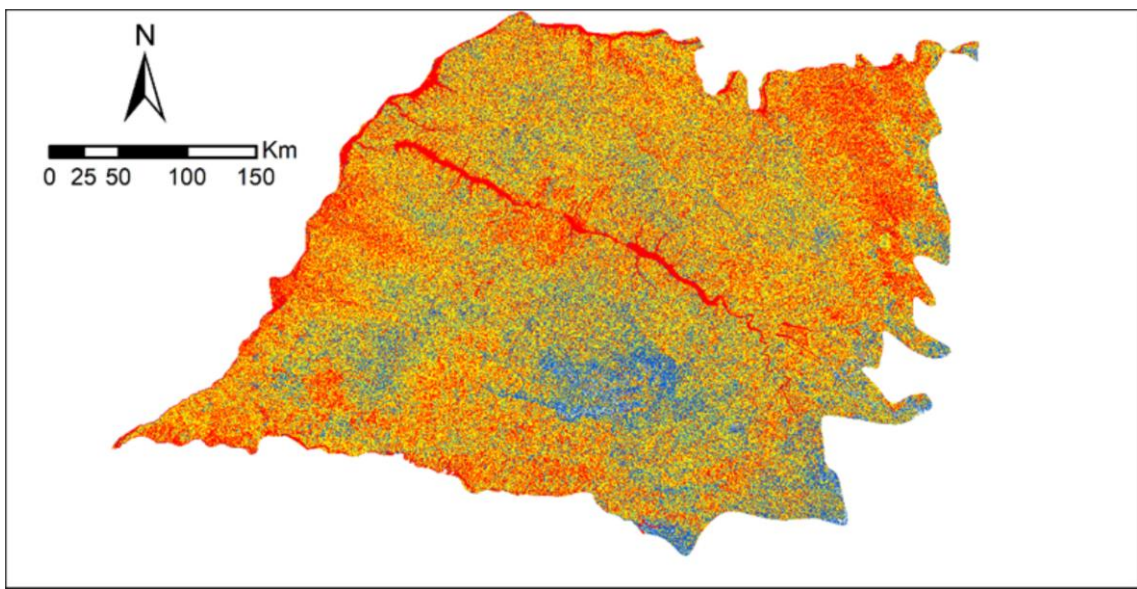
Figure 5 – Slope classification map of the Western Paulista Plateau, obtained from the C_{max} and C_{if} of correlation curve between class intervals and pixel frequency.



Basic Relief Units

- | | |
|--|--|
| Class 11 - 0 to 200 m, and 0-6% slope | Class 23 - 361 to 806 m, and 6.1-18% slope |
| Class 12 - 201 to 360 m, and 0-6% slope | Class 31 - 0 to 200 m, and >18% slope |
| Class 13 - 361 to 806 m, and 0-6% slope | Class 32 - 201 to 360 m, and >18% slope |
| Class 21 - 0 to 200 m, and 6.1-18% slope | Class 33 - 361 to 806 m, and >18% slope |
| Class 22 - 201 to 360 m, and 6.1-18% slope | |

Figure 6. Final map of Basic Units Relief of the Western Paulista Plateau.



Dissecation in the Western Paulista Plateau

High Intermediary Less intense

Figure 7. Final dissecation map (eroding process) of the Western Paulista Plateau.